TECHNICAL REPORT STANDARD TITLE PAGE

1. Report No.	2. Government Accession No.	3. Recipient's Catalog No.
FHWA/TX-81/14+208-3F		

4. Title and Subtitle	5. Report Date
DESIGN OF POST-TENSIONED GIRDER ANCHORAGE ZONES	June 1981
	6. Performing Organization Code

7. Author(s)	8. Performing Organization Report No.
W. C. Stone and J. E. Breen	Research Report 208-3F

9. Performing Organization Name and Address	10. Work Unit No.
Center for Transportation Research The University of Texas at Austin Austin, Texas 78712	11. Contract or Grant No. Research Study 3-5-77-208
	13. Type of Report and Period Covered
12. Sponsoring Agency Name and Address Texas State Department of Highways and Public Transportation; Transportation Planning Division P. O. Box 5051 Austin, Texas 78763	Final
	14. Sponsoring Agency Code

15. Supplementary Notes

Study conducted in cooperation with the U. S. Department of Transportation, Federal Highway Administration. Research Study Title: "Influence of Casting Position and of Shear on the Strength of Lapped Splices"

16. Abstract

Several large thin-webbed box girders, with post-tensioned anchorage zones designed in accordance with AASHTO and ACI requirements, have experienced large cracks along the tendon path in the anchorage zones at the design stressing load. Cracking of this nature provides a path for penetration of moisture and salts and thus presents a potential corrosion and frost damage threat. In addition, such cracking negates a major reason for the use of prestressed concrete, the minimization of service load cracking.

This report summarizes the major design-related observations and conclusions from an extensive analytical and experimental program which studied anchorage zone behavior of post-tensioned box girders. The experimental program investigated the primary variables affecting the formation of the tendon path crack: tendon inclination and eccentricity, section height and width, tensile splitting strength of the concrete, anchor width and geometry, and the effect of supplementary anchorage zone reinforcement, both active and passive. An extensive series of three-dimensional linear elastic finite element computer analyses was used to generalize these results and develop a failure theory to explain tendon path crack initiation based upon specified peak spalling strains at the edge of the anchorage. The theory agreed well with the experimental data over a wide spectrum of variables.

17. Key Words	18. Distribution Statement
box-girders, thin-webbed, anchorage zones, post-tensioned, cracks, tendon path, reinforcing	No restrictions. This document is available to the public through the National Technical Information Service, Springfield, Virginia 22161.

19. Security Classif. (of this report)	20. Security Classif. (of this page)	21. No. of Pages	22. Price
Unclassified	Unclassified	158	

Form DOT F 1700.7 (8-69)

DESIGN OF POST-TENSIONED GIRDER ANCHORAGE ZONES

by

W. C Stone and J. E. Breen

Research Report No. 208-3F

Research Project No. 3-5-77-208

"Design Criteria for Post-Tensioned Anchorage Zone Bursting Stresses"

Conducted for

Texas Department of Highways and Public Transportation

In Cooperation with the
U.S. Department of Transportation
Federal Highway Administration

by

CENTER FOR TRANSPORTATION RESEARCH
BUREAU OF ENGINEERING RESEARCH
THE UNIVERSITY OF TEXAS AT AUSTIN

June 1981

The contents of this report reflect the views of the authors, who are responsible for the facts and the accuracy of the data presented herein. The contents do not necessarily reflect the official views or policies of the Federal Highway Administration. This report does not constitute a standard, specification, or regulation.

There was no invention or discovery conceived or first actually reduced to practice in the course of or under this contract, including any art, method, process, machine, manufacture, design or composition of matter, or any new and useful improvement thereof, or any variety of plant which is or may be patentable under the patent laws of the United States of America or any foreign country.

PREFACE

This is the final report in a series which summarizes the detailed investigation of the effects and control of tensile stresses in the anchorage zones of post-tensioned girders. The first report in the series summarizes the state-of-the-art and presents a three-dimensional finite element analysis procedure which is of great use in understanding the development of these tensile stresses. The second report in this series summarizes an extensive series of model and full-scale physical tests which were performed to document the problem and further explore the effect of variables. This third and final report in the series draws on the analytical and experimental results presented in the first two reports. It uses these results to develop design procedures and suggested AASHTO specification provisions to control the problem. This report also contains several examples to illustrate the application of the design criteria and procedures.

This work is a part of Research Project 3-5-77-208, entitled "Design Criteria for Post-Tensioned Anchorage Zone Bursting Stresses." The studies described were conducted at the Phil M. Ferguson Structural Engineering Laboratory as a part of the overall research program of the Center for Transportation Research, Bureau of Engineering Research of the University of Texas at Austin. The work was sponsored jointly by the Texas Department of Highways and Public Transportation and the Federal Highway Administration under an agreement with The University of Texas at Austin and the Texas Department of Highways and Public Transportation.

Liaison with the Texas Department of Highways and Public Transportation was maintained through the contact representative Mr. Alan Matejowsky, the Area IV committee chairman Mr. Robert L. Reed and

the State Bridge Engineer, Mr. Wayne Henneberger; Mr. Randy Losch was the contact representative for the Federal Highway Administration. Special thanks are due to Dr. E. B. Becker and Dr. C. P. Johnson of The University of Texas at Austin, who gave a great deal of assistance and encouragement in developing the program PUZGAP-3D used in the analytical phase. Special thanks are also extended to Messrs. Wanderlan Paes-Filho and John Sladek, Assistant Research Engineers, at the Phil M. Ferguson Structural Engineering Laboratory, who made major contributions to the design, fabrication and testing of the specimens.

The overall study was directed by Dr. John E. Breen, The J. J. McKetta Professor of Engineering. The detailed analysis was carried out under the immediate supervision of Dr. William C. Stone, Research Engineer, Center for Transportation Research.

S U M M A R Y

Several large thin-webbed box girders, with post-tensioned anchorage zones designed in accordance with AASHTO and ACI requirements, have experienced large cracks along the tendon path in the anchorage zones at the design stressing load. Cracking of this nature provides a path for penetration of moisture and salts and thus presents a potential corrosion and frost damage threat. In addition, such cracking negates a major reason for the use of prestressed concrete, the minimization of service load cracking.

This report summarizes the major design-related observations and conclusions from an extensive analytical and experimental program which studied anchorage zone behavior of post-tensioned box girders. The experimental program investigated the primary variables affecting the formation of the tendon path crack: tendon inclinationn and eccentricity, section height and width, tensile splitting strength of the concrete, anchor width and geometry, and the effect of supplementary anchorage zone reinforcement, both active and passive. An extensive series of three-dimensional linear elastic finite element computer analyses was used to generalize these results and develop a failure theory to explain tendon path crack initiation based upon specified peak spalling strains at the edge of the anchorage. The theory agreed well with the experimental data over a wide spectrum of variables.

Experimental data from the prototype tests revealed an interesting additional failure mechanism due to "multistrand" effects. Sections with significant curvature in the tendon profile and with multiple strands in the same duct generated large lateral splitting forces at the point of minimum radius of curvature due to the flattening out of these multiple strands in the tendon within the confines of the duct. A method of designing reinforcement to resist this effect was presented.

A new design procedure is suggested for control of tendon path cracking and suggested code provisions are furnished. Emphasis is placed on methods of designing the section to remain uncracked at the maximum temporary post-tensioning load. Various reinforcing schemes for the anchorage zone proper (both active and passive) were investigated and a general reinforcement design procedure was developed. The concept of limit state design of the anchorage zone is discussed and load factors are developed with respect to cracking and ultimate load.

I M P L E M E N T A T I O N

This report summarizes the most important findings of an extensive experimental and analytical investigation of tension stresses in the anchorage zones of thin post-tensioned concrete structures. Specific suggestions for AASHTO Specification changes are presented along with a general design methodology for eliminating or controlling the occurrence of this cracking.

The study shows that current AASHTO provisions are ineffective, misleading, and incomplete. Adoption of the suggested specifications and design criteria and procedures will lessen the owner or designer reliance on the supplier of the anchorage system to provide correct anchorage zone hardware and details of supplementary reinforcement. The designer or constructor is given a procedure to more realistically evaluate the acceptability of a proposed anchorage system. The present AASHTO Specification places great reliance on the anchorage supplier and creates substantial conflict of interest and division of responsibility in case of subsequent problems due to the detailing provisions.

Comparative study of various details indicate that use of spirals or transverse prestressing can greatly improve anchorage behavior and capacity. Substantial economies can result from the relaxation of some present requirements which are shown to be grossly conservative, while improved performance will result if cracking is eliminated or minimized by use of the improved detailing provisions suggested.

TABLE OF CONTENTS

L I S T O F F I G U R E S

LIST OF TABLES

CHAPTER 1

INTRODUCTION

1.1 Problems in Thin Web Post-Tensioned Structures

Current trends in bridge construction show increased utilization of precast and prestressed concrete.

A number of problems have occurred in post-tensioned applications in both the bridge and the building field which indicate that the design procedures and design criteria for post-tensioned anchorage zone tensile stresses need further examination and refinement [1]. Substantial cracking along the tendon path has been experienced in a precast segmental bridge in Texas [3] (see Fig. 1.1) and in a cast-in-place box girder bridge reported by Dilger and Ghali [4]. In both of these bridges the cable profiles had significant curvature, inclination, and eccentricity in and near the anchorage zones. In the case of the Texas bridge, there was some concern over the possible effects of the anchorage hardware geometry. Similar cracking was reported in construction of the Olympic Stadium in Montreal and in post-tensioned slab structures and other thin web applications. Significant anchorage zone cracking was experienced in preliminary tests for a major lightweight concrete bridge in California which indicated lightweight concrete may be even more vulnerable.

The cracking which occurred in these anchorage regions was controlled by auxiliary reinforcement and the member strength was not appreciably reduced. However harmless these cracks may appear, they provide a path for penetration of moisture and salts and thus present potential corrosion and frost damage threats. The formation of these

Fig. 1.1 Resident engineer pointing to tendon path crack

cracks negates one of the major factors leading to the choice of prestressed concrete, the minimization of service load cracking.

Major and contradictory changes have taken place in the AASHTO, ACI, and PCI design specifications for anchorage zones in recent years, based more on the results of field experience and proprietary data than on published analyses or test procedures. Current design recommendations [4,5], while vague, seem both conservative and workable for many applications where massive end blocks with large cover can be used with relatively straight or gently curving tendons in cast-in-place post-tensioned construction. However, they do not give sufficient guidance for the wide range of thin web post-tensioned applications currently in use today, or the many new applications being suggested as the industry develops. Thus, this study of the development and control of critical anchorage zone tensile stresses was undertaken. Its goal was to provide more specific guidance to bridge design and construction personnel regarding the behavior of anchorage systems so that they could better assess the performance of a post-tensioning system without having to rely wholly on the recommendations of the hardware supplier.

1.2 The Anchorage Zone Stress State

1.2.1 The Nature of Anchorage Zone Stresses. Application of linear, elastic theory shows that if a concentrated load is applied through a bearing plate across the width of a finite rectangular block, compressive and tensile stresses are set up, as shown in Fig. 1.2. Two important tension fields are shown in this figure: those acting along the line of the load, and those acting on or near the end face at points removed from the load. The two tensile stress zones are generally called:

(1) Bursting Stress--located along the line of loading, normal to it, and away from the point of loading.

(2) Spalling Stress--located along the loading surface, parallel to it and away from the point of loading.

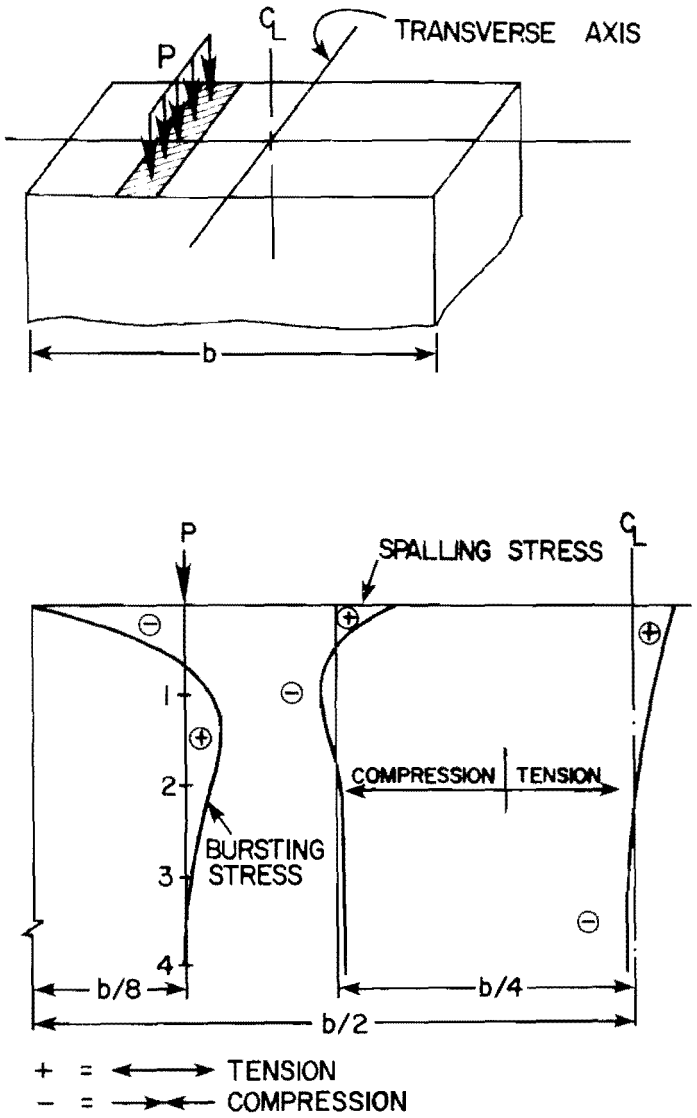

Fig. 1.2 Transverse stresses in a rectangular block loaded by a plate

In dealing with a specific post-tensioned anchorage, the load must be applied over a finite area. The compressive stress immediately under the anchor is called:

(3) Bearing Stress--The load divided by the net bearing area.

An extensive literature study presented in Ref. 1 shows that the precise role that each of these three stresses plays in the behavior of the anchorage zone has not been fully understood. No method has been proposed to predict the cracking loads. Little information is available on efficiency of reinforcement for controlling cracking caused by these tensile stresses.

1.2.1.1 Bursting Stress. Distress in the anchorage zone is signalled by the sudden formation of a crack along the line of the load. The load at which this occurs depends not only on the size of the loaded area in relation to the geometry of the loaded surface but additionally on the geometry of the surface itself, i.e., the eccentricity, inclination, and curvature of the tendon. In addition, the shape of the anchorage device as well as the action of supplemental reinforcement affect the load at which crack formation occurs.

St. Venant's principle applied to a member subjected to a concentrated load P as in Fig. 1.3(a) states that a section at a distance approximately equal to the depth of the section from the applied load should exhibit an essentially uniform normal stress distribution. The longitudinal stress distribution within the zone ABCD is not uniform and cannot be analyzed by the usual laws of strength of materials. In fact, the distribution of stresses on Section EE′ is completely discontinuous, with very high stresses at points near the applied load P and practically zero stress at all other points. This zone of disturbance is called the lead-in zone. Fig. 1.5(b) is a free body of the upper part of the lead-in zone. Equilibrium of horizontal forces requires the shear stress τ. Transverse stresses f_x are required for equilibrium of moments about M. Finally, the vertical equilibrium of forces requires the transverse stress

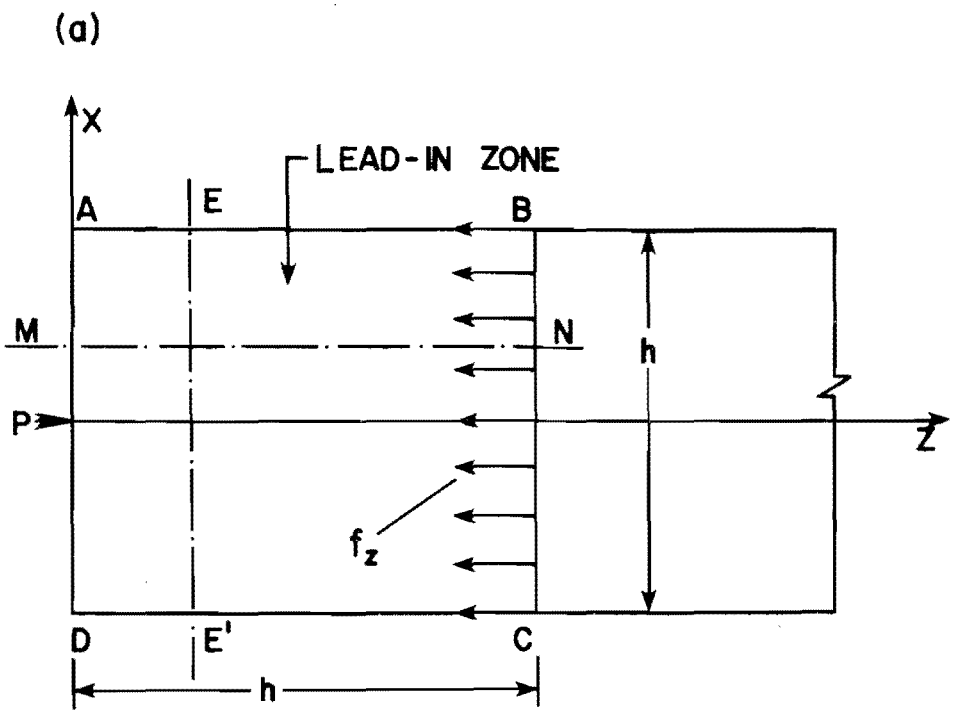

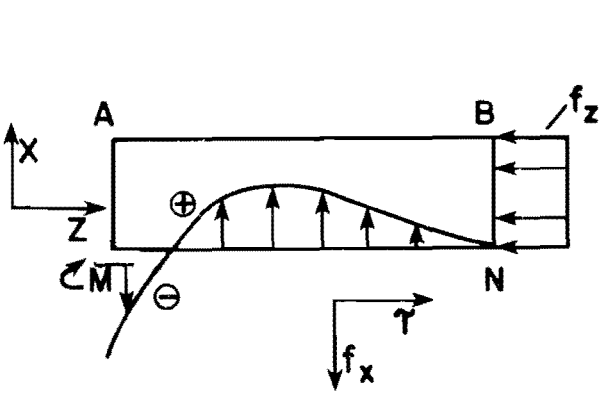

f_x = BURSTING STRESS DISTRIBUTION

$\Sigma F_x = 0 : \Sigma f_x^{\ominus} + \Sigma f_x^{\oplus} = 0$

Fig. 1.3 Equilibrium considerations within the lead-in zone

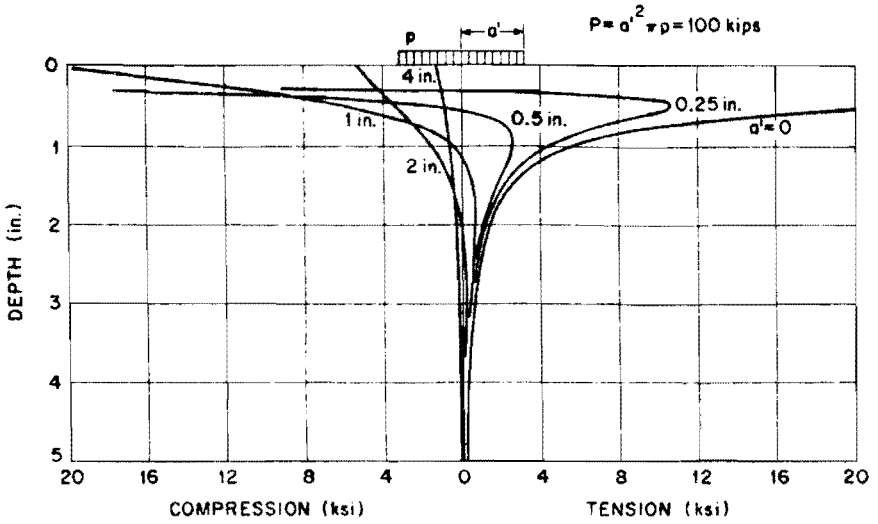

Fig. 1.4 Bursting stresses in semi-infinite body for various loaded areas (from Ref. 7)

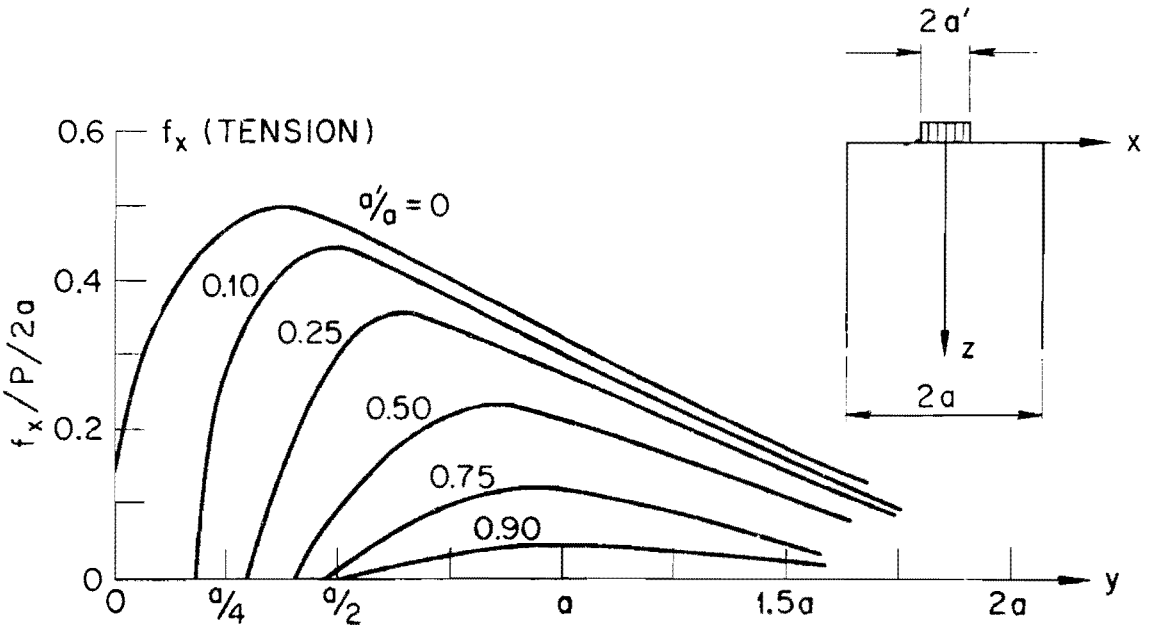

Fig. 1.5 Bursting stresses for various loaded areas (Guyon) (from Ref. 7)

distribution resultant to be equal to zero. Therefore, tensile and compressive transverse stresses must occur within the lead-in zone. However, these equilibrium considerations are not sufficient for the determination of the transverse stress distribution. Various analytical approaches to the solution of the stress distribution in the anchorage zone were discussed in detail in the first report in this series [1].

In actual anchorage practice, the load acts over a finite area with a reasonably large radius. For this case the classical elasticity analysis indicates that the stresses are relatively small. These stresses are plotted for a constant load P in Fig. 1.4 for various values of a'/a, where 2a denotes the section breadth and $2a'$ denotes the anchor breadth. Standard design practice in many countries has been to provide massive reinforcement for the total resultant tensile force obtained by integrating the area under curves such as those shown in Figs. 1.5 and 1.6. Experience gained from anchorage zone cracking problems with the Texas bridge at Corpus Christi [3], in which the anchorage zones were reinforced based on a similar set of experimentally derived bursting curves [8] indicated that design based solely upon such consideration of bursting stresses may be unconservative.

1.2.1.2 Spalling Stress. The spalling tensile stresses are maximum at the loaded surface and decrease rapidly away from the surface (see Fig. 1.2). The total spalling tensile force is thus relatively small. In contrast to the attention paid to bursting stresses, the spalling stresses have sometimes been neglected or dismissed because they are so localized. However, the peak spalling stress can be very high, indeed much higher in almost every practical anchorage application examined by the authors than the bursting stresses. This takes on great significance since in the currently reported experimental program cracking occurred along the tendon path with calculated bursting stresses far below the tensile

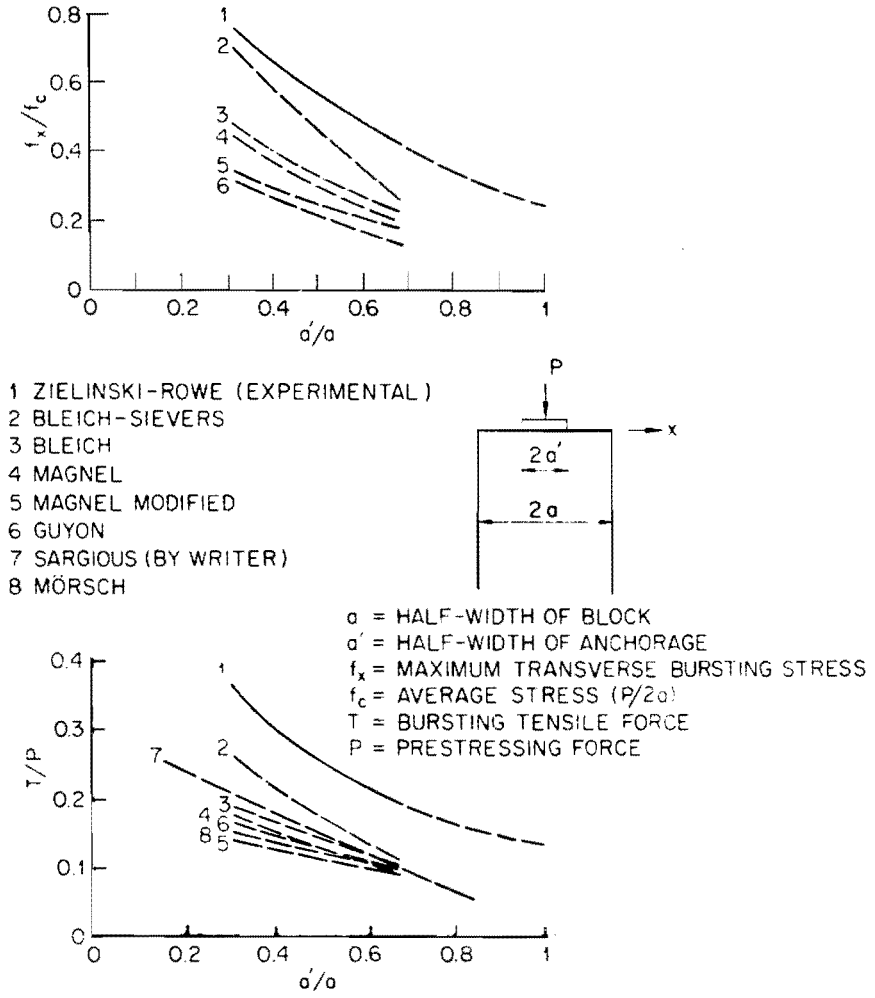

Fig. 1.6 Maximum bursting stress and tensile force (from Ref. 7)

strength of the concrete. Like bursting stresses, the spalling stress distribution is greatly affected by the geometric variables such as eccentricity, inclination, and proportions of the section. Most of the previous research on post-tensioned anchorage zones has been limited to analysis for straight tendons and has been interpreted in the context of the role of the bursting stresses. The advent of comprehensive finite element programs in the last decade allowed more realistic modeling for specimens with complex geometries. The results of these analyses reported in Refs. 1 and 2 indicate a key role of spalling stresses in crack formation.

1.2.1.3 Bearing Stress. The maximum compressive stress developed by a post-tensioning system occurs beneath the anchor. In the case of a flat plate, or bearing-type anchor, the average bearing stress is equal to the post-tensioning load divided by the net area of the anchor defined as the projected plate area minus the tendon duct area. Current design specifications in the United States, while specifying the need to examine bursting and spalling stresses, usually phrase their strictest recommendations in terms of allowable bearing stress. Most European specifications permit significantly higher allowable bearing stresses in post-tensioned design [9]. Whether this apparent over-conservatism in the American codes is justified has been a question much pondered but under-researched.

1.2.1.4 Additional Considerations. In addition to the geometric effects such as inclination, eccentricity, width, and bearing area, the effects of friction and normal forces along the tendon duct for curved tendons (see Fig. 1.7), the effect of anchor hardware geometry (see Fig. 1.8) and other externally applied loads such as lateral post-tensioning must all be considered to fully grasp the anchorage zone stress state.

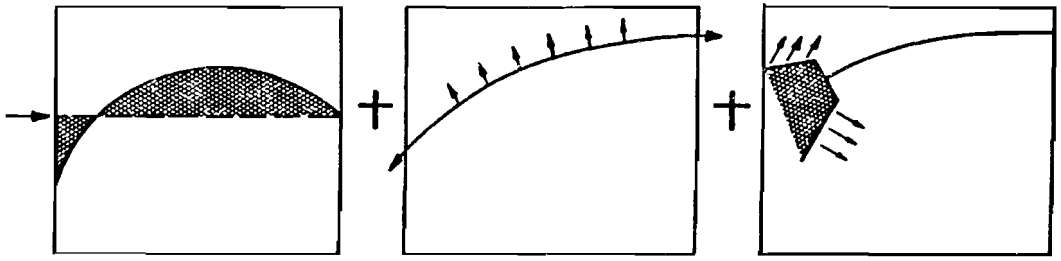

Fig. 1.7a Combination of end zone, radial, and inclined wedge effects

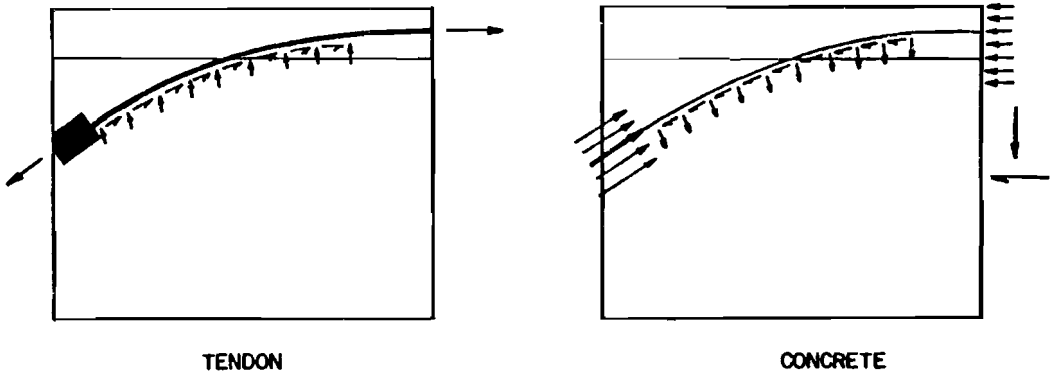

Fig. 1.7b Forces due to tendon curvature

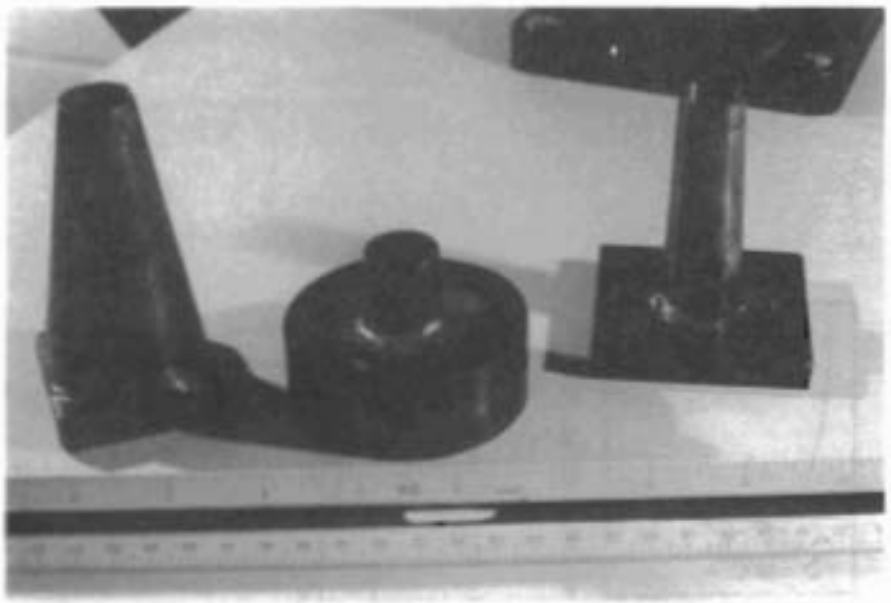

Cone Bell Plate

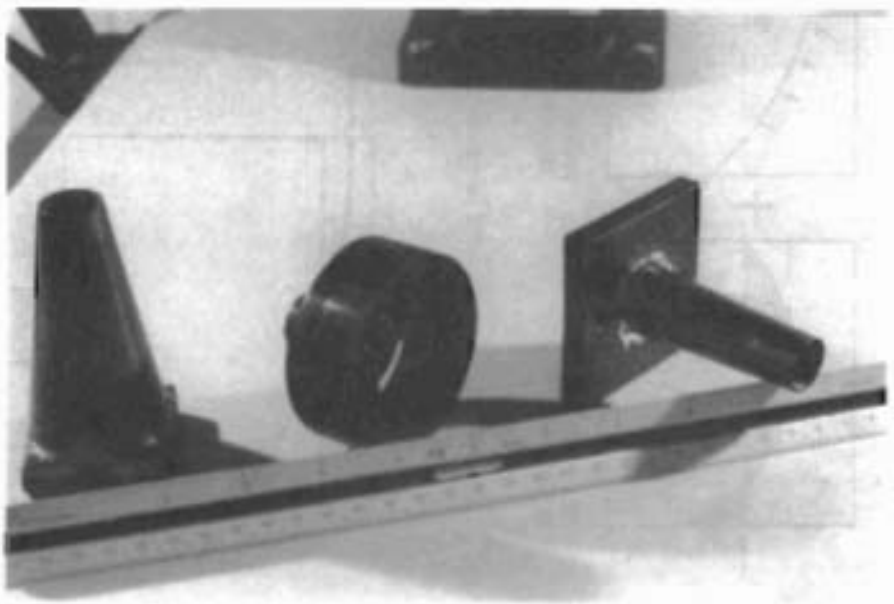

Fig. 1.8 Models of typical anchors used in post-tensioned construction

1.3 Overview of the Project

1.3.1 Objectives. The overall research program was broken into six interactive phases which constitute its specific objectives. These were:

(1) To document the state-of-the-art based on an extensive literature study of all analytical, experimental, and design-related papers and reports concerning anchorage zone stresses for post-tensioned applications.

The results of this survey were presented in detail in the first report [1].

(2) To survey the wide range of post-tensioning anchorage systems currently available in the United States and to make a classification according to general anchorage principles, sizes, and shapes.

Figure 1.8 shows the three distinct types of anchorages in use. These are the bearing or plate-type anchor, the cone or wedge anchor, and a "bell" shaped anchor. There are also three basic schemes used in making up the tendon. These use either 250 or 270 ksi 7 wire strand tendons where the load is locked off using conical chucks, 240 ksi wire where the load is locked off by "button-heading" the ends of the wire, or 160-170 ksi bars, smooth or deformed. The latter uses a heavy duty nut which conveniently screws down once the post-tensioning load has been applied. Bar type tendons cannot be used where a sharp curvature is required and wire type tendons usually require specialized anchorage procedures in the field. For these reasons the 7 wire strand tendons have been widely used in post-tensioned applications. While theoretically the anchorage zone cannot detect whether it is being loaded by strand, wire, or bar, the overall performance of anchorage in regions where significant curvature of the tendon is required has shown that cracking can occur at locations well removed from the immediate anchorage area [2]. This effect occurs primarily for multiple strand tendons, but can occur for single strand tendons as well, and is discussed in this report.

(3) To survey present and projected tendon path and anchorage zone characteristics in post-tensioned bridge applications.

A detailed examination of available bridge plans for several segmental projects both in the United States and Europe was reported on in Ref. 1. In many cases tendons are curved, inclined at anchors, and have significant eccentricity. These characteristics and their effects on the anchorage zone are illustrated in Fig. 1.7. There is a current trend to anchor out of the web for speed of construction. This technique uses side "blisters" in the interior of the box section to anchor the tendon. Aside from moving the anchorage away from the congestion at the end of the web section, this method often does not eliminate the above factors and in fact may give rise to an additional out-of-plane curvature effect.

(4) To study systematically by both analytical and experimental procedures, the development of critical tensile stresses in the anchorage zone for typical applications using representative anchorage systems.

In essence this was the core of the project. In this phase the principal variables, inclination, cover (width), eccentricity, bearing areas, and anchorage type were examined using both accurate 1/4-scale models and full-scale prototype specimens in the laboratory, as reported in the second report of this series [2]. A parallel effort was initiated to predict stress distributions in the physical specimens through the use of two- or three-dimensional static, linear elastic finite element programs. As primary emphasis was placed on developing a behavioral mode for first cracking, the linear elastic assumption proved to be sufficiently accurate. The development and calibration of the analytical programs are detailed in the first report of this series [1].

(5) To evaluate the efficiency of various active and passive reinforcement in anchorage zones, including spirals, conventional reinforcing bars, and lateral prestressing.

This objective was an outgrowth of the experimental program but dealt with crack control rather than the behavioral mechanism by which the crack was initiated. If the cracking load could be altered and the ultimate load enhanced by the addition of reinforcement, then major design interest focuses on the most efficient scheme for placement of this reinforcement. Placement was the primary question concerning passive reinforcement. With lateral prestressing, or active reinforcement, a powerful new option was opened. This was due to the fact that the stress field in the anchorage zone could be significantly altered by the addition of a transverse compressive force. Experimental results were reported in the previous report of this series [2]. Detailed design recommendations are given herein.

(6) To develop recommendations for specific design criteria for post-tensioned anchorage zone tensile stresses.

Based upon experimental and analytic data these recommendations can be broken down into two categories:

(a) If the structure is to be located in a highly corrosive environment where not even minor cracking can be tolerated, what is the maximum permissible stressing load, given the geometry of the anchorage zone?

(b) Given rigid geometric conditions and required load, what is an "acceptable" crack and how can this be controlled through an active or passive reinforcing scheme?

In either case the structure must be capable of performing satisfactorily under service load conditions and with an adequate factor of safety under failure conditions. The design recommendations and examples based on this investigation are contained in this report.

CHAPTER 2

ANCHORAGE ZONE BEHAVIOR DESIGN IMPLICATIONS

2.1 Introduction

2.1.1 General. In the preceding report in this series [2], detailed experimental data and photos were presented for both model and prototype specimens. Comparisons were provided between the analytical model [1] and the physical tests, and similitude relationships between model and prototype were developed. In this chapter, the overall trends obtained experimentally will be summarized, trends will be extrapolated using the analytical program PUZGAP and design implications will be indicated.

An extensive comparison was made of experimental data and the finite element analysis results. A semi-empirical calibration procedure provided a method by which the cracking load could be predicted with reasonable accuracy from the results of an analytical analysis using the three-dimensional finite element program (PUZGAP). The development of this semi-empirical method is presented in Sec. 2.2, while the actual calculations are illustrated in Sec. 2.3. Using these procedures, cracking loads for the major geometric variables were calculated and compared to the experimental results in Secs. 2.4 through 2.7. The solid line on each figure in those sections represents the finite element predicted cracking load. Analytical results were extrapolated to include regions beyond the range of the experimental data to establish design trends. Sections 2.4 through 2.7 present the observed normalized load trends causing initiation of the tendon path cracks for the major geometric variables: cover, inclination, bearing area, and eccentricity.

Since the test specimens used to explore those effects contained no supplementary anchorage zone reinforcement, ultimate loads for most cases occurred at loads only nominally above the load to cause cracking. Thus, no ultimate load conclusions should be drawn from these tests. Since both the cracking and ultimate load can be raised significantly through the use of supplementary anchorage zone reinforcement, the effects of such reinforcement are dealt with in Sec. 2.8. Major emphasis is placed on the development of simplified multipliers which can be applied to the cracking load of the specimen without supplementary reinforcement to predict the expected cracking and ultimate loads for the same section with supplemental reinforcement. To complete the generalization, the cracking trends presented in Secs. 2.4 through 2.7 (for unreinforced sections) are reduced in Chapter 3 to a design expression through a regression analysis of the experimental data.

2.1.2 Methods of Comparing Test Results. The cracking behavior of the anchorage zone is very much a function of the tensile capacity of the concrete. Two measures of this capacity are the indirect tensile strength as measured by the split cylinder test and the computed tensile strength based on measured compressive strength, which is usually expressed as $\times\sqrt{f'_c}$. Since the split cylinder strength proved to be the most accurate normalizer when comparing model and prototype performance, it will be used in developing the mathematical model and for comparison with test results. On the other hand, for design applications and regulations most practicing engineers would rather deal with a function of the compressive strength, since this is the general control specimen used. There is a large amount of data relating f'_c and f_{sp} so that a suitable conversion factor can be derived. This will be presented in Chapter 3.

2.2 General Concepts of Thin Web Anchorage Zone Failure

2.2.1 Anchorage Zone Failure. In spite of the many variables investigated in the experimental program reported in detail in Ref. 2, the post-tensioned anchors in thin web girders tended to exhibit a generally consistent behavior in sequence of failure. The actual loads at which various stages were reached were affected by variables such as inclination, eccentricity, and supplementary reinforcement but the sequence was generally the same.

The failure sequence for a plate anchor specimen with no supplementary reinforcement is shown in photographs in Fig. 2.1 and summarized in Fig. 2.2. The basic stages are:

(a) Initial cracking along the tendon path, beginning at a distance about the bearing plate width in front of the anchor

(b) With increased load, the crack extends both towards the loaded face and away from it

(c) Formation of diagonal cracks on the end face, emanating from the four corners of the bearing plate

(d) Propagation of the diagonal cracks on the side faces

(e) A generally sudden explosive-type failure, with complete destruction of the side face and a noticeable formation of a cone of crushed concrete ahead of the anchor.

In specimens with no supplementary reinforcement, stages (d) and (e) are often almost simultaneous. The main effect of the supplementary anchorage zone reinforcement is to raise the initial cracking loads and to provide a significant amount of reserve strength between cracking and ultimate.

2.2.2 The Bearing Stress Role. As documented in the tests reported in Ref. 2, the cracking load is fairly insensitive to appreciable changes in the bearing area. The two full-scale tests, FS1A and FS1B, had identical cracking loads and had differences in normalized cracking loads of only 12 percent, despite a 73 percent difference in anchorage bearing area. Furthermore, these tests were

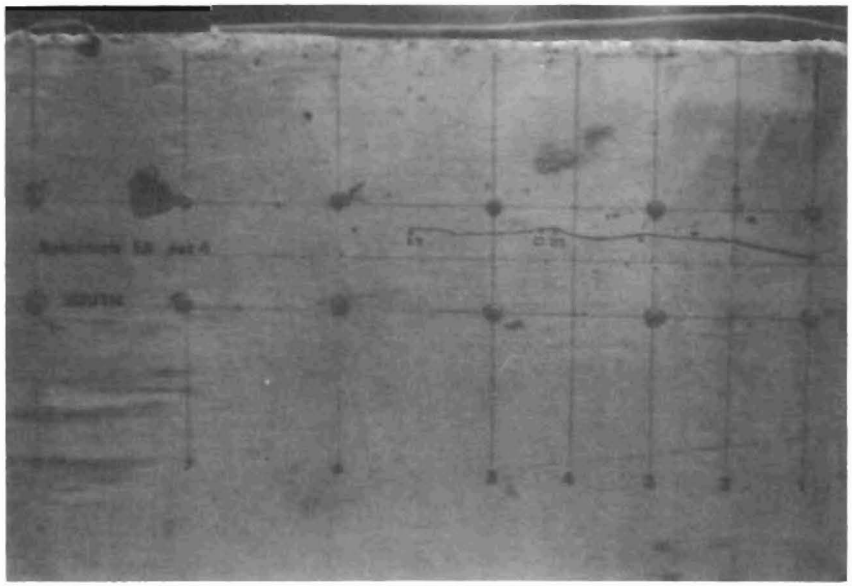

(a) Tendon path crack

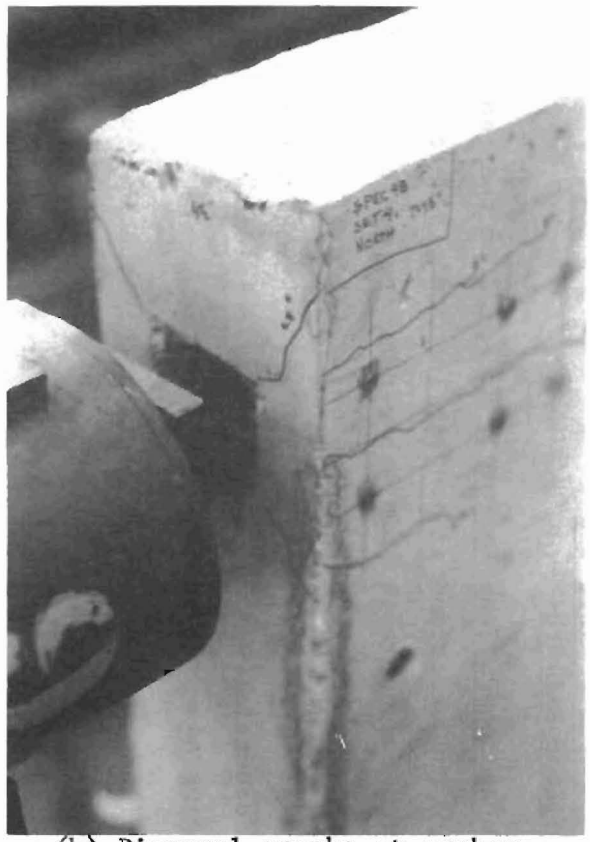

(b) Diagonal cracks at anchor

Fig. 2.1 Failure sequence--plate anchors

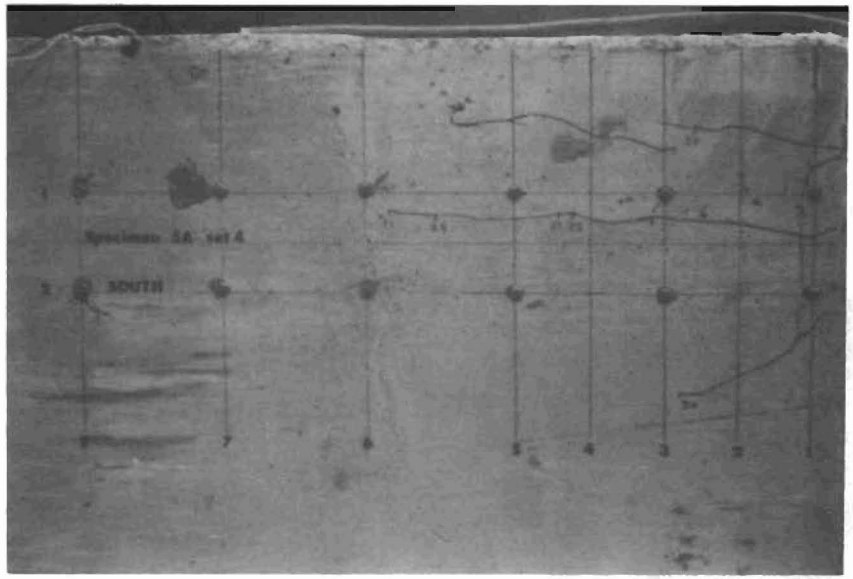

(c) Diagonal cracks propagate

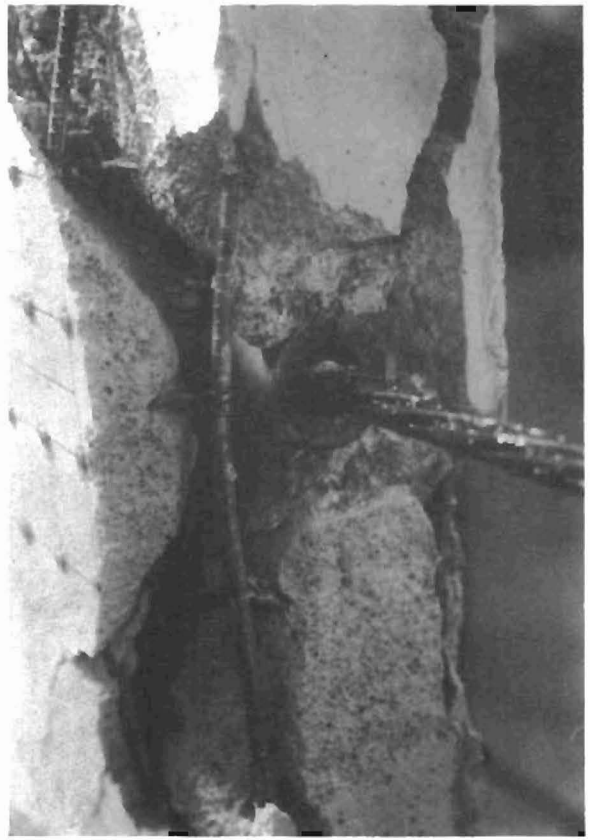

(d) Ultimate failure

Fig. 2.1 (Continued)

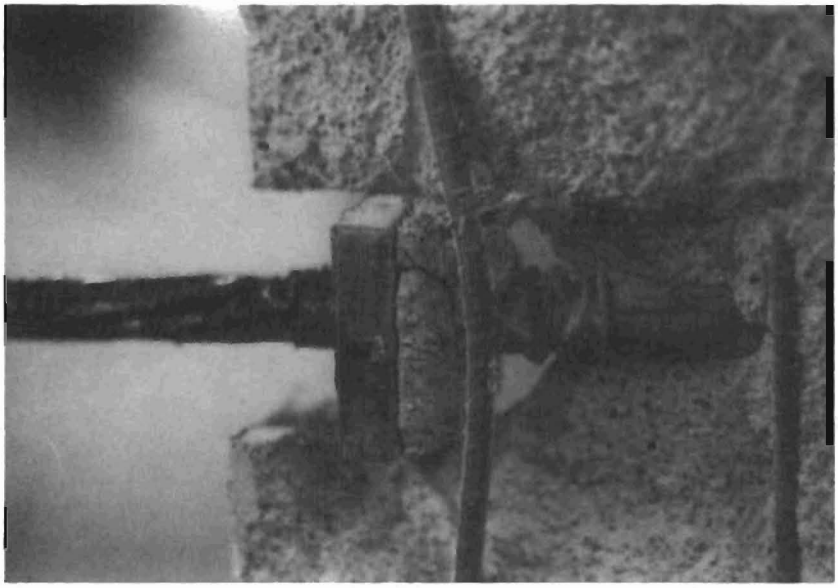

(e) Cone of crushed concrete

Fig. 2.1 (Continued)

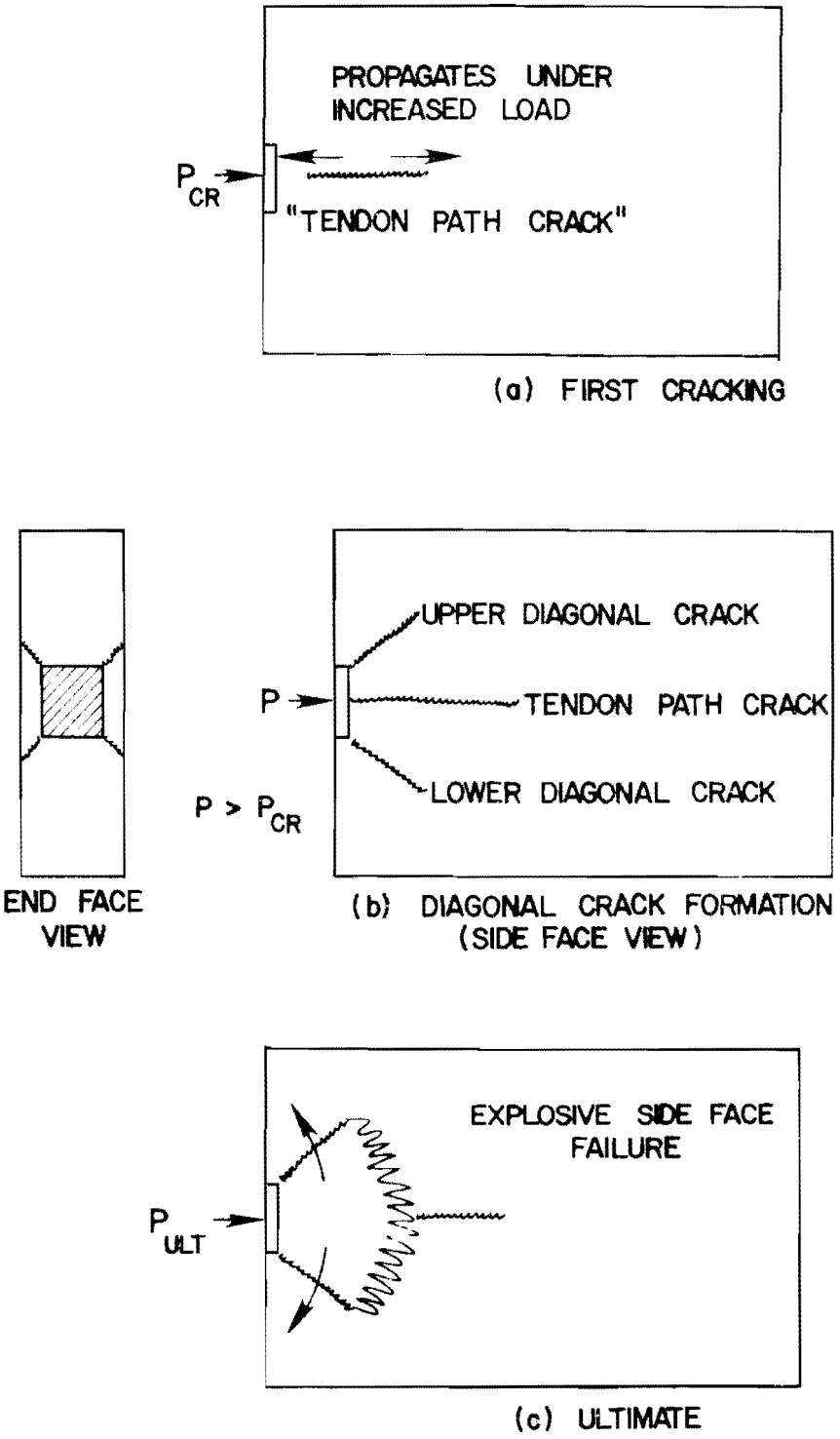

Fig. 2.2 Failure sequence for plate anchors

conducted on straight tendon, concentrically loaded specimens. Cracking loads for inclined and eccentric tendons with no supplementary anchorage reinforcement are substantially less than those for a straight concentric tendon, given identical anchors. While bearing stress should be a factor in a design equation, results indicate it should be a minor one. The factor $2a'/t$, which indirectly reflects cover as a function of the anchor width ($2a'$) and the web thickness (t) is considerably more important than the factor $(2a'/t)^2$ which reflects the bearing area. Present specifications which base anchorage design principally on bearing stress are not only overconservative for straight tendon, concentric load applications, but inapplicable and generally unconservative for inclined and eccentric tendon situations. A more accurate general indicator of cracking trends is thus needed.

2.2.3 The Bursting Stress Role. Since most previous research [1] focused on a bursting stress design criterion it is important to have a clear understanding of the bursting stress variation for all geometric variables studied. One measure of this is the peak tensile bursting stress developed for a given load. As the analytically computed bursting and spalling stresses (strains) were in general agreement with the physical test strainmeter data it will simplify comparisons to use the 3D FEM analytical solution results. Reference will be made to specific measured data where important trends were observed. Table 2.1 provides a summary of all three-dimensional finite element studies pertinent to the physical test program. Data are provided for a 1 kip load. Since the solution is linear, comparable data for any tendon load can be obtained by multiplication of the indicated results by the load. Values corresponding to specific test specimens at their measured cracking loads are presented later in Sec. 2.3.

For concentric straight tendon specimens with varying thicknesses, column σ_{xb} in Table 2.1 indicates that the maximum

TABLE 2.1

3D-FEM SUMMARY

	Geometric Variables					Maximum values at 1 kip load				
	t (in.)	2a (in.)	e (in.)	2a' (in.)	θ (degrees)	Spalling Strain (με) ε_{xs}	Spalling Stress (psi) σ_{xs}	Bursting Strain (με) ε_{xb}	Bursting Stress (psi) σ_{xb}	
Eccentricity	3	20	0	2	0	5.04	19.2	2.88	6.48	*
	3	20	4	2	0	13.72	51.2	2.8	5.76	*
	3	20	6	2	0	16.48	123.0	2.8	4.72	*
	3	20	8	2	0	22.9	171.0	2.0	3.36	*
Bearing Stress	3	20	0	3	0	3.92	19.2	2.48	5.84	*
	3	20	0	2.625	0	4.24	16.48	2.8	6.0	*
	3	20	0	2.125	0	4.88	18.76	2.56	5.68	*
	3	20	0	2	0	5.04	19.2	2.72	6.1	*
	3	20	0	1.5	0	5.84	22.0	2.48	5.3	*
Width	1	20	0	1	0	10.4	39.6	8.0	20.6	*
	2	20	0	2	0	7.6	28.8	4.0	10.1	*
	3	20	0	2	0	5.04	19.2	2.88	6.48	*
	4	20	0	2	0	4.4	18.4	2.0	4.64	*
	5	20	0	2	0	3.8	13.08	1.6	3.68	*
	6	20	0	2	0	3.12	9.68	1.28	3.2	*

TABLE 2.1 (Continued)

	Geometric Variables					Maximum values at 1 kip load				
						Spalling		Bursting		
	t (in.)	2a (in.)	e (in.)	2a' (in.)	θ (degrees)	Strain (με) ε_{xs}	Stress (psi) σ_{xs}	Strain (με) ε_{xb}	Stress (psi) σ_{xb}	
Inclination	3	20.5	0	2.625	0	8.04	34.0	5.02@	13.9@	**
	3	20.5	0	2.625	15	40.32	164.0	3.76@	11.5@	**
	3	20.5	0	2.625	30	57.76	229.0	2.87@	9.12@	**
								6.72#	23.9#	**
	3	20.5	0	2.625	45	80.8	325.0	3.16@	9.52@	**
								8.72#	32.3#	**
LPT	3	20.5	0	2.625	30	24.1	94.4	1.68@	2.99@	**,I
								5.52#	19.4#	**,I
	3	20.5	0	2.625	30	50.24	197.6	-0.856@	-7.04@	**,II
								4.32#	13.6#	**,II

Notes:

* Tendon duct not included in FEM mesh.
** Duct, friction and normal (radial) forces included in mesh.
I 0.3 kip LPT at 0.146a from loaded face.
II 0.3 kip LPT at 0.780a from loaded face.
@ Peak bursting stress (strain) at 4a' from loaded face along tendon duct.
# Peak transverse stress (strain) at point of maximum tendon curvature (not a conventional bursting stress).

bursting stress decreases exponentially with increasing thickness. This is expected, and the trend is illustrated in Fig. 2.3. The solid line in this figure represents the predicted peak bursting stress at the model tendon design load of 25 kips (400 kips prototype) (0.8 f_{pu}). Even at the higher loads which actually caused cracking in the test specimens the measured peak stresses are insufficient to explain why cracking occurred, since the tensile strength of the concrete (which is shown on Fig. 2.3) is considerably in excess of the highest bursting stress expected or measured. For example, in the first line of the table with t = 3 in., e = 0, θ = 0, Table 2.1 indicates the calculated peak bursting stress at a 1 kip load to be 6.48 psi. The cracking load for the corresponding test specimen (M2-2) was 34 kips. Thus, at cracking, the calculated peak bursting stress is 6.48 (34) = 220 psi, as plotted on the dashed line of Fig. 2.3. This value is well below the measured tensile capacity of the concrete for that particular specimen (f_{sp} = 627 psi). The experimentally measured values showed peak stresses at cracking based on measured strains to be approximately 30 to 50 percent higher than those predicted by the computer analysis, as shown in Fig. 2.3. These values are plotted above the 3D FEM predicted values and again clearly fall well below the measured tensile strength of the concrete. The observed bursting strains at cracking were generally well below the 150 microstrain recommended by Rüsch [10] as the lowest limiting strain which would cause cracking.

The most important evidence that the bursting stress is not the proper criteria for anchorage zone cracking behavior comes from eccentric straight tendon tests. The survey of design methods outlined in Ref. 1 showed that in the widely accepted symmetrical prism analogy of Guyon [7], to treat the case of an eccentric tendon, the distance from the eccentric load centerline to the nearest face (denoted a_1) is used in place of the value a (half height of the section). For increasingly eccentric loads, the value a_1 thus

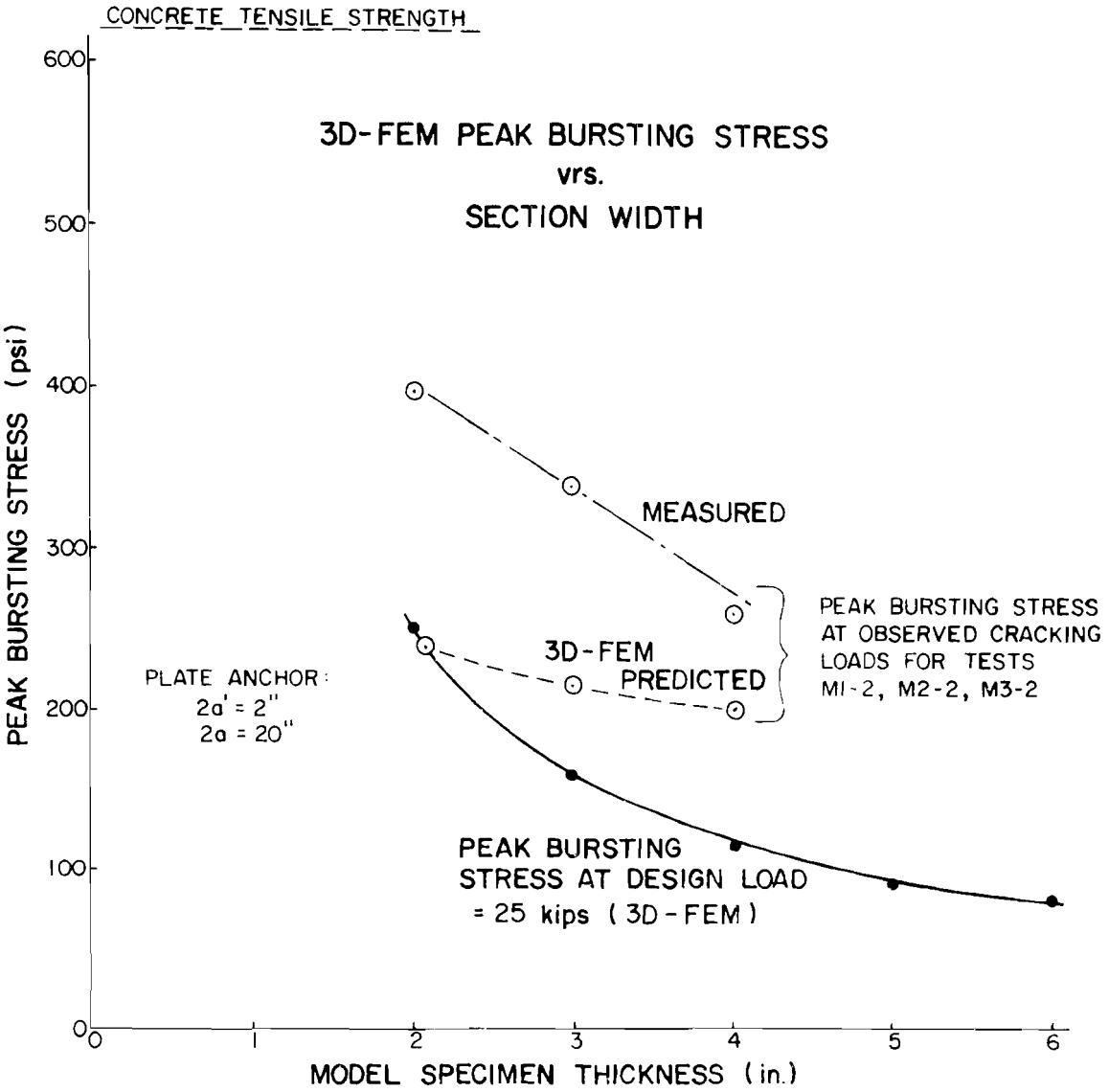

Fig. 2.3 Peak bursting stress as a function of section thickness

becomes smaller and smaller. For a given anchor plate the depth of the plate $2a'$ remains constant. Thus for eccentric tendons the value of $2a'/2a_1$ becomes larger. Since the value $2a_1$ essentially represents an effective section height 2a for the symmetrical prism, it can be seen from Fig. 1.5 that for increasing eccentricities the value of a'/a (or a'/a_1 for the eccentric section) approaches 1 and the peak bursting stress decreases. The 3D FEM analysis results and the experimental results shown in Fig. 2.4 both indicate decreased bursting strains with increased eccentricity.

The test results, however, showed that cracking load was appreciably reduced with increasing eccentricity. Thus, there is a direct conflict between the experimental results and the bursting stress criteria theory. This is an extremely important statement!! It means that if design of reinforcement for the anchorage zone is based upon bursting stresses using the Guyon symmetrical prism analogy or the FEM analysis, less supplementary reinforcement would be required for loads with higher eccentricities. The experimental results clearly indicate the cracking load is reduced with increased eccentricity and show that there is a serious error in this logic. The decrease in bursting stress trend with increased eccentricity predicted by Guyon appears to be qualitatively valid when compared with finite element data (Table 2.1) and experimental data obtained in this study. It is the correlation of calculated or measured bursting stress with experimental cracking loads which does not agree.

For inclined tendon specimens, Table 2.1 shows that the computed bursting stress also decreases with increases in the angle of inclination. Figure 2.5 shows clear experimental verification that the measured bursting stress (strain) decreased with increases in the tendon inclination. This directly contradicts the experimentally observed cracking trend which showed that cracking loads decrease with increasing inclination.

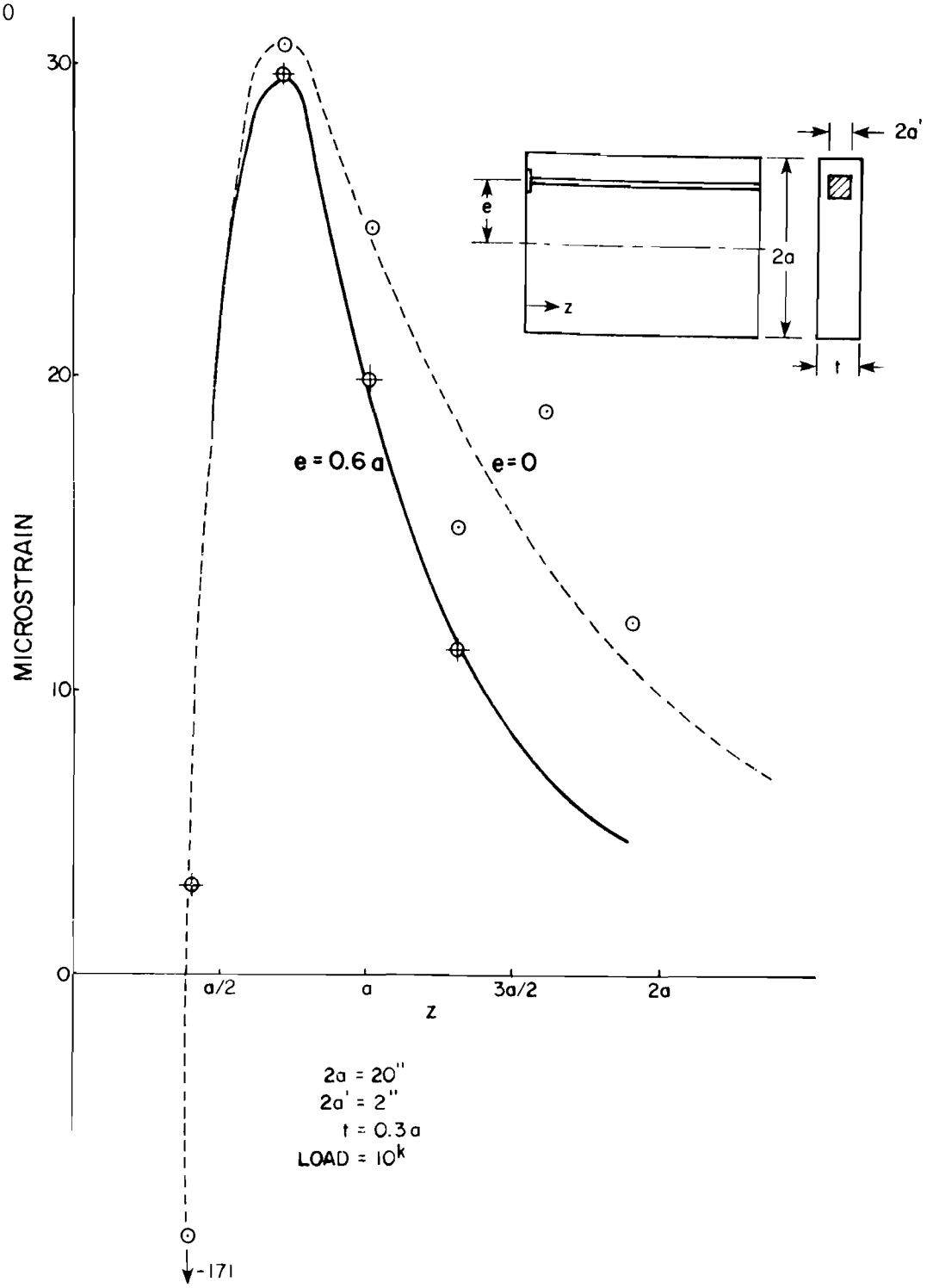

Fig. 2.4 Experimental bursting strain distribution--eccentricity series

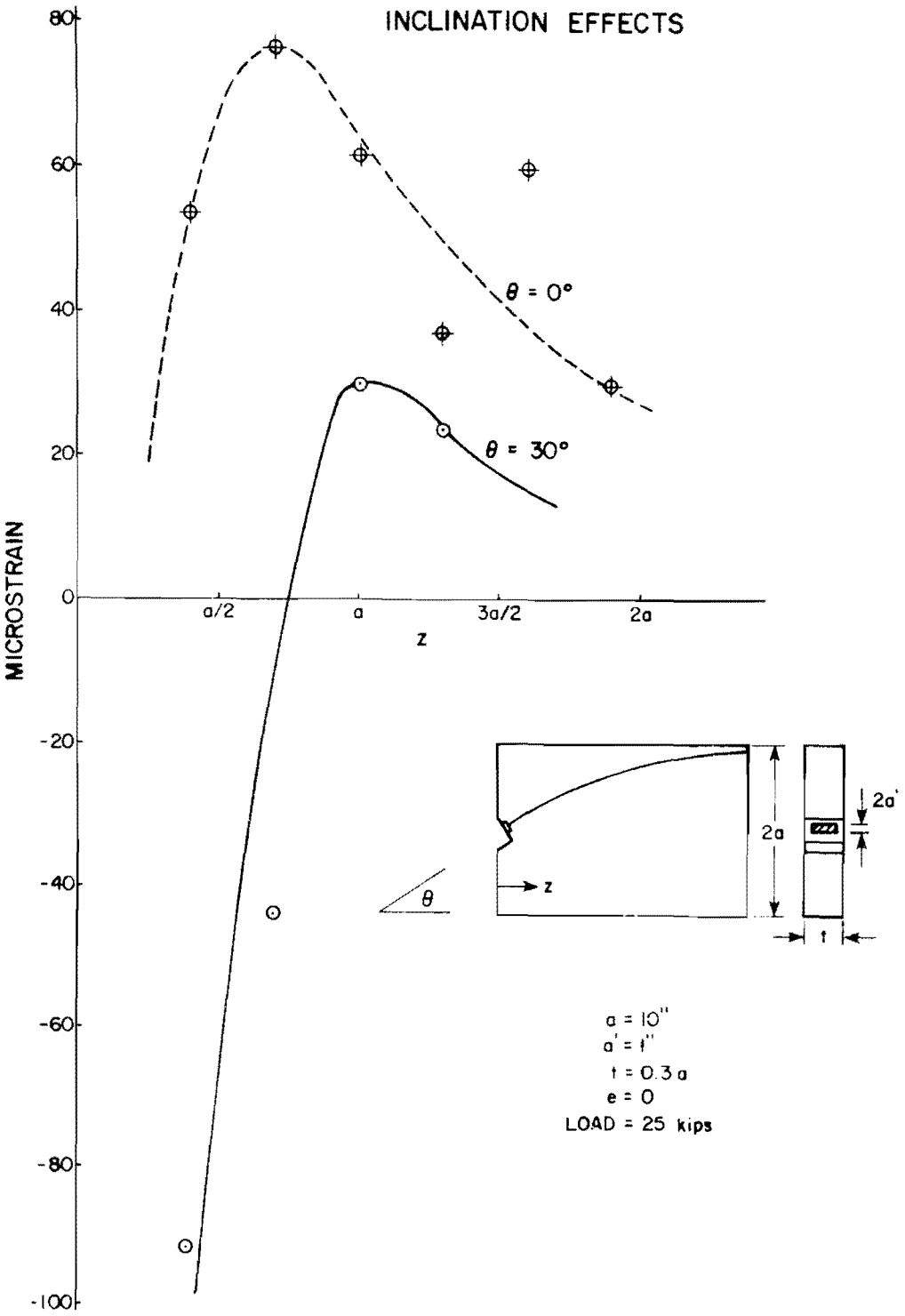

Fig. 2.5 Experimental bursting strain distribution--inclination series

Although not a conventional bursting stress from the elasticity definition given in Chapter 1, Table 2.1 shows that for highly inclined multiple strand tendons (note 30, 45 degree values specifically) the transverse tensile stress along the tendon path at points near the region of maximum curvature begins to increase. The two values shown in the table (labeled # in Table 2.1) represent the 3D FEM predicted transverse stress at the point of maximum curvature developed by applying appropriate friction and normal forces along the tendon duct. The true peak conventional "bursting" stress occurs at approximately a distance of $4a'$ from the loaded face. These values are marked with the symbol @ in Table 2.1 and show the general decrease with increased inclination. The bursting stress in the anchor region marked with @ is insufficient to cause cracking at the loads observed experimentally.

For example specimen FS2B (30 degree tendon) cracked at a load of 330 kips. Using the results shown in Table 2.1 and scaling the prototype load to a quarter-scale load by $(1/4)^2 = 1/16$ would indicate a peak bursting stress of $(330)(9.12)/16 = 187$ psi, considerably less than the measured 455 psi indirect tensile strength of the concrete used in that specimen. On the other hand, the transverse peak stress at the point of maximum curvature, $330\ (23.9)/16 = 490$ psi would probably cause cracking, and, in fact, the crack did initiate from this location in specimen FS2B. While the conventional bursting stress clearly is an inappropriate indicator of the cracking behavior in the anchorage zone, the special case of the highly inclined curved multiple strand tendon poses an additional mechanism for crack formation. For this case the calculated transverse tensile stress at the point of maximum curvature does agree qualitatively with experimentally observed cracking data. Design of reinforcement to resist the transverse tensile stress in the region of maximum curvature is, therefore, a requisite when dealing with curved tendons. This is discussed in Section 2.2.5.

Conventional bursting stress analysis is not a proper criterion for control of anchorage zone cracking.

2.2.4 Spalling Stress Role. When the major contradiction outlined in the previous section was noted between the predicted bursting stress and the actual eccentric tendon cracking load trends, a detailed examination was undertaken of the state of stress in the anchorage zone using the three-dimensional finite element program. Somewhat unexpectedly it was found that the computed tensile spalling stress along the end face increased rapidly with increasing eccentricity. The maximum value calculated was located near the lower edge of the plate anchor. While no evidence was seen in any test specimens of external cracks due to spalling stresses, the variation in magnitude of the computed spalling stress also correlated with the observed variations in the inclined, bearing stress, and cover series specimens.

Studies of the role of the spalling stresses in anchorage zone behavior led to the formulation of a failure hypothesis outlined in Sec. 2.2.5. Since the spalling stress (strain) seems to be the best indicator of tendon path crack initiation, even though "spalling cracks" do not occur, a method of predicting first cracking through the use of analytically derived spalling stresses (strains) was developed, as outlined in Sec. 2.2.6.

2.2.5 Anchorage Failure Mechanism. Detailed comparison of analytical and experimental data for a wide variety of variables indicated that several key phases were common in the overall loading behavior of plate (bearing) type anchorages. These phases suggested a general failure mechanism which could also be adapted to cone and bell anchors.

The key phases were:

(1) Appearance of the longitudinal tendon path crack, usually beginning at a distance approximately $2a'$ from the loaded face.

(2) Appearance of upper and lower diagonal cracks emanating from the corners of square anchors or of radial cracks from circular anchors.

(3) Ultimate failure consisting of an explosive side face blow out, usually occurring shortly after formation of the diagonal cracks.

(4) After failure a cone (pyramid) of crushed concrete was observed beneath the anchor plate with the telltale presence of powdered concrete along its edges indicative of a shear failure.

To further investigate the shear type failure noted in phase (4), a study was made of both the calculated spalling tensile stress (strain) and maximum shearing stress (strain) in the vicinity of the anchor plate edge. The shearing stress values offered no direct correlation which would explain the cracking behavior. The spalling stress values, however, followed a definite trend which indicates that the following sequence is the probable mechanism leading to anchorage zone failure for bearing plate anchors and with minor modifications for cone and bell type anchors:

(1) Due to large friction forces developed directly beneath the anchor plate, Poisson ratio type lateral expansion of the concrete in this vicinity is constrained.

(2) A complex, triaxial compressive stress state is thus set up which permits development of extremely high direct bearing stresses (up to $3f'_c$) beneath the plate (see Fig. 2.6a).

(3) The confining lateral forces at the edge of the plate are reduced by the presence of the spalling tensile stress (strain). As this reduction in lateral confining stress takes place the effect on the state of stress would be to increase the shearing stress, as can be seen from the increase in diameter of the Mohr's circle as illustrated in Fig. 2.6b.

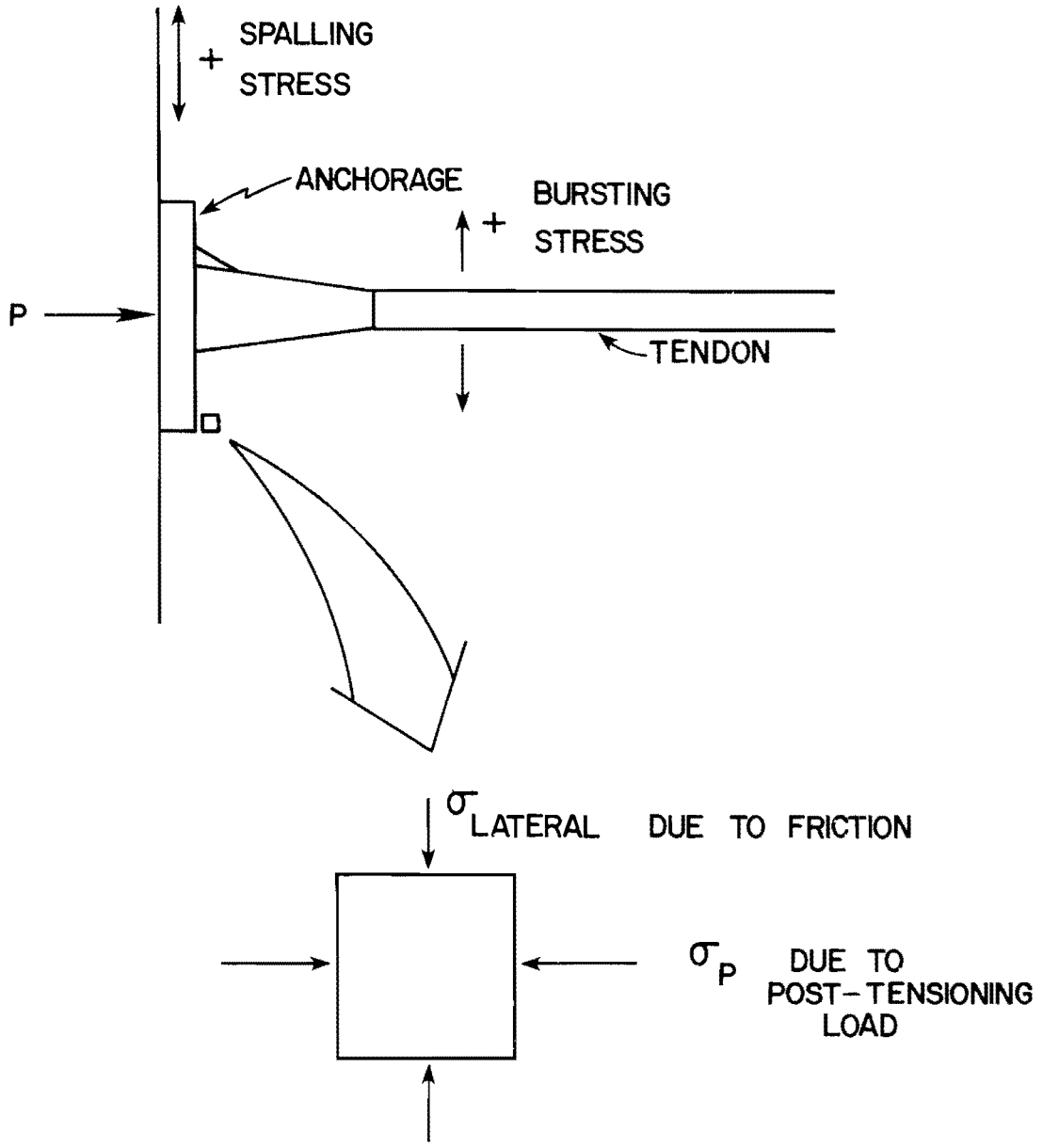

Fig. 2.6 Spalling initiated shear failure theory

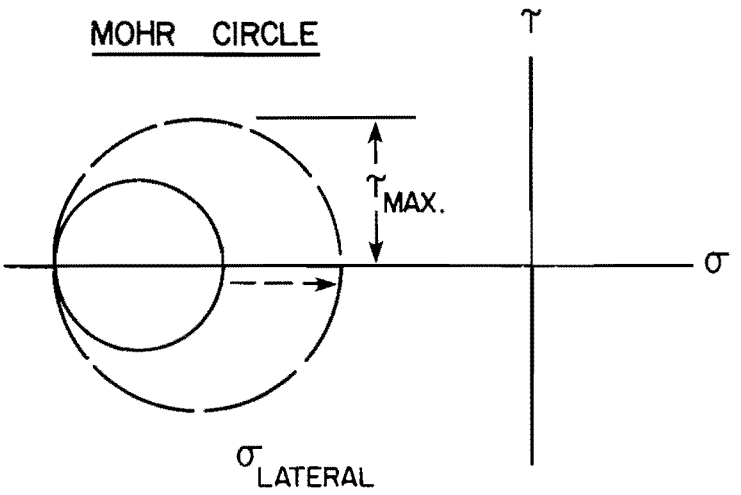

(b)

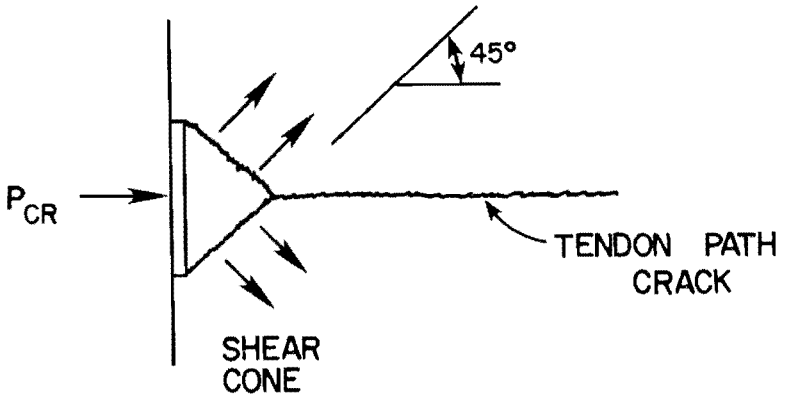

(c)

Fig. 2.6 (Continued)

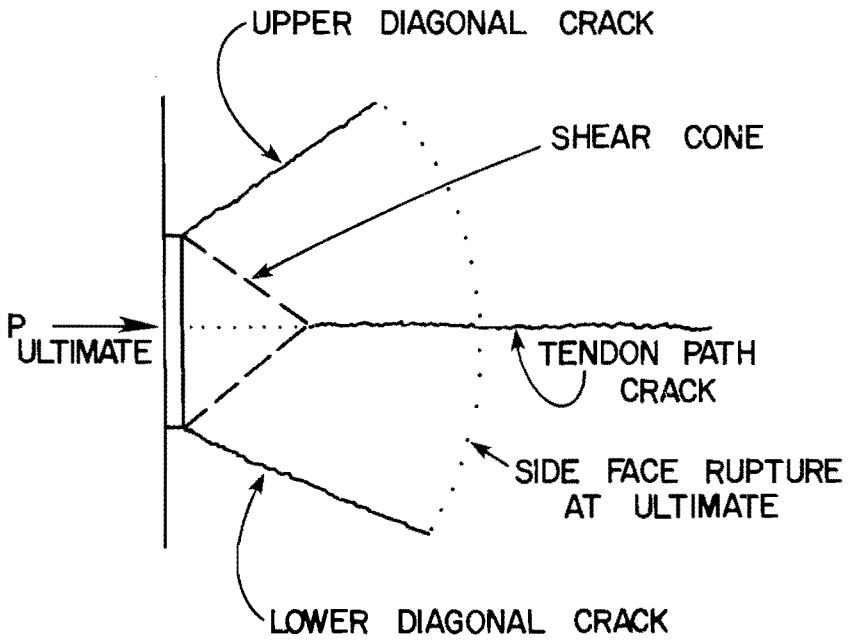

(d)

Fig. 2.6 (Continued)

(4) At some level of applied load the confining stress is sufficiently reduced (though still in compression) that an internal shear failure occurs along the plane of maximum shear stress.

(5) The maximum shearing stress plane occurs at an angle of 45° counterclockwise from the primary stress σ_p axis and thus propagates to form the 45° pyramidal "cone" seen for all plate-type anchors (see Figs. 2.1e and 2.6c).

(6) Simultaneous with the formation of the cone, a tendon path crack propagates from the tip of the cone, as shown in Fig. 2.6c.

(Phases 5 and 6 can be delayed by the presence of supplementary anchorage zone reinforcement. This delay can be substantial when spirals and lateral post-tensioning which enhance confinement are used.)

(7) The cone is forced into the anchorage zone, setting up large lateral forces which eventually produce the upper and lower diagonal cracks.

(8) Increases in load above that required for formation of diagonal cracks lead to ultimate explosive failure of the side faces, bounded by the upper and lower diagonal cracks (see Fig. 2.6d).

2.2.6 Prediction of First Cracking Based on Analytical Studies. A summary of the three-dimensional finite element analysis findings was presented in Table 2.1. Dimensions correspond to those of the quarter-scale specimens at a load of 1 kip. For full-scale comparison, dimensions should be multiplied by a scale factor S_ℓ of 4 and the stresses and strains shown would correspond to a load of S_ℓ^2 or 16 kips.

As pointed out in Sec. 2.2.4, the spalling stress-strain trends seem to be the best indirect indicator of crack initiation. As a means of comparing the maximum tensile spalling strain, all

values in Table 2.1 which corresponded to physical specimens were multiplied by the respective measured cracking loads to obtain the predicted peak spalling strain at the plate edge. These values are presented in Table 2.2.

2.2.6.1 Straight Tendons. For straight tendon specimens the mean tensile spalling strain at cracking was 190 $\mu\epsilon$ (microstrain) with a standard deviation of 18 $\mu\epsilon$. A value one standard deviation below the mean, 172 $\mu\epsilon$, was assumed to be a limiting spalling strain at internal crack initiation. This value, incidentally, compares well with Rüsch's value of 150 for the lower tensile strain capacity for concrete, although, as explained earlier, the formation of the tendon path crack is a complex mechanism and not a simple propagation of a spalling crack or a "bursting" crack. Any 3D FEM analysis results for straight tendons with calculated spalling strains greater than 172 $\mu\epsilon$ can be viewed as a trigger threshold for formation of the tendon path crack in specimens without supplementary anchorage zone reinforcement.

2.2.6.2 Inclined tendons. In modeling the anchorage zone for an inclined tendon it is usually necessary to provide a "block out" so that the anchorage can be positioned at the proper angle without altering the vertical end face which must mate with successive elements. The presence of the blockout introduces a right angle, or so-called re-entrant corner, in the geometry at a position close to the application point of the post-tensioning load. This gives rise to a stress concentration at this location of approximately 6 to 7, slightly less than that given by Peterson [11] for a loaded T-head. Rather than attempting to determine the precise effects on the spalling tensile strain of the change in inclination and the presence of the idealized perfect right angle, a different strain threshold for inclined tendons was assumed. The average value for inclined tendons in Table 2.2 was 1150 $\mu\epsilon$ (roughly 6 to 7 times that for straight tendons) with a standard deviation of 58 $\mu\epsilon$. The limiting value for crack initiation in the anchorage zone for

TABLE 2.2

3D-FEM PEAK SPALLING STRAIN AT FIRST CRACKING

Variable	$\varepsilon_{xs} \cdot P_{cr}$	$\frac{\varepsilon_{xs} \cdot P_{cr}}{f_{sp}}$	Corresponding Specimen ID
e = 0	172	0.274	M2-2
e = .3A	168	0.513	M7A-4
e = .6A	205	0.414	M1A-4
2a' = 0.875t	165	0.244	MR1A
2a' = 0.875t	207	0.317	MI1A
2a' = 0.875t	201	0.501	FS1B
2a' = 0.71t	209	0.309	MR1B
2a' = 0.71t	200	0.329	MI1B
t = 0.2a	183	0.292	M3-2
t = 0.3a	172	0.274	M2-2
t = 0.4a	210	0.334	M1-2
θ = 15	1109	2.08	FS2A
θ = 30	1191	2.61	FS5B
θ = 30 60^{k} LPT @ 0.15a	845	1.5	FS5B

(continued)

TABLE 2.2 (Continued)

Variable	$\epsilon_{xs} \cdot P_{cr}$	$\frac{\epsilon_{xs} \cdot P_{cr}}{f_{sp}}$	Corresponding Specimen ID
$\theta = 30$ 60^k LPT @0.78a	1444	2.56	FS5A

Straight Tendon Specimens:

$\overline{\epsilon_{xs} P_{cr}} = 190$

S.D. = 18

$\overline{\frac{\epsilon_{xs} P_{cr}}{f_{sp}}} = 0.345$

S.D. = 0.09

Inclined Tendon Specimens:

$\overline{\epsilon_{xs} P_{cr}} = 1150$

S.D. = 58

$\overline{\frac{\epsilon_{xs} \cdot P_{cr}}{f_{sp}}} = 2.34$

S.D. = 0.26

inclined tendons was thus set at 1092 $\mu\epsilon$. A rezone technique was necessary to refine the mesh in the vicinity of the anchor for accurate resolution of the above values. The transition between this value and the much smaller one for straight tendons needs further study to adequately treat the effect of very small inclinations.

2.2.6.3 Multistrand Effect in Curved Tendons. Cracking loads predicted from the use of the assumed critical spalling strains assume first cracking to occur in the anchorage zone via the mechanism discussed in Sec. 2.2.5. For the case of highly inclined, curved multiple strand tendons the cracking load may be significantly less due to failure initiating at the point of maximum tendon curvature. This independent failure mechanism should be checked in accordance with the theory presented in Sec. 2.2.7 and the reinforcement recommendations presented in Chapter 3.

2.2.7 Multistrand Side Face Failure Mechanism. For thin web post-tensioning applications where significant tendon curvatures are required and multiple strand tendons are used, a second mechanism may govern the failure of the section. Any time a loaded tendon follows a curved path, normal and friction forces will be set up as shown in Fig. 2.7. Equilibrium of forces in the vertical (x) direction yields:

$$P \sin \frac{d\theta}{2} + (P + dP) \sin \frac{d\theta}{2} - N = 0 \qquad (2.1)$$

$$2P \sin \frac{d\theta}{2} + dP \sin \frac{d\theta}{2} = N \qquad (2.2)$$

where N = summation of all normal components over ds. The normal force applied to the tendon duct per unit length is thus:

$$p = N/ds \qquad (2.3)$$

Also, from small angle theory

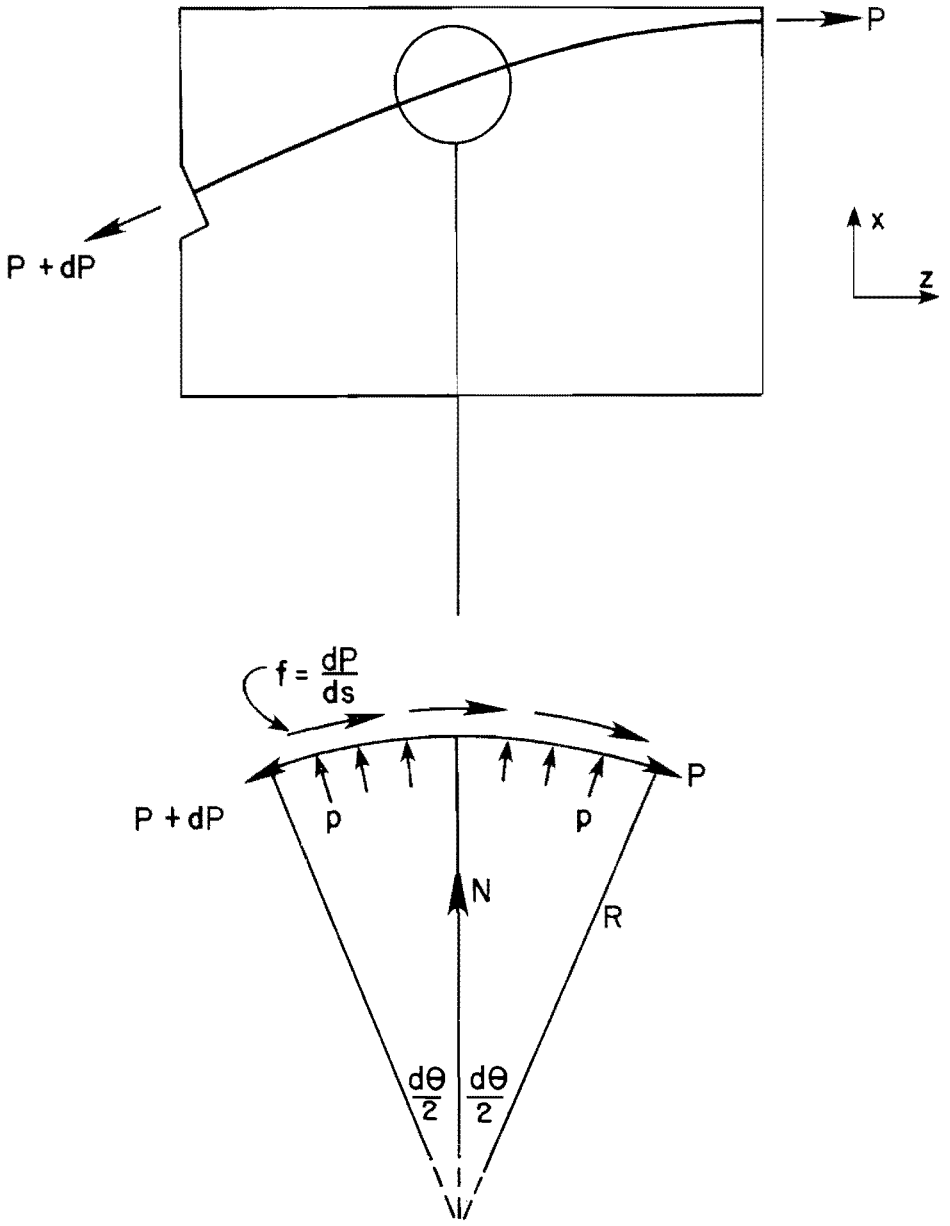

Fig. 2.7 Radial and friction forces due to tendon curvature

$$\sin \frac{d\theta}{2} = \text{ARC} \frac{d\theta}{2} \tag{2.4}$$

Substituting (2.4) into (2.2) yields

$$2P \frac{d\theta}{2} + dP \frac{d\theta}{2} = N \tag{2.5}$$

But $dP \frac{d\theta}{2} \sim 0$ thus

$$Pd\theta = N \tag{2.6}$$

Substituting (2.3) into (2.6) yields

$$p = P \frac{d\theta}{ds} = \frac{P}{R} \tag{2.7}$$

where P = post-tension load (kips)

R = radius of curvature at a given point (in.)

p = normal load on tendon duct per unit length (kips/in.)

From calculus

$$R = \frac{\left[1 + \left(\frac{dx}{dz}\right)^2\right]^{3/2}}{\left|\frac{d^2x}{dz^2}\right|} \tag{2.8}$$

Most curved tendon profiles can be described by the equation

$$X = Az^3 + Bz^2 + Cz + D \tag{2.9}$$

Substitution into (2.8) yields

$$R = \frac{[1 + (3Az^2 + 2Bz + C)^2]^{1.5}}{|6Az + 2B|} \tag{2.10}$$

If the value of R is relatively small, very large normal components of the post-tensioning force are set up which can cause tendon path cracking at loads below those which would initiate

cracking in the anchorage zone proper. This is more likely to occur when the anchorage zone is well-reinforced and the point of maximum curvature occurs well away from the anchorage and does not have supplementary reinforcement. Figure 2.8 illustrates this failure sequence which was observed in the full-scale tests, as shown in Fig. 2.9. An empirical design method to control this effect will be presented in Chapter 3.

2.3 Major Effects of Variables

In this section the measured cracking loads of the physical test specimens reported in Ref. 2 and the predicted cracking loads using the 3D FEM analysis with cracking criteria based on the empirically based spalling strain levels developed in the preceding section are discussed as functions of the major variables in the program. Use of the 3D FEM procedure allows a more general comparison of the effect of variables. As a means of nondimensionalizing the data presented in the following sections, the normalized cracking load P_{cr}/f_{sp} (which has units of square inches), is divided by the cross-sectional area of the web--2at.

2.3.1 Cover and Thickness Effects. For most specimens in the scale model and full-scale tests, the web thickness was a constant, as was the section height. To investigate the effect of cover, however, one model series was conducted wherein similar anchors were used while varying the web thickness. Rather than dealing in absolute web thickness (t = 6 in., for example), the cover is expressed indirectly as a ratio of the width of the bearing plate divided by the thickness ($2a'/t$) or expressed directly as the cover/thickness ratio on a face ($C/t = 1/2 - a'/t$). Table 2.3 lists the data pertinent to this series, while Fig. 2.10 shows the nondimensional cracking trends with respect to cover. The solid line, which forms a reasonable and conservative lower bound for the experimental data, was based on the three-dimensional finite element predictions discussed in Sec. 2.2.6.

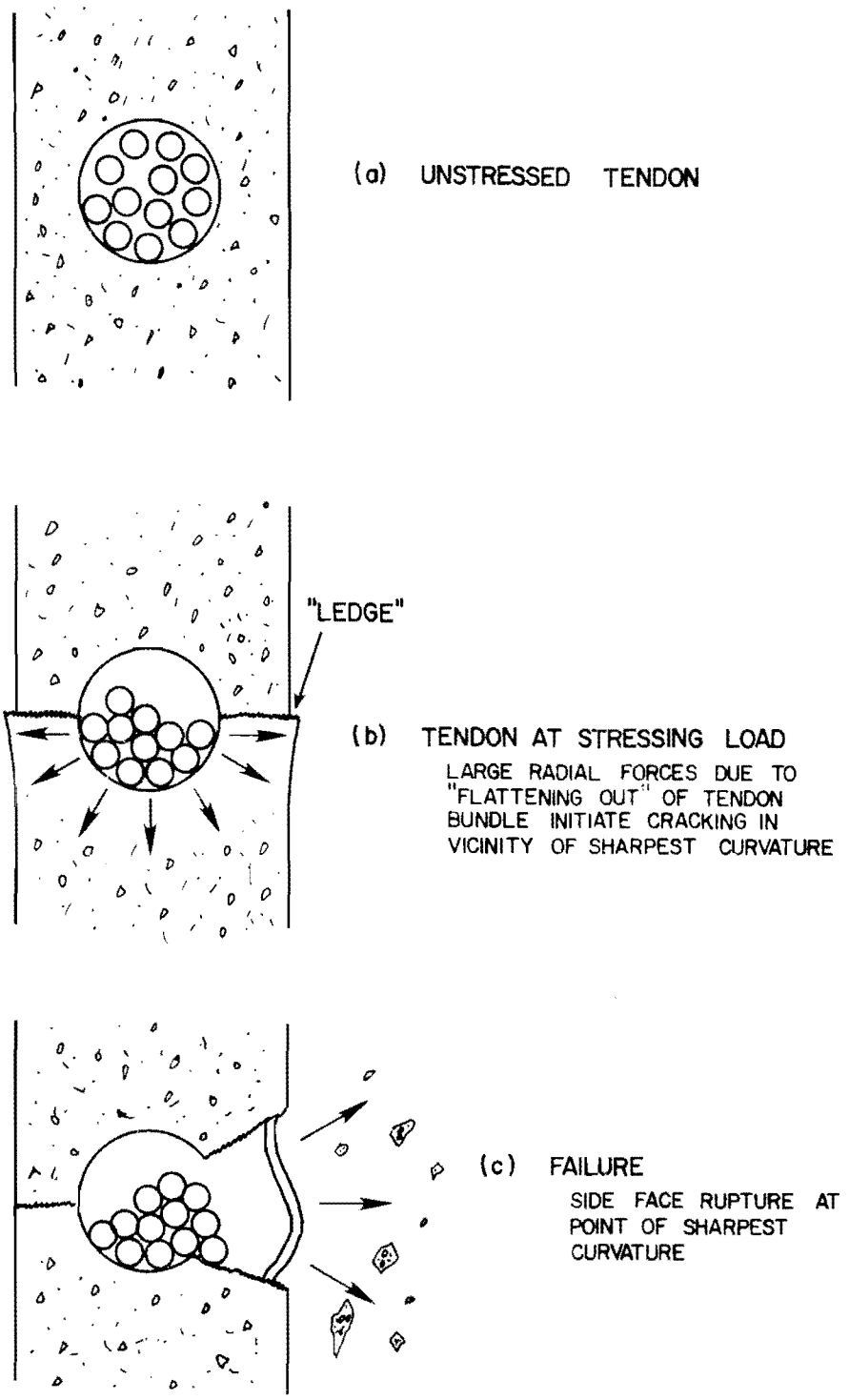

Fig. 2.8 Multistrand failure in a curved tendon

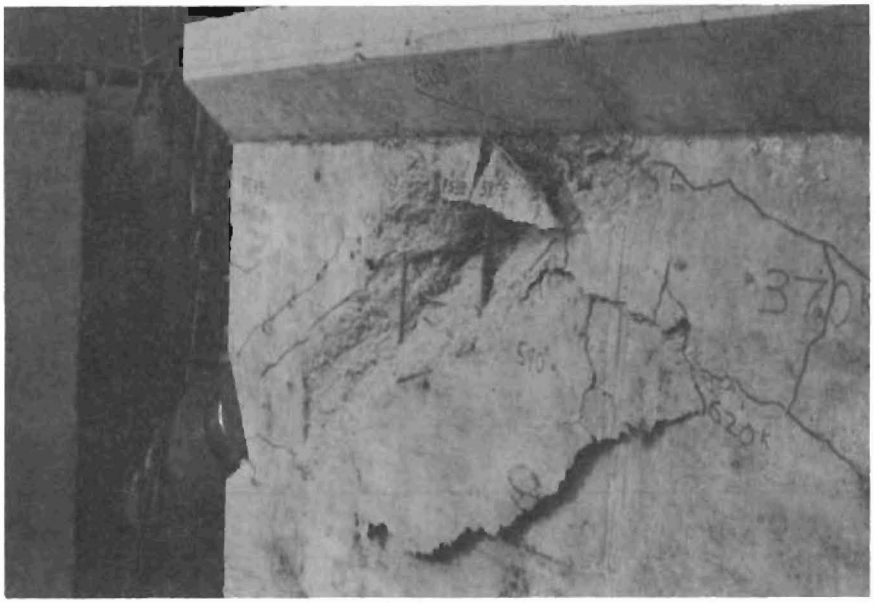

(a) Ultimate load: 590 kips. Side face rupture at point of maximum curvature

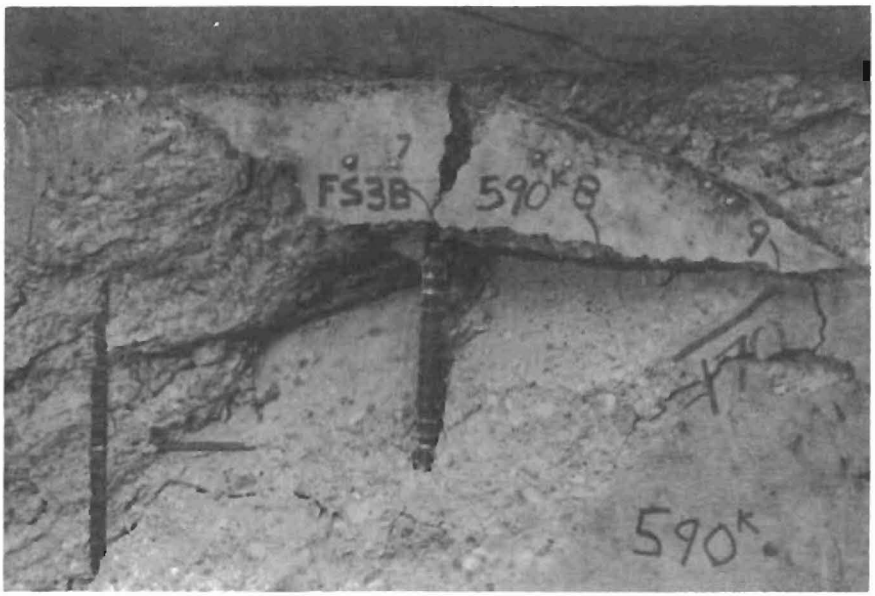

(b) Close up of failure zone. Vertical bar in center has been forced outward

Fig. 2.9 Failure due to multistrand effect in specimen FS3B

TABLE 2.3

COVER EFFECTS

Specimen	Cover Ratio $2a'/t$	$\frac{P_{cr}}{f_{sp}}$ (in.^{2})	$\frac{P_{cr}}{\sqrt{f'_c}}$ (in.^{2})	$\frac{P_{ult}}{f_{sp}}$ (in.^{2})	$\frac{P_{ult}}{\sqrt{f'_c}}$ (in.^{2})	$\frac{f_{sp}}{\sqrt{f'_c}}$	$\frac{P_{cr}}{(2f_{sp}at)}$
M1-2	0.50	68	659	68	659	9.6	0.85
M2-2	0.66	54	521	54	521	9.6	0.90
M3-2	1.00	38	368	38	368	9.6	0.95
M3-2R	1.00	39	333	41	351	8.5	0.975
MR1A	0.875	54	529	76	734	9.7	0.878
MR1B	0.71	59	573	73	706	9.7	0.959
M1A	0.875	71	677	86	815	9.5	1.154
MI1B	0.71	59	560	72	683	9.5	0.959
FS1A	0.71	55*	352*	--	--	6.4	0.894
FS1B	0.875	62*	328*	--	--	5.3	1.008

*Adjusted to 1/4 model values. Multiply above numbers by 16 to obtain prototype values.

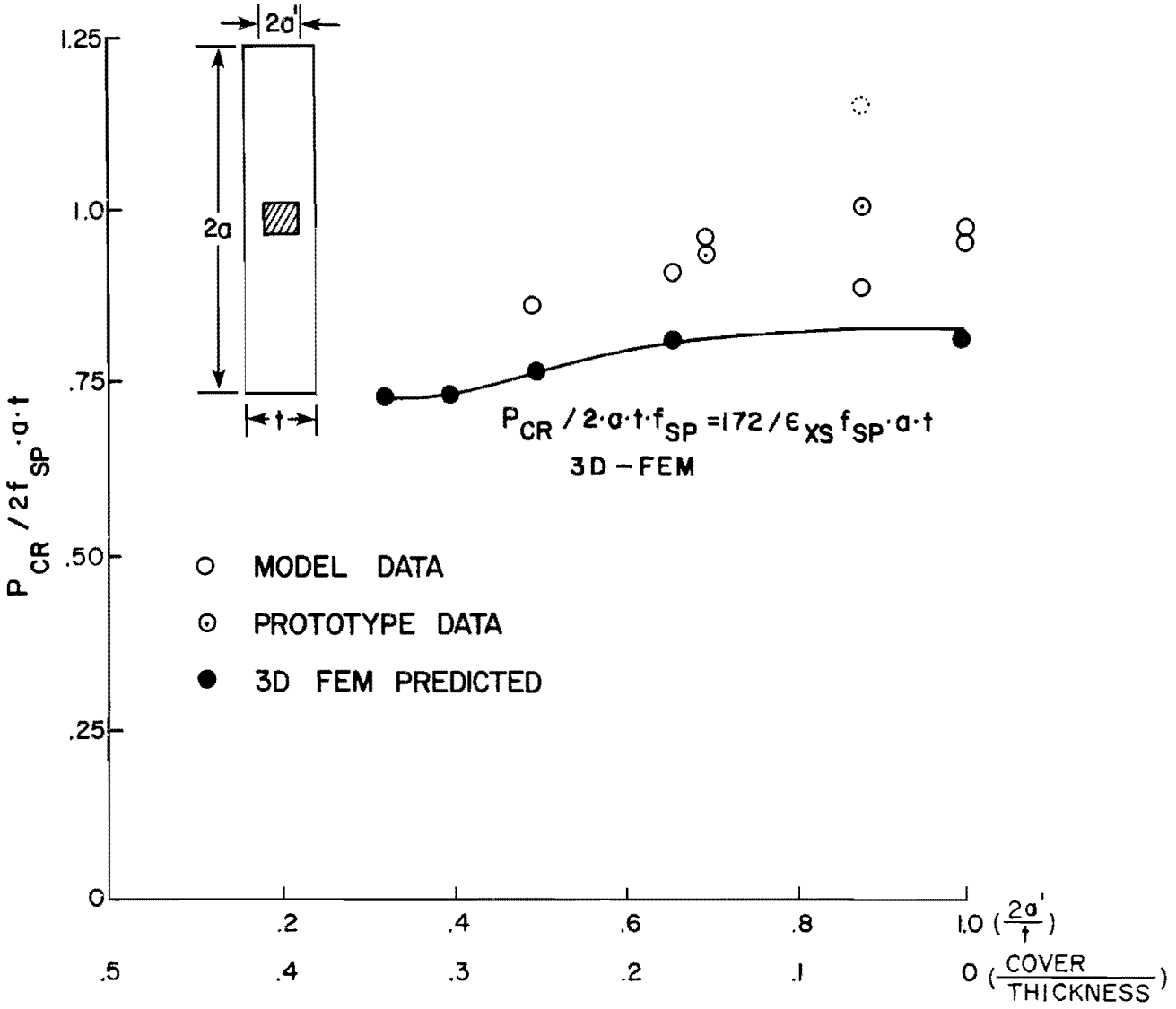

Fig. 2.10 Cover effects

The trend exhibited in Fig. 2.10 would tend to indicate that for specimens with like values of f_{sp}, it would appear that sections will crack when about the same uniform compressive stress ($P_{cr}/2at$) is applied, irrespective of the ratio of cover concrete (C/t). It does not mean the absolute cracking load remains the same as cover is increased.

Clearly the thickness of the section is an important variable. Since the sections with like values of f_{sp} crack when a specified uniform compressive stress ($P_{cr}/2at$) is reached, thicker sections will require higher loads to achieve that specified stress. The effect can be illustrated by factoring out the nondimensionalizing term (2at), and plotting P_{cr}/f_{sp} in Fig. 2.11. Here it can be clearly seen that, for any given anchor size, as the thickness of the section increases due to increased cover the cracking load also increases significantly.

2.3.2 Inclination Effects. A summary of specimens with inclined tendons is presented in Table 2.4. The angle of inclination is measured from the axis normal to the end face. In general, as the angle of inclination increases, the cracking load drops. This trend is clearly illustrated in Fig. 2.12. The solid line was generated from the finite element predicted cracking loads. An approximate value for the decrease in the normalized cracking load ($P_{cr}/2atf_{sp}$) is 1 percent per degree of inclination as measured from the normal to the loaded face, as shown in Fig. 2.12.

2.3.3 Bearing Area Effects. A summary of the seven specimens which dealt with the effect of bearing area on the behavior of the anchorage zone is presented in Table 2.5. In contrast to the cover series, the width of the specimen was kept constant and the size of the anchorage was successively reduced to obtain higher bearing stresses for a given load. In general, it was observed that the cracking load increased slightly for increases in the size of the bearing plate, as shown in Fig. 2.13. The results of the FEM analysis agree with the test data. The relative flatness of the curve

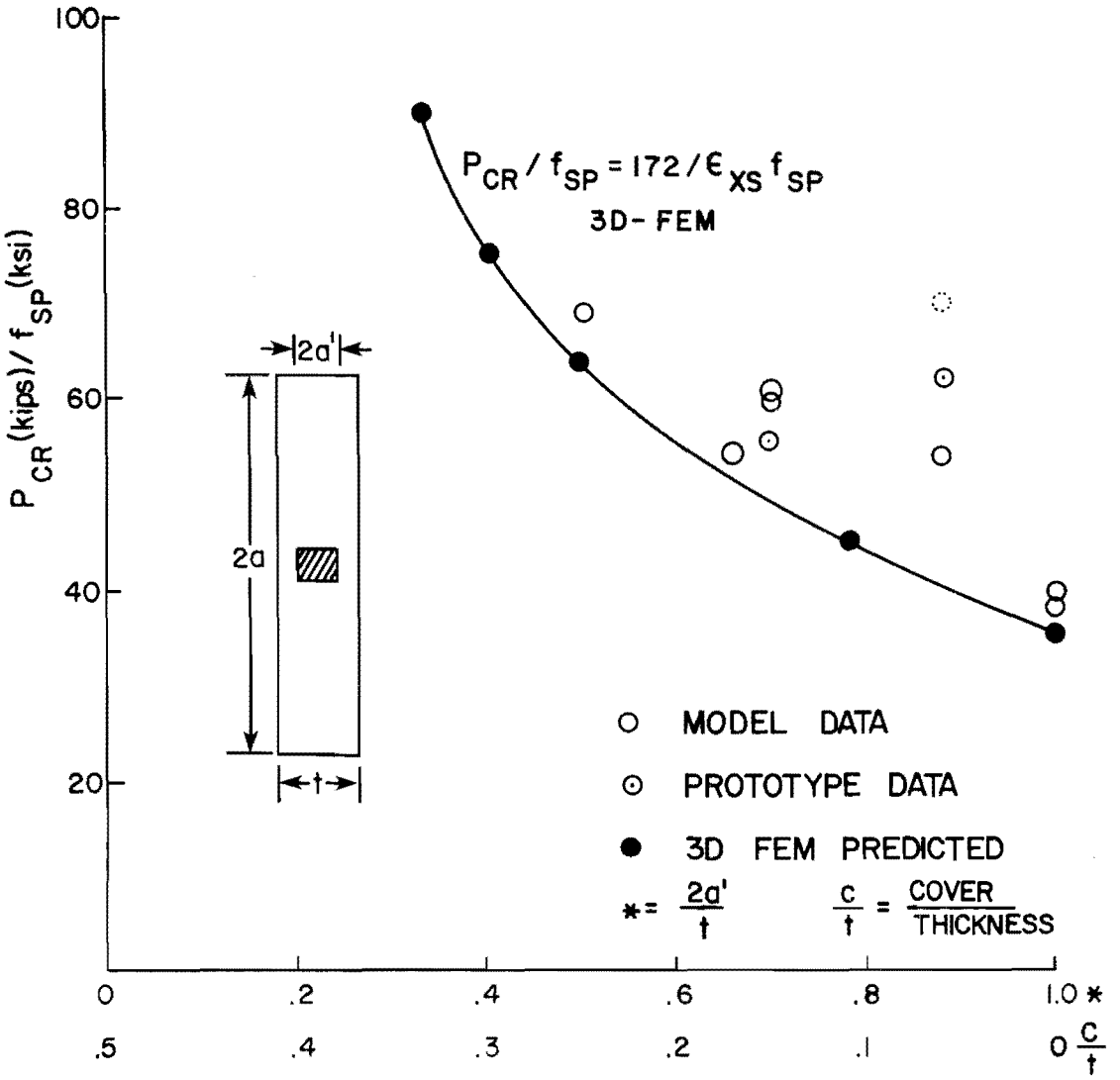

Fig. 2.11 Thickness effects

TABLE 2.4

INCLINATION EFFECTS

Specimen	Inclination	(in^2) P_{cr}/f_{sp}	(in^2) $P_{cr}/\sqrt{f'_c}$	(in^2) P_{ult}/f_{sp}	(in^2) $P_{ult}/\sqrt{f'_c}$	$f_{sp}/\sqrt{f'_c}$	$P_{cr}/2f_{sp}$ at
PSIB*	0	62	328			6.4	1.008
MI1A	0	71	677	86	815	9.5	1.154
MI1B	0	59	560	72	683	9.5	0.959
MR1A	0	54	520	76	734	9.7	0.878
MR1B	0	59	573	73	706	9.7	0.959
FS2A*	15	51	387	--	---	7.4	0.829
FS2B*	30	45	303	--	---	6.6	0.731
M1-3	30	45	468	52	535	10	0.750
MI2	30	51	411	82	659	8	0.829

*Full scale values adjusted by scale factor of 1/16. For comparison multiply above values by 16 to obtain prototype equivalents.

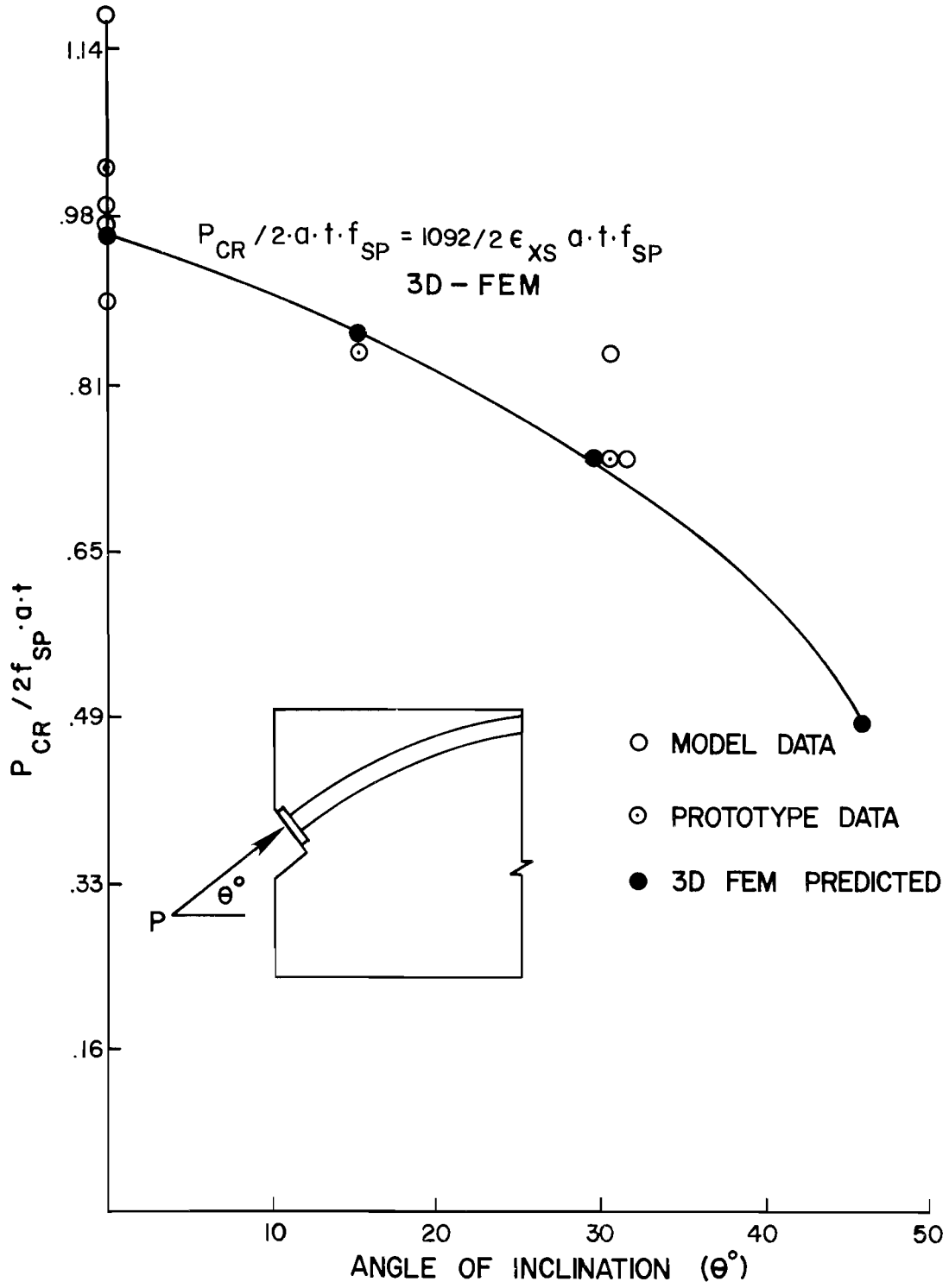

Fig. 2.12 Inclination effects

TABLE 2.5

BEARING AREA EFFECTS

Specimen	Bearing Ratio A_1/A_2	P_{cr}/f_{sp}	$P_{cr}/\sqrt{f'_c}$	P_{ult}/f_{sp}	$P_{ult}/\sqrt{f'_c}$	$f_{sp}/\sqrt{f'_c}$
M2-2	0.44	54	521	54	521	9.6
MI1B	0.50	59	560	72	683	9.5
MR1B	0.50	59	573	73	706	9.7
FS1A*	0.50	55	352	--	---	6.4
MI1A	0.76	71	677	86	815	9.5
MR1A	0.76	54	520	76	734	9.7
FS1B*	0.76	62	328	--	---	5.3

*Adjusted by scale factor of 1/16. Multiply above values by 16 to obtain prototype equivalents.

can be seen by observing the increase in $P_{cr}/2atf_{sp}$ for dramatic changes in A_1/A_2 where A_1 = the area of the bearing plate and A_2 = the area concentric with and geometrically similar to the plate (these definitions are as given in the ACI Building Code). For instance, for $A_1/A_2 = 1$, the cracking load is 40 percent above that for the case of $A_1/A_2 = 0.2$. Thus, the 40 percent increase in cracking load corresponds to a 500 percent increase in bearing area. It should be noted that increased A_1/A_2 values correspond to increased a'/a values which should result in decreased bursting stresses.

With slight rearranging, the ACI equation for bearing stress after allowance for prestress losses (Sec. 18.13 ACI 318-77 Commentary) yields the following formula:

$$f_{allow} = 0.6f'_c \sqrt{A_2/A_1} \leq f'_c \quad \text{(from ACI)}$$

$$P_{allow} = f_{allow} \times A_1 = 0.6f'_c \sqrt{A_2/A_1} \times A_1$$

for f'_c = 4000 psi (average, most tests), and f_{sp}

$= 8.3 \sqrt{f'_c}$ (models) [A lower value of around $6.5\sqrt{f'_c}$ would be more appropriate for prototype concretes.]

$$P_{allow}/f_{sp} = 4.57 \sqrt{A_2 A_1} \qquad (2.11)$$

As a comparison, these values are plotted as a broken line below the experimental data in Fig. 2.13. Also plotted is a similar curve based on the ACI bearing stress equation immediately after tendon anchorage $f_{allow} = 0.8\ f'_{c_i} \sqrt{A_2/A_1 - 0.2} \leq 1.25\ f'_{c_i}$. This expression is in very

good agreement with the data trends and is quite conservative. They follow the correct trend but are indeed conservative, especially since the ACI formula is based on ultimate load (not cracking). Since, with supplementary reinforcement, the cracking and ultimate loads can be raised significantly, the ACI curve is in actuality very conservative.

A similar examination can be made of the AASHTO Anchorage Bearing Stress criterion of AASHTO Sec. 1.6.1.(B)(4). This allows a post-tensioned anchorage bearing stress at service load of 3000 psi but not to exceed $0.9\, f'_{c_i}$. For the model series f'_c was about 4000 psi, 2a was 20 in. and t was 3 in. To illustrate the effects of this criterion in Fig. 2.13 the following procedure was used

$$f_{allow} = 3000 \leq 0.9(4000)$$

$$P_{allow} = f_{allow} \times A_1 = 3000A_1$$

Again, for the models $f_{sp} = 8.3\sqrt{f'_c}$, so

$$\frac{P_{allow}}{f_{sp}} = \frac{3000A_1}{8.3\sqrt{4000}} = 5.72A_1$$

Nondimensionalizing as in Fig. 2.13

$$\frac{P_{all}}{f_{sp}2at} = 5.72\,\frac{A_1}{2at} = \frac{5.72(2a')^2}{2at} \cdot \frac{t}{t} = 5.72\,\frac{A_1}{A_2} \cdot \frac{t}{2a}$$

For 2a = 20 t = 3

$$\frac{P_{all}}{f_{sp}2at} = 0.86\,\frac{A_1}{A_2}$$

The AASHTO values for various A_1/A_2 ratios are shown on Fig. 2.13. The AASHTO procedures become increasingly conservative as smaller bearing plates are used in a constant thickness web and also severely penalize small anchors in high strength concrete. The

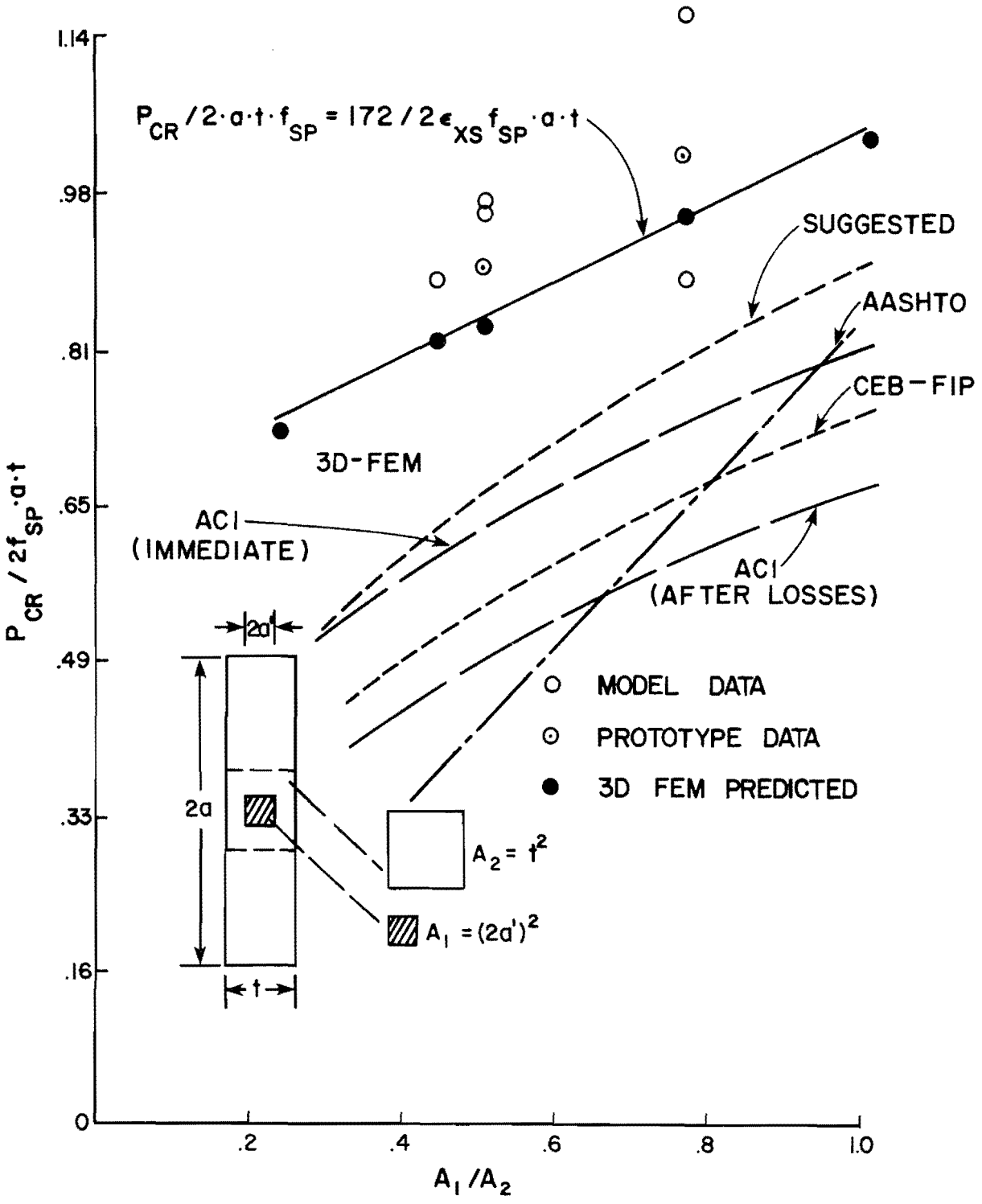

Fig. 2.13 Bearing area effects

CEB-FIP expression ($P_u = f_{cd}\sqrt{A_1 A_2} \leq 3.3\, f_{cd} A_1$) is shown in roughly comparable terms ($P_u = 0.67 f'_c \sqrt{A_2 A_1} \leq 2.2\, f'_c A_1$) in Fig. 2.13. It is similar to and falls in between the ACI expressions.

The general trend of the ACI and CEB expressions is much more in agreement with the experimental and analytical results than are the AASHTO expressions. Remembering that all experimental and analytical data are for specimens with no supplementary anchorage zone reinforcement, the suggested design expressions for bearing stress for post-tensioned anchorages could be liberalized significantly. The AASHTO expression should be changed to reflect cover effects.

A reasonable expression would be

$$f_b = 0.8 f'_{c_i} \sqrt{A_2/A_1} \leq 1.33 f'_{c_i}$$

which is shown as a "suggested" curve on Fig. 2.13.

2.3.4 Eccentricity Effects. A series of nine tests dealt with the effect of eccentricity of the anchorage in a web. Data for these tests are given in Table 2.6. The general trend, shown in Fig. 2.14 indicates that increased eccentricity results in a decrease in the cracking load. As a measure of this, an anchor located 1/3 of the distance from the centroidal plane toward the edge will crack at a load 25 percent below that for centroidal loading. An anchor located 2/3 of the way toward the edge will crack at a load approximately 50 percent below that for centroidal loading. The trend appears to be fairly linear. The superimposed solid line represents the finite element analysis predicted cracking load. If the anchor is so eccentric that it is located within the flange region, these results may not be meaningful.

2.3.5 Passive Reinforcement Effects--Spirals, Orthogonal Grids. There are basically two reasons for adding supplementary reinforcement to the post-tensioned anchorage zone. The most important is to prevent complete failure in the event that cracking should occur, and thus to ensure that the safety of the structure is

TABLE 2.6

ECCENTRICITY EFFECTS

Specimen		$(in.^2)$ P_{cr}/f_{sp}	$(in.^2)$ p_{cr}/f_{sp}	$(in.^2)$ $P_{ult}/\sqrt{f_c'}$	$(in.^2)$ $P_{ult}/\sqrt{f_c'}$	$f_{sp}/\sqrt{f_c'}$	$\frac{P_{cr}}{2f_{sp}at}$
M7A-4	e = 0.3a	46	306	52	347	6.6	0.76
M7C-4	e = 0.3a	58	508	65	572	8.7	0.96
M1A-4	e = 0.6a	36	301	36	301	8.3	0.6
M8B-4	e = 0.6a	43	475	49	537	10.8	0.716
MR1A	e = 0	54	520	76	634	9.7	0.88
MR1B	e = 0	59	573	73	706	9.7	0.959
M 1A	e = 0	71	677	86	815	9.5	1.15
MI1B	e = 0	59	560	72	683	9.5	0.959
FS1B*	e = 0	62	328	--	--	5.3	1.008

*Values adjusted by 1/16 to model scale. To obtain equivalent values for prototypes multiply above values by sixteen.

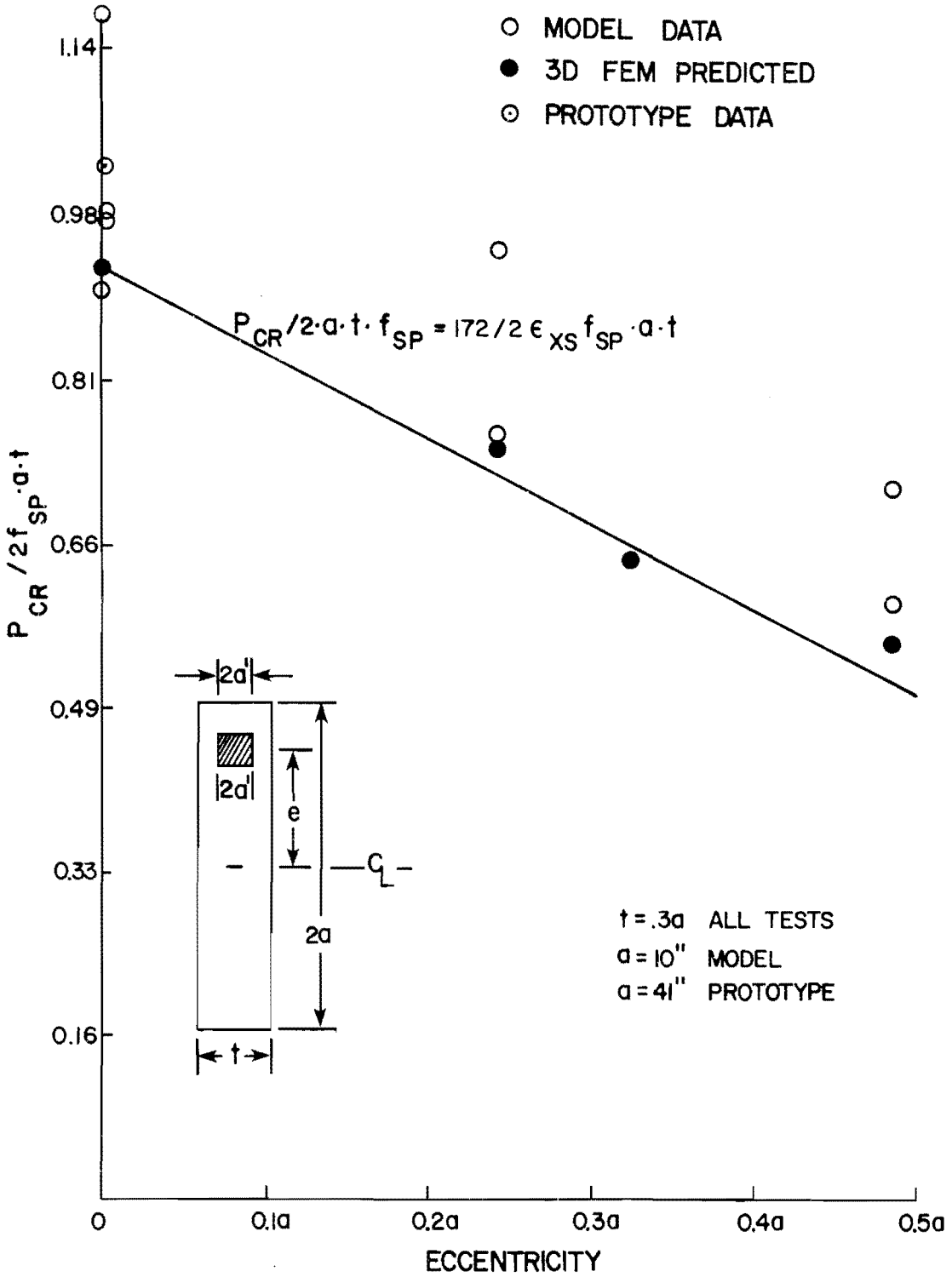

Fig. 2.14 Eccentricity effects

unimpaired. However, in most cases, the addition of supplementary reinforcement will also tend to raise the cracking load, due to the confinement of the concrete. Thus, the second reason for adding supplementary reinforcement is to increase the surface crack formation load adding to the resistance to corrosion and to the aesthetics of the post-tensioned application.

The reinforcing schemes tested during the rectangular model series [2] indicated that spiral reinforcement was far superior to conventional orthogonal or grid-type reinforcement. However, in many cases it may be impractical to use spiral reinforcement because of congestion in the anchorage zone. For such situations, orthogonal reinforcement, while less efficient, will provide some increase in the cracking load and a substantial increase in the ultimate capacity. General trends for both types of passive reinforcement are discussed below.

2.3.5.1 Spiral Reinforcement. Test results for spirally reinforced specimens (summarized in Tables 2.7 and 2.8 and shown in Fig. 2.15) indicate the following trends:

(1) For a given volumetric percentage of spiral reinforcement, the spirals fabricated from smaller diameter bar stock (3/8 in. versus 1/2 in. for the prototype tests) were observed to perform better than identical spirals fabricated from larger bar stock. While this trend may not be a general rule, it indicates that for a given required quantity of reinforcement, the most efficient means of deployment is through the use of spirals fabricated from smaller bars at a closer pitch, rather than from large bars at a greater pitch.

(2) Within the range investigated in the full-scale tests, long spirals (26 in. in length affixed to the anchor) performed no better than short spirals (13 in. in length). For the case of the inclined, curved, multiple strand tendons, however, careful attention must be paid to the possibility of cracking along the tendon path at the

TABLE 2.7

REINFORCEMENT EFFICIENCY SUMMARY -- INCLINED TENDON TESTS

Specimen	Reinforcement	A ($in.^2$) P_{cr}/f_{sp}	B ($in.^2$) P_{ult}/f_{sp}	$(\frac{A}{A_c} - 1)$ × 100%	$(\frac{B}{A} - 1)$ × 100%	$(\frac{B}{A_c} - 1)$ × 100%	$\frac{A_s f_y}{10,000}$ (kips)
FS2B	Control (Full Scale) No Reinforcement	725	--	0	--	--	0
FS3A	D = 8" , ℓ = 13" S = 2" , d = 3/8"	787	1361	9	73	88	10.6
FS3B	D = 8" , ℓ = 13" S = 2" , d = 1/2"	636	1250	-12 **	96	72	18.84
FS4A	D = 8" , ℓ = 26" S = 2" , d = 3/8"	779	1267	8	63	75	21.2
FS5A	60 kips LPT at 32"	845	--	17	--	--	8.26
FS5B	60 kips LPT at 6"	959	1599	33	66	120	8.26

(continued)

TABLE 2.7 (Continued)

Specimen	Reinforcement	A (in^2) P_{cr}/f_{sp}	B (in^2) P_{ult}/f_{sp}	$(\frac{A}{A_c} - 1)$ × 100%	$(\frac{B}{A} - 1)$ × 100%	$(\frac{B}{A_c} - 1)$ × 100%	$\frac{A_s f_y}{10,000}$ (kips)
MI2*	Control for MI3	825	1319	0	--	--	0
MI3*	D = 2" , ℓ = 6.5" S = 1/4", d = 13 gage	976	1610	18	65	95	20.2

Notes:

A_c = Normalized control cracking load (no reinforcement)
A,B = Normalized specimen cracking and ultimate loads
D = Overall spiral diameter (inches)
ℓ = Overall length of spiral (inches)
d = bar diameter (60 ksi) used to fabricate spiral
LPT = lateral post-tensioning (active reinforcement). Distance is from loaded face.
* : Model values for $A_s f_y/1000$, P_{cr}/f_{sp}, P_{ult}/f_{sp} adjusted by scale factor $1/S^2 = 16$
**=Specimen cracked prematurely due to multistrand effects.
A_s = The area of supplementary reinforcement which crosses perpendicularly the tendon path in the anchorage zone. For practical purposes, the anchorage zone is assumed to extend a maximum distance of 6a' from the primary loaded face.
All specimens had plate type anchors.

TABLE 2.8 REINFORCEMENT EFFICIENCY SUMMARY--STRAIGHT TENDONS WITH SPIRAL REINFORCEMENT

Specimen	Reinforcement	A (in^2) P_{cr}/f_{sp}	B (in^2) P_{ult}/f_{sp}	$(\frac{A}{A_c} - 1)$ × 100%	$(\frac{B}{A} - 1)$ × 100%	$(\frac{B}{A_c} - 1)$ × 100%	$\frac{A_s f_y}{10{,}000}$ (kips)
M2B-4	Control for (t = 0.45a) M5A-4 , M5B-4	421.0	421.0	--	0	--	0
M5A-4*	D = 2" , ℓ = 6" S = 0.75" , d = 13 gage	768.0	1136.0	82	47	170	18.5
M5B-4*	D = 2" , ℓ = 6" S = 0.75" , d = 10 gage	823.0	1184.0	95	43	181	33
M1B-4*	Control for M6A-4 (t = 0.3a) M6B-4	323.0	452.8	--	40	--	0
M6A-4*	D = 2" , ℓ = 6" S = 0.75" , d = 13 gage	736.0	1043.0	127	41	222	18.5
M6B-4*	D = 2" , ℓ = 6" S = 0.75" , d = 10 gage	823.0	1053	154	28	226	33

Notes:

A_c = Normalized control cracking load (no reinforcement)

A,B = Normalized specimen cracking and ultimate loads.
Same as for Table 7.5a. All values for P_{cr}/f_{sp}, P_{ult}/f_{sp} and $A_s f_y$ have been scaled from model data by a factor of 16. All tendons have eccentricity of .6a.

TABLE 2.9

REINFORCEMENT EFFICIENCY SUMMARY -- STRAIGHT TENDONS WITH ORTHOGONAL REINFORCEMENT

Specimen	Reinforcement	A (in^2) P_{cr}/f_{sp}	B (in^2) P_{ult}/f_{sp}	$(\frac{A}{A_c} - 1)$ × 100%	$(\frac{B}{A} - 1)$ × 100%	$(\frac{B}{A_c} - 1)$ × 100%	$\frac{A_s f_y}{10,000}$ (kips)
M2B-4	Control for t = 0.45a M4A-4 , M4B-4	421	421	--	0	--	0
M4A-4	5 - 10 gage stirrups at 2" spacing	716	777	70	8.5	127	13.74
M4B-4	17 - 6mm stirrups at 1" spacing	832	958	97	15.1	127	143.0
M1B-4	Control for M3A-4, M3B-4 t = 0.3a	323	452.8	--	40	--	0
M3B-4	11 - 6 mm stirrups at 1.6" spacing	596	688	84	15.4	113	92.5

Notes:

Same as 7.5a,b.
All specimens had cone type anchors.

TABLE 2.10

RECOMMENDED DESIGN VALUES

I.) Straight Tendon Tests

Reinforcement	Increase in Cracking Load			Increase in Ultimate Load		
	$\bar{x}$ (%)	σ (%)	$\bar{x} - 2\sigma$ (%)	$\bar{x}$ (%)	σ (%)	$\bar{x} - 2\sigma$ (%)
Spiral	141	19	103	224	2.8	218
Orthogonal	84	11	61	106	18	71

II.) Inclined Curved Tendon Tests

Spiral (multiple strand tendon)	8.5	0.7	7	78	8.5	61
Spiral (single strand tendon)	18	2.07*	14	95	9.22*	77
100 psi LPT (multiple strand tendon)	33	3.8*	25.4	120	11.6*	97

*Estimates based on mean variance of other tests.
$\bar{x} - 2\sigma$ represents the recommended % increase above the cracking load for a specimen with no supplemental reinforcement (from Fig. 2.10-2.13 or Eq. 3.2).

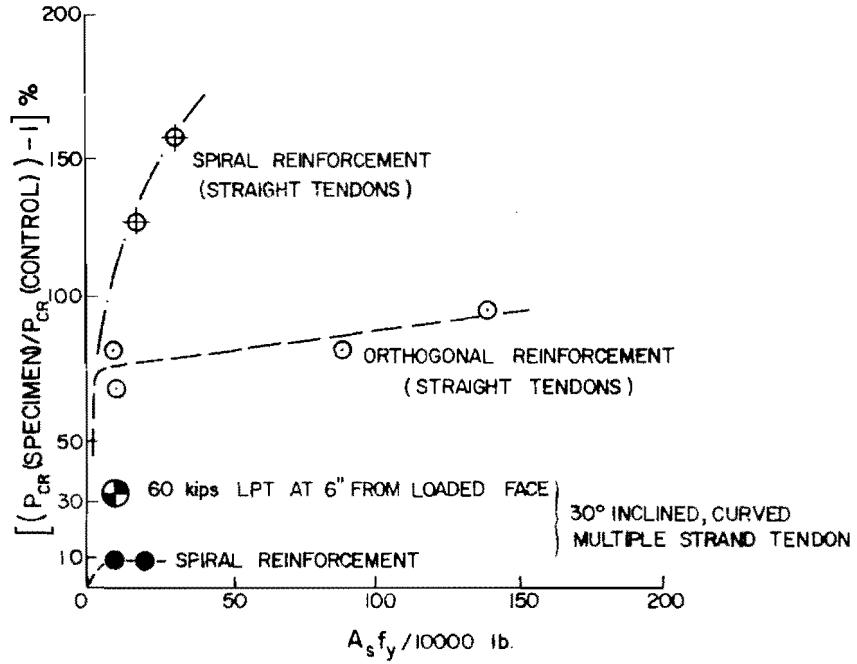

(a) PERCENT INCREASE IN CRACKING LOAD ABOVE UNREINFORCED SECTION

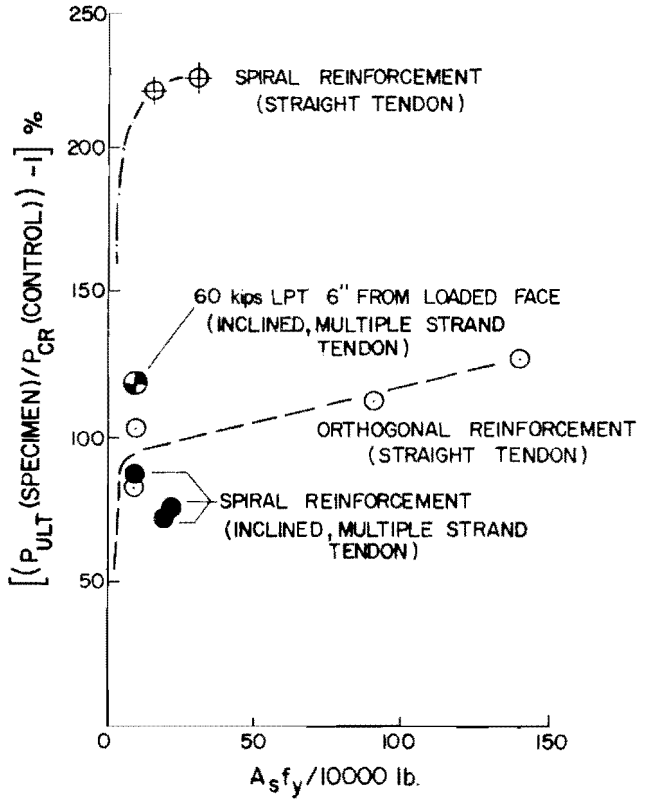

(b) PERCENT IN ULTIMATE LOAD ABOVE CRACKING LOAD FOR UNREINFORCED SECTION

Fig. 2.15 Supplementary reinforcement efficiency

point of maximum tendon curvatures. In most practical applications that point would be well-removed from the anchorage zone, and from the influence of any spiral reinforcement in the anchorage zone. While continuing anchorage zone reinforcement into the zone of maximum curvature would seem logical in such situations, calculations which will be presented in the next chapter indicate that the reinforcement required to resist multistrand effects is much smaller than that required for confinement in the anchorage zone.

(3) At first cracking, all spiral confinements tested in the prototype specimens series maintained crack widths below the maximum 0.013 in. currently implicitly specified by ACI.

A measure of the spiral's effectiveness in delaying surface cracking and in increasing the ultimate anchorage capacity can be clearly seen in Fig. 2.15 and is summarized in Table 2.10. In straight tendon specimens the spiral reinforcement raised the cracking load by 100 percent (i.e., more than twice the cracking load) over that witnessed in companion tests with no supplementary anchorage zone reinforcement. Ultimate loads were increased more than 200 percent above the cracking load for the unreinforced section. These results would apply to both single and multiple strand tendons. The values in Table 2.10 represent conservative results two standard deviations below the observed mean.

For specimens with 30-degree inclined, curved, multiple strand tendons, supplementary spiral reinforcement in the anchorage zone raised cracking loads by only 7 percent. Part of the reason for this was due to the fact that first cracking for the specimens in this series occurred beyond the zone of spiral reinforcing, in the area of maximum tendon curvature. The anticipated rise in cracking load with the addition of the spiral is thus counterbalanced by the tendency for cracking which occurs due to the multistrand effects discussed in Sec. 2.2.7. However, model tests of single strand tendons (see Table 2.10) indicate that if cracking were

prevented in the region of maximum curvature (say, by the proper use of spiral reinforcement in that zone), first cracking would occur in the anchorage zone at a load approximately 14 percent above that for a specimen without reinforcement. Figure 2.15 clearly indicates that passive supplementary reinforcement is significantly less effective in raising cracking loads for inclined tendon applications than for straight tendons. However, the ultimate load can be substantially raised by the addition of spiral reinforcement, although again not as much as for straight tendon applications. For supplementary spiral confinement with inclined tendons (at 30°), the ultimate loads will be conservatively 61 percent and 77 percent above the cracking load for the unreinforced section for multiple strand tendons and single strand tendons, respectively. It may be possible to raise the ultimate capacity of multiple strand tendons still further by the addition of supplementary spiral reinforcement in the region of maximum curvature, but no experimental verification of this is available at present. The design of such reinforcement is discussed in a later section. For tendons inclined at angles other than 30°, it would seem reasonable, pending further experimental study, to assume a linear variation in the increases in cracking and ultimate loads between the sets of values given for straight and 30° inclined tendons.

The percentage increases stated above reflect the observed mean less two standard deviations for each grouping. Spiral reinforcement is assumed to be designed in accordance with the method described in Ref. 2 which suggests a minimum confinement similar to an ACI column spiral. Design procedures and recommendations for spirally reinforced anchorage zones are summarized in Chapter 3. The method will be illustrated in an example in Chapter 3. Data for specimens with straight tendons and a width of $t = 0.45a$ were not used in deriving these values as the spiral used was considered to be of insufficient diameter for that section. Proper design of the

spiral will yield values of $A_s f_y/10000$ (lb) of about 20 for the prototype used in this study. The value A_s for the spiral is determined by the area of spiral steel crossing perpendicular to a horizontal plane along the tendon path. Values for other applications will depend upon spiral diameter, pitch, the post-tensioning load and the yield strength of the spiral. Increasing the amount of spiral steel beyond that calculated probably would not greatly modify the percentage increases given in Table 2.10. Figure 2.16 indicates the strength gain to be flat-topped for increasing amounts of spiral reinforcement.

2.3.5.2 Orthogonal Reinforcement. While spiral reinforcement is the most efficient means of providing passive reinforcement in anchorage zones, it may not always be feasible to use it due to problems of congestion. For such cases, orthogonal reinforcement in the form of closely spaced closed stirrups, or mats similar to those recommended by Guyon and shown in Fig. 2.17, is an acceptable remedial method of raising the cracking and ultimate loads.

A study dealing with widely varying amounts of passive reinforcement in Ref. 2 reveals that heavily reinforced specimens exhibited only nominally higher cracking and ultimate loads than those with fairly light amounts of reinforcement. This effect is summarized in Table 2.9.

As shown in Fig. 2.15 and Table 2.10, for straight tendon applications orthogonal reinforcement raises the cracking load by 60 percent above the observed cracking load in companion specimens with no reinforcement. Ultimate failure occurred at loads at least 70 percent above the cracking load for the unreinforced section. No tests were done to investigate the performance of orthogonal reinforcement for inclined tendon applications because the spiral was so clearly superior.

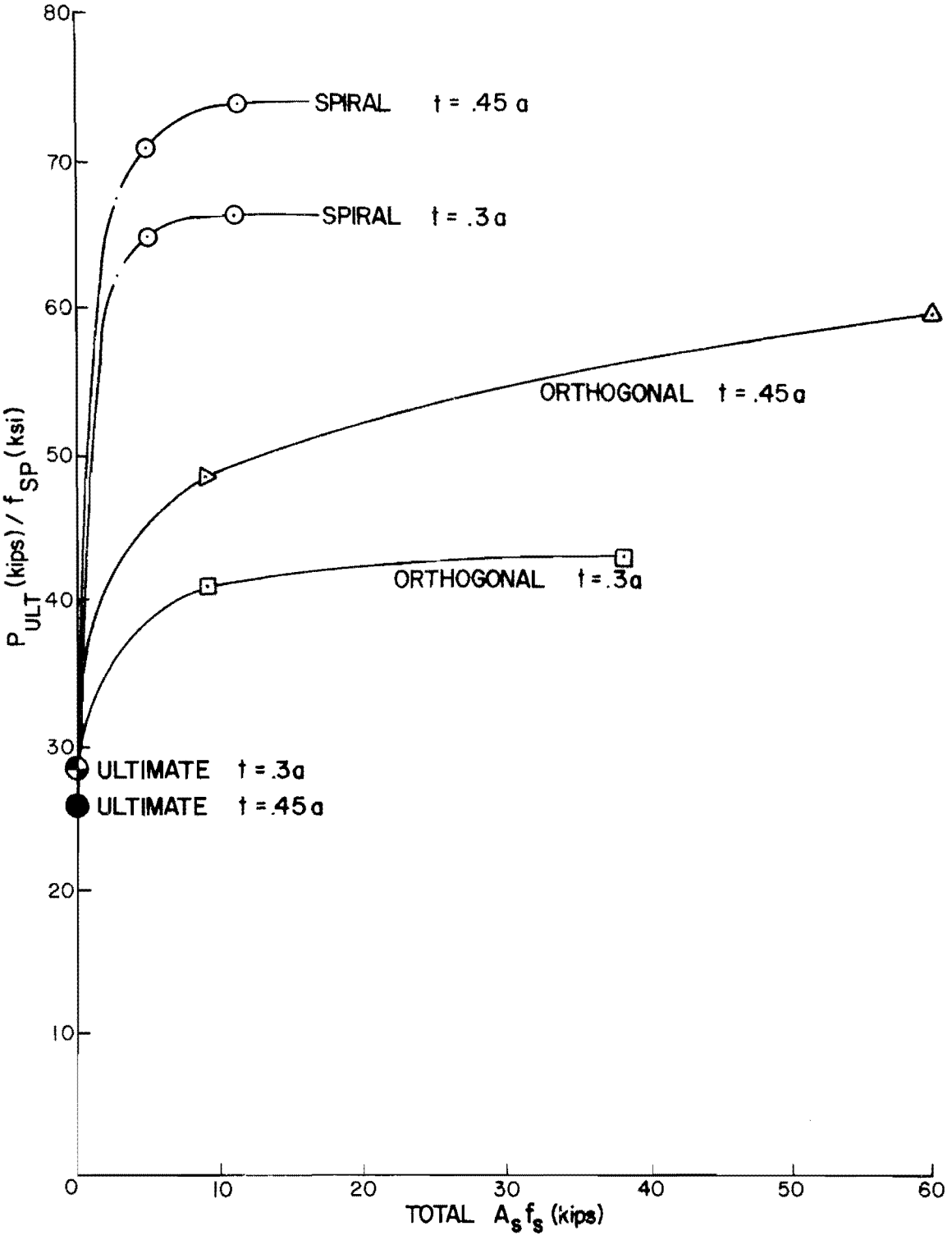

Fig. 2.16 Normalized ultimate loads--reinforcement series

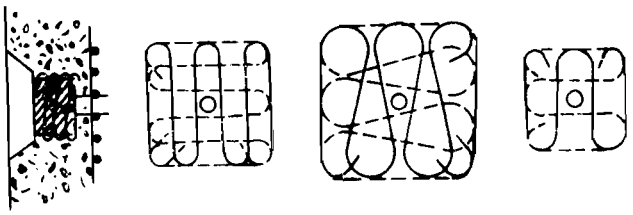

Mesh reinforcement immediately behind anchors

Fig. 2.17 Anchorage zone reinforcement design as per Guyon (from Ref. 5)

Figure 2.15 shows the relative insensitivity of the anchorage zone to massive amounts of orthogonal reinforcement, both for cracking and ultimate loads. Following an initial rise both curves flatten out.

2.3.6 Active Reinforcement Effects. For most practical situations, the inclusion of passive reinforcement in the form of spirals will be the most convenient method of anchorage zone reinforcement. However, in situations where complete prevention of cracking is desirable, the use of lateral prestress in the anchorage zone offers the designer a powerful tool. Perhaps the most important need for the use of lateral prestressing occurs when, due to geometric limitations or construction schedules which require stressing before the concrete has reached its maximum tensile strength, it is not possible to provide a section which would remain uncracked at service load using passive reinforcement. In such cases, by judicious use of lateral prestress the cracking load can be raised significantly.

Test specimens FS5A and FS5B and the results of the three-dimensional finite element analysis indicated the following:

(1) The optimum location for the lateral prestress load is as close to the loaded face as is feasible, as shown in Fig. 2.18.

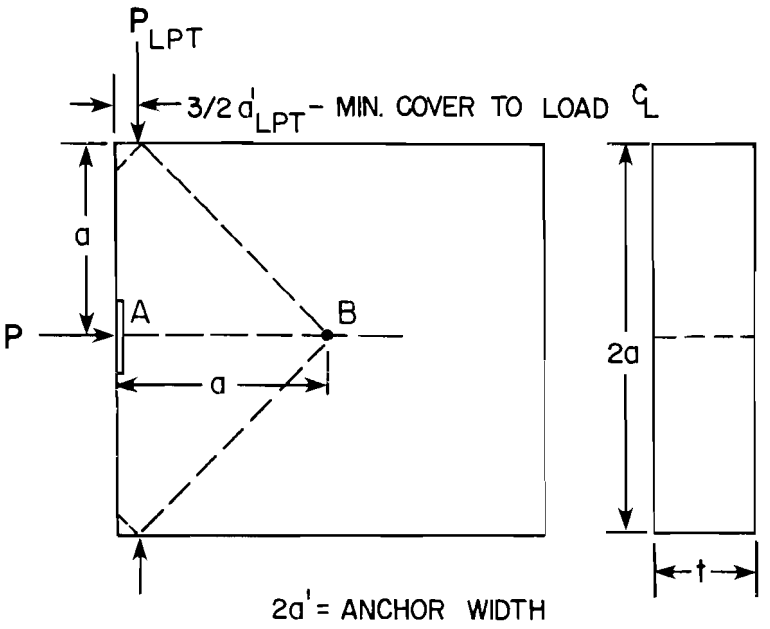

(a) LATERAL COMPRESSIVE STRESS ALONG AB ≅ LPT / a·t

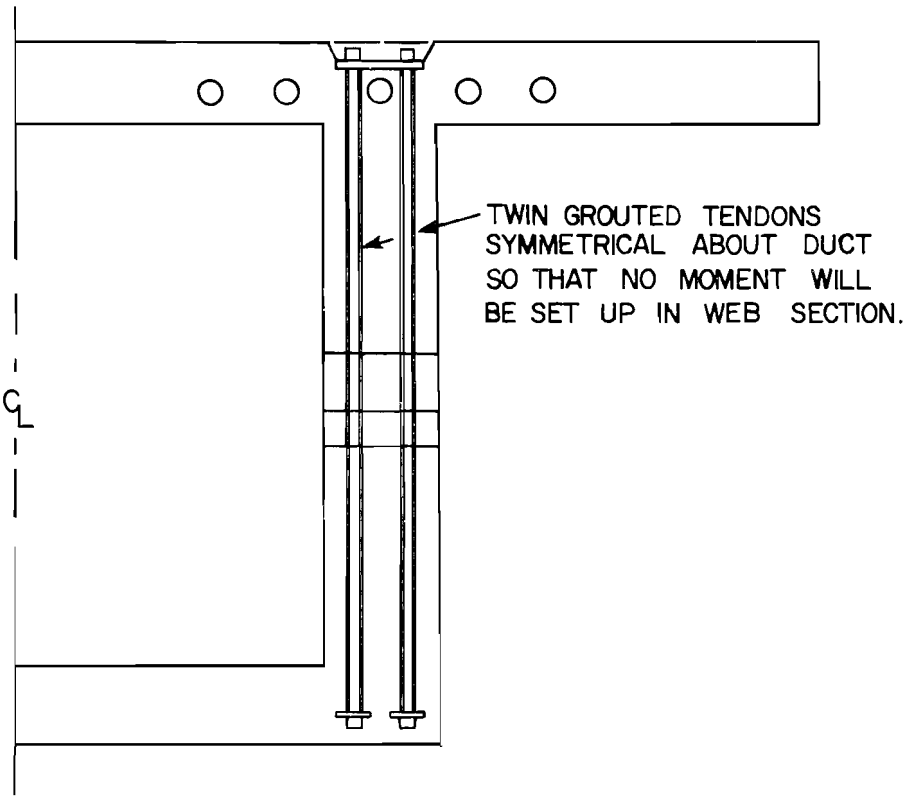

(b) TYPICAL IMPLEMENTATION IN ACTUAL BOX SECTION WEB TO AVOID MOMENT SET UP.

Fig. 2.18 Lateral post-tensioning details

(2) For a lateral post-tension load of 60 kips (100 psi nominal lateral precompression of the web over a length equal to one-half of the section depth [see Fig. 2.18a] for the prototype section of this study) placed at the optimum location, the cracking load was observed to be 33 percent higher than that for an identical specimen without supplementary reinforcement (active or passive). Cracking occurred on a plane following the tendon path, but slightly above it and extended from the loaded face to the web-flange junction. Crack width measurements indicated that the crack initiated in the region of maximum curvature where the widest cracks were observed. Thus, first cracking appeared at a load somewhat lower than that predicted by the program.

(3) Given that the inclined, curved, multiple strand tendon appears to be the worst case for design, it can be seen in Fig. 2.15 that lateral post-tensioning offers the most effective means of raising both the cracking and ultimate loads. Although no LPT tests were done for straight tendons, it seems reasonable to assume that its performance relative to the spiral will be similar.

(4) As only one test was performed with the lateral post-tensioning load at the optimum location, estimates of the expected standard deviation were calculated from the mean variance of the other tests dealing with reinforcement effects. By subtracting twice this deviation from the observed values, the allowable increase in cracking load shown in Table 2.10 was 25 percent above that for the unreinforced curved tendon section. Likewise, the ultimate load increase is 97 percent above that for the unreinforced section. These values pertain to the inclined, curved, multiple strand tendon pattern.

Several additional important points should be made concerning the implementation of lateral post-tensioning (LPT) in practical situations. Upon first consideration it might be assumed that

shrinkage and creep losses would be a severe deterrent to the use of lateral post-tensioning, owing to the short length of the tendon. For the case of a segmental bridge using precast box sections (one of the most likely situations to need LPT), three considerations make LPT highly practical and easy to implement:

(1) Since most segmental bridges are now built using fast-track procedures, the precast box segments are constructed well before they are erected. This reduces shrinkage problems to a minimum, since nearly all losses due to shrinkage occur in the first 100 days from the date of casting.

(2) A lateral prestress load capable of raising the cracking load by 33 percent only required 100 psi compression across the web section. At this pressure, creep losses are small.

(3) Losses at the LPT anchorage due to slip associated with seating the chucks can be minimized by using a positive seating method such as a secondary jack for pressing the wedges in before the load is released from the stressing jack. Alternatively, threaded bar-type tendons with lock-off nuts can be used.

Grouted tendons are recommended to prevent possible loss of the tendon should a failure occur at the anchorage sometime after stressing.

CHAPTER 3

DESIGN CRITERIA AND PROCEDURES

3.1 Introduction

The design engineer has two general approaches available for the design of post-tensioned anchorage zone reinforcement. These are:

(1) To design the section geometry and supplementary anchorage zone reinforcement so that cracking will not occur at maximum stressing load levels.

(2) To allow anchorage zone cracking to occur during stressing but to provide proper reinforcement so that crack widths at the stressing load will not exceed an allowable value selected to minimize the possibility of water penetration and corrosion.

In either case the anchorage ultimate load capacity must be kept well above the cracking load to ensure adequate safety and to give warning of structural distress well in advance of failure.

In this chapter specific methods of predicting cracking and ultimate loads are presented based on a comprehensive regression analysis of the test data and on the indications of the 3D-FEM analysis procedures. A limit state design philosophy with appropriate factors of safety for cracking and ultimate loads is presented. Suggested code and commentary language is presented and several design examples are included to illustrate the procedures suggested.

3.2 Cracking Load Prediction

A step-wise linear regression analysis considering all geometric variables in the test program was performed using the results [2] of the 20 tests for which no supplementary anchorage zone reinforcement was provided. Both model and full-scale data were included.

Using the data from Table 3.1 a large number (approximately 50) of variable combinations were examined. The regression analysis was performed interactively using the program STEP 01 (available at The University of Texas at Austin) and a CDC Cyber 750/175 computer. In this manner a large number of runs could be made efficiently and the variables with low statistical meaning were gradually eliminated. The primary goal of the regression study was to minimize the mean standard error which is a measure of the difference between the measured and calculated cracking loads, using a reasonable expression. The resulting general cracking equation is expressed as a function of six major variables. Elimination of any of these variables made major and undesirable changes in the correlation. The resulting expression is:

$$\begin{aligned} P_{cr_{(plate)}} &= 0.7928(2at)f_{sp} - 9.0965 - 6.913t + 19.3894(2a') \\ &+ 33.228f_{sp} - 48.762(2a'/t)^2 f_{sp} - 4.9848tf_{sp} \\ &- 0.0247297\theta t^2 - 22.891(e/2a)t + 6.2175(e/2a)t^2 f_{sp} \end{aligned} \tag{3.1}$$

where, as shown in Fig. 3.1:

$P_{cr_{(plate)}}$ = plate anchor cracking load in kips for section without supplementary anchorage reinforcement

e = eccentricity (in.) (always assumed positive)

2a = section height (in.)

2a′ = width and depth of bearing plate (assumed square, in.)

t = section thickness (in.)

θ = tendon inclination at loaded face (degrees) (always assumed positive)

f_{sp} = split cylinder tensile strength (ksi)

For convenience in use, an equivalent form of Eq. 3.1, with simpler coefficients, was developed as follows:

TABLE 3.1

REGRESSION ANALYSIS DATA

Case	Specimen	P_{cr}	t	2a'	f_{sp}	2a	e	θ
1	MR1A	39	3	2.625	0.723	20.5	0	0
2	MR1B	43	3	2.125	0.725	20.5	0	0
3	MI1B	41	3	2.125	0.697	20.5	0	0
4	MI2	30	3	2.625	0.582	20.5	0	30
5	FS1A	400	12	8.5	0.451	82	0	0
6	FS1B	400	12	10.5	0.401	82	0	0
7	FS2B	330	12	10.5	0.455	82	0	30
8	M7A-4	15	3	2	0.327	20	3	0
9	M7C-4	32	3	2	0.548	20	3	0
10	M1A-4	18	3	2	0.495	20	6	0
11	M8B-4	31	3	2	0.707	20	6	0
12	M1-2	43	4	2	0.627	20	0	0
13	M2-2	34	3	2	0.627	20	0	0
14	M3-2	24	2	2	0.627	20	0	0
15	M3-2R	18	2	2	0.460	20	0	0
16	M2A-4	22	4.5	2	0.495	20	6	0
17	M1A-4	18	3	2	0.495	20	6	0
18	FS2A	440	12	10.5	0.532	82	0	15
19	M1-3	28	3	2	0.610	20	0	30
20	M2-3	32	4.5	2	0.637	20	0	30

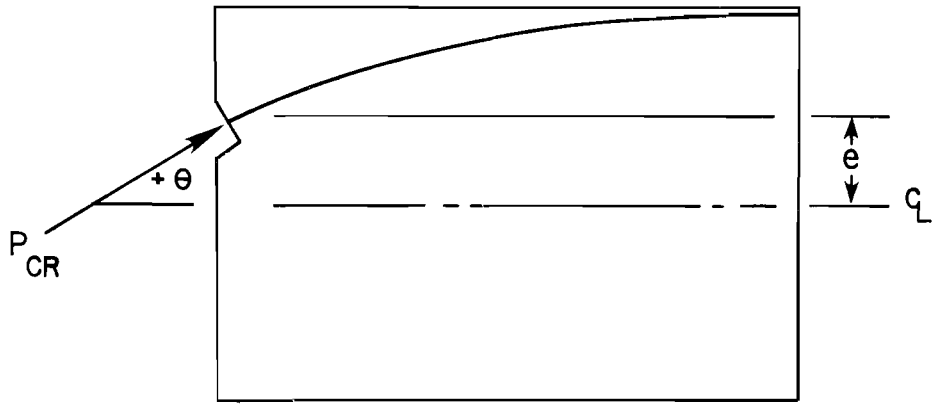

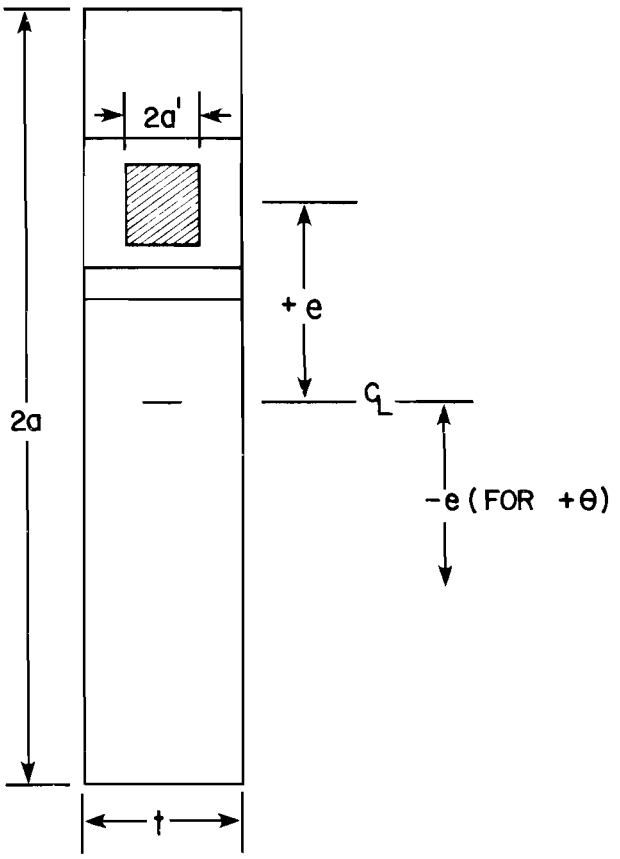

Fig. 3.1 Geometric data for Eqs. 3.1 and 3.2

$$P_{cr_{(plate)}} = t\left[\frac{f_{sp}}{24}(38a - 120) - \frac{t}{81}[2\theta - 252(e/a)f_{sp}] - \frac{103}{9}(e/a) - 7\right] + 39a' + \frac{f_{sp}}{5}[166 - 975(a'/t)^2] - 9.1 \quad (3.2)$$

To demonstrate the accuracy of Eq. 3.2, Table 3.2 compares the measured experimental cracking load against the calculated value. The mean of P_{cr}(test)/P_{cr} (calculated) was 1.004 with a standard deviation of 0.072. As an external check, Eq. 3.2 was used to calculate the expected cracking loads for a number of physical specimen tests performed by Cooper [3] and Berezovytch [12]. The results are shown in Table 3.3. For the 16 comparisons made of these independent tests, the mean value of P_{cr}(test)/P_{cr}(calculated) was 1.127, indicating a moderate conservatism in the calculated values. The standard deviation was 0.23, which is high but not unreasonable given the expected scatter for tests which depend heavily on the tensile strength of concrete specimens.

Equation 3.2 can be used to predict the plate anchor load which will cause cracking in a section without supplementary anchorage zone reinforcement. For those sections which do have supplementary anchorage zone reinforcement, either passive or active, the expected increase in cracking load above that calculated from Eq. 3.2 can be obtained by using the appropriate factor from Table 2.10. This will be discussed further in Sec. 3.2.2.

Equation 3.2 was developed from test results for bearing or plate-type anchors. The results from Eq. 3.2 should be modified for "bell" and "cone" type anchors. Test results reported in Ref. 2 indicate the following factors are appropriate:

TABLE 3.2

REGRESSION ANALYSIS RESULTS--COMPARISON OF PREDICTED AND ACTUAL CRACKING LOADS

Case	Specimen	P_{cr}(test)	P_{cr} (Eq. 3.1)	$\frac{P_{cr}(test)}{P_{cr}(Eq.\ 3.1)}$	P_{cr} (Eq. 3.2)	$\frac{P_{cr}(test)}{P_{cr}(Eq.\ 3.2)}$
1	MR1A	39	42.5	0.9176	42.5	0.9176
2	MR1B	43	42.2	1.0189	42.2	1.0189
3	MI1B	41	41.0	1.0	41.0	1.0
4	MI2	30	31.6	0.9493	31.7	0.9464
5	FS1A	400	401.5	0.9963	400.9	0.998
6	FS1B	400	398.7	1.003	398.4	1.004
7	FS2B	330	330.5	0.998	330.35	0.999
8	M7A-4	15	15.8	0.949	15.8	0.949
9	M7C-4	32	27.4	1.167	27.5	1.163
10	M1A-4	18	18.5	0.973	18.5	0.973
11	M8B-4	31	31.4	0.9873	31.4	0.9873
12	M1-2	43	42.5	1.011	42.3	1.016
13	M2-2	34	36.6	0.929	36.6	0.929
14	M3-2	24	19.7	1.21	19.85	1.21
15	M3-2R	18	18.7	0.962	18.8	0.958
16	M2A-4	22	22.2	0.991	22.1	0.995
17	M1A-4	18	18.5	0.973	18.5	0.973
18	FS2A	440	439.1	1.002	438.8	1.0027
19	M1-3	28	29.2	0.959	29.1	0.962
20	M2-3	32	29.7	1.077	29.6	1.081
				$\bar{X} = 1.0037$		$\bar{X} = 1.0041$
				$\sigma = 0.072$		$\sigma = 0.072$

TABLE 3.3

EXTERNAL CHECK OF EQUATION 3.2

	Specimen	P_{cr} (kips)	f'_c (psi)	# f_{sp} (ksi)	t (in.)	2a (in.)	θ (degrees)	e (in.)	2a' (in.)	(kips) P_{cr} Eq. 3.2	$\frac{P_{cr}(\text{Test})}{P_{cr}(\text{Eq. 3.2})}$
Cooper[3]	Spiral Reinf. No. 1 Set 3	12.6	7480	0.707	1.67	16	28	1.5	1.42	11.52*@	1.09
	Spiral Reinf. No. 1 Set 4	12.1	5550	0.595	1.67	16	28	1.5	1.42	10.11*@	1.19
	LPT Reinf. No. 1 Set 10	19.6	6830	0.661	1.67	16	28	1.5	1.42	16.76*@	1.16
Berezovytch[12]	II-1	37	3160	0.365	3	36	0	0	2	38.96	0.949
	II-2	36	3850	0.403	3	36	0	0	2	33	1.09
	II-3	40	3850	0.403	5	36	0	0	2	52	0.78
	II-4	44	3850	0.403	5	36	0	0	2	52	0.846
	III-1	40	2860	0.347	5	36	0	0	2	45	1.34
	III-2	54.5	2860	0.347	5	36	0	0	2	45	1.21

(continued)

TABLE 3.3 (Continued)

	Specimen	P_{cr} (kips)	f'_c (psi)	# f_{sp} (ksi)	t (in.)	2a (in.)	θ (degrees)	e (in.)	(in.)	Eq. 3.2 P_{cr} (kips)	$\frac{P_{cr}(\text{Test})}{P_{cr}(\text{Eq. 3.2})}$
Berezovytch (12)	III-4	40	2860	0.347	3	36	0	0	2	38	1.05
	III-5	75	4470	0.434	5	36	0	0	2	57	1.31
	III-6	100	4470	0.434	7	36	0	0	2	66	1.51
	III-8	107	4315	0.426	7	36	0	0	2	64	1.6
	IV-1	32	2460	0.323	3	36	0	0	2	35.4	0.904
	IV-2	32.5	2460	0.323	3	35	0	0	2	35.4	0.92
	IV-3	55	3535	0.386	5	36	0	0	2	50.2	1.09

* Modified to account for reinforcement as per section 3.2.2.

@ Anchor laterally eccentric in web. Effective thickness used. (As per Fig. 3.2)

f_{sp} for Cooper's test estimated at $8\sqrt{f'_c}$; $6.5\sqrt{f'_c}$ for Berezovytch's tests.

$\bar{X} = 1.127$

$\sigma = 0.23$

Plate: $P_{cr} = 1.00 P_{cr_{(plate)}}$ (3.3a)

Bell: $P_{cr} = 1.08 P_{cr_{(plate)}}$ (3.3b)

Cone: $P_{cr} = 0.61 P_{cr_{(plate)}}$ (3.3c)

3.2.1 Limitations. Equation 3.3, although intended for general applications, has certain restrictions due to lack of data in some areas. These include:

(1) Inclinations are always assumed positive, as are eccentricities (see Fig. 3.1). Any combination of negative tendon eccentricity (i.e., below the centroid rather than above it) with positive tendon inclination or vice versa is not directly covered. It is likely that in such cases the tendon would have a higher cracking load than when both inclination and eccentricity are positive. However, by using absolute values for angles and eccentricities, Eq. 3.3 should yield conservative solutions for such problems.

(2) Thin web sections are assumed. The limits of the experimental and computer data are for $0.05 \leq t/2a \leq 0.25$.

(3) Multiple tendons anchored in the same web section are not covered. Limited experimental evidence [2] indicates further conservatism is warranted.

(4) The anchorage is assumed to be square. Until further information is available, the shorter edge distance should be used for $2a'$ when rectangular anchors are used (see Fig. 3.2d).

Although not specifically tested in this study, several practical applications should be soluble using Eq. 3.3, and proper consideration of the geometry. These are:

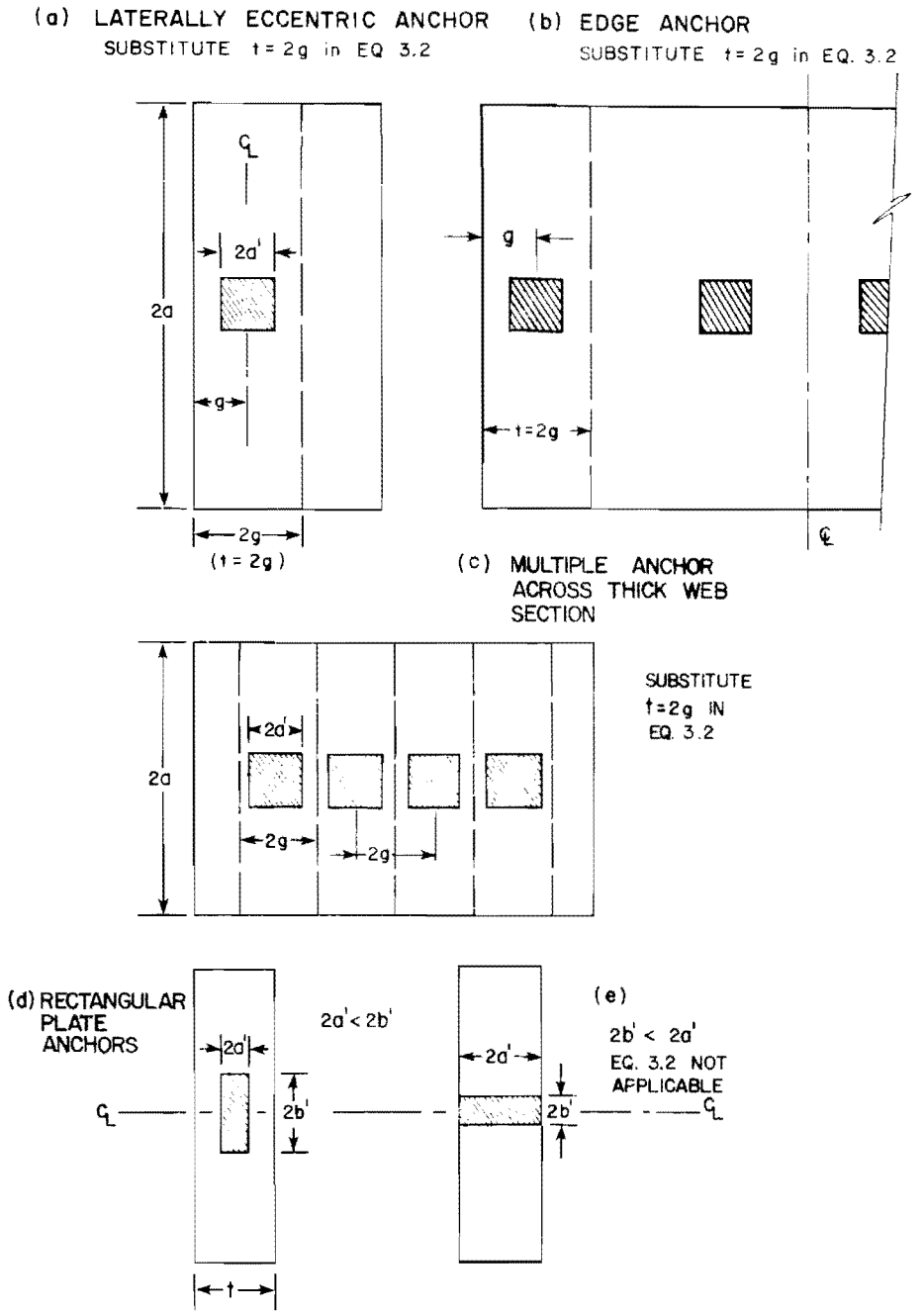

Fig. 3.2 Special cases for Eq. 3.2

(a) Laterally eccentric anchors and edge anchors, particularly in thick web sections.

(b) Multiple anchors across thick web sections.

(c) Rectangular anchor plates oriented such that $2a' < 2b'$.

These cases are illustrated in Fig. 3.2. Figures 3.2a through c indicate that a conservative solution should be obtained by replacing the value t in Eq. 3.2 with the value 2g which equals twice the edge distance or the distance between the anchors. Strip type rectangular anchors such as shown in Fig. 3.2e where $2b' < 2a'$ cannot be accurately handled by Eq. 3.2 without further experimental or analytical investigation. However, rectangular anchors, such as shown in Fig. 3.2d, where $2a' < 2b'$ can be conservatively designed using Eq. 3.2.

For other complex applications, a more exact solution should be obtained as described in Sec. 2.2.6 using a linear elastic, three-dimensional finite element analysis, or by further experimental investigation.

3.2.2 Effect of Supplementary Reinforcement. Cracking loads calculated from Eq. 3.3 represent the minimum value to be expected for a normally reinforced section without supplementary anchorage zone reinforcement. A substantial number of tests dealing with various supplementary reinforcing methods indicated that cracking loads could be raised significantly by the addition of such reinforcement (passive or active). The expected rise in cracking load for a given type of reinforcement was given in Table 2.10. Using these percentage increases and assuming a linear variation between the values for straight and inclined tendons the cracking load for the reinforced anchorage zone is given by:

$$P'_{cr} = (2.03 - 0.032\theta)P_{cr} \qquad \text{Spiral Reinforcement} \qquad (3.4a)$$

$$P'_{cr} = (1.61 - 0.019\theta)_{P_{cr}} \qquad \text{Orthogonal Reinforcement} \qquad (3.4b)$$

$$P'_{cr} = (2.37 - 0.0372\theta)P_{cr} \qquad \text{Active Reinforcement} \qquad (3.4c)$$

where P'_{cr} = the predicted cracking load with supplemental reinforcement (kips)

θ = angle of tendon inclination (degrees)

P_{cr} = cracking load for the section with no supplementary reinforcement as calculated from Eqs. 3.3 and 3.2.

These equations are valid only for reinforcement amounts and locations designed in accordance with Sec. 3.5.3.

3.3 Ultimate Strength Prediction

A review of the ultimate load data for specimens without supplemental anchorage zone reinforcement shows a considerable amount of scatter. Some inclined tendon models developed ultimate loads 60 percent above cracking. Most, particularly among the straight tendon tests, exhibited very brittle behavior with an explosive failure of the anchorage zone occurring at a load coincident with or only slightly above that which caused formation of the tendon path crack. For this reason the ultimate load for an anchor with no supplementary reinforcement should conservatively be equated with the cracking load. The ultimate load, however, is substantially increased for sections containing supplementary reinforcement in the anchorage zone (active or passive), thus providing a desirable margin of safety between cracking and ultimate load. The relative increase in the ultimate load for a given supplementary anchorage zone reinforcing method is presented in Table 2.10. Again assuming a linear variation between the straight and inclined values from Table 2.10, the ultimate load for a given situation can be calculated as:

$$P_{ult} = (3.18 - 0.053\theta)P_{cr} \qquad \text{Spiral Reinforcement} \qquad (3.5a)$$

$$P_{ult} = (1.71 - 0.017\theta)P_{cr} \qquad \text{Orthogonal Reinforcement} \qquad (3.5b)$$

$$P_{ult} = (3.89 - 0.064\theta)P_{cr} \qquad \text{Active Reinforcement} \qquad (3.5c)$$

where P_{ult} = ultimate load for the supplementary reinforced section (kips)

θ = angle of tendon inclination (degrees)

P_{cr} = cracking load for the section with no supplementary reinforcement as calculated from Eqs. 3.3 and 3.2 (kips).

These equations are valid only for reinforcement amounts and locations designed in accordance with Sec. 3.5.3.

3.4 Limit State Design

In general, when a structure or structural element becomes unfit for its intended use, it is said to have reached a limit state [13]. Limit state design is a design process which involves identification of all possible modes of failure (limit states), determination of an acceptable level of safety against occurrence of each limit state and consideration by the designer of the significant limit states. Limit states for the post-tensioned anchorage zone fall into two basic groups:

(1) Ultimate limit states which are related to the structural collapse of part or all of the structure. Such a limit state should have a low probability of occurrence since it may lead to loss of life and major financial losses. Ultimate limit state for the post-tensioned anchorage zone would be evidenced by:

(a) Explosive rupture of the anchorage zone.

(b) Complete side face blow-out of a multiple strand curved tendon at the point of maximum curvature.

(2) Damage limit states which are related to damage of the structure in the form of premature or excessively wide cracks. For the post-tensioned anchorage zone the damage limit state falls into two categories:

(a) If the environment is a hostile one (corrosion and freeze-thaw damage possibilities) formation of any tendon path crack would constitute a damage limit state.

(b) If the environment is nonhostile and minor cracking can be tolerated, the limit state would constitute the load at which crack widths became excessive (greater than about 0.012 in.-0.013 in. as currently implicitly specified).

Since there is less danger of loss of life in the second group, a higher probability of occurrence can be tolerated than in the case of the ultimate limit state.

The design philosophy for these two limit state groups is to arrive at a best estimate of the highest load that will come onto the structure with respect to a particular limit state. This load is then multiplied by an appropriate factor of safety which takes into account possibilities of overload, as well as anticipated variations in the maximum load due to material tolerances. This new load (with safety factor included) must be less than the best estimate of the nominal resistance of the structure to a particular limit state multiplied by a strength reduction factor (ϕ-factor) which takes into account both the undesirability of a particular type of failure, as well as the possibility of material and construction defects (sub-standard concrete, e.g.). Expressed in equation form:

$$(P_{LS})(L.F.) \leq \phi P_{nom_{LS}} \tag{3.6}$$

where P_{LS} = the best estimate of the highest load to come onto the structure at a particular limit state

$P_{nom_{LS}}$ = best estimate of nominal strength of structure with respect to a particular limit state

L.F. = the load factor representing a factor of safety against reaching a particular limit state.

ϕ = strength reduction factor--accounts for material and construction defects and undesirability of a particular limit state.

3.4.1 Limit State Design for Cracking. The maximum permissible specified temporary prestressing load to be applied to any structure is $0.8f_{pu}$, that is to say, 80 percent of the guaranteed ultimate tensile strength of the prestressing tendon. Thus $P = 0.8f_{pu}A_s$, where A_s is the nominal area of the tendon. In practice, a 10 percent overload could occur due to a jacking error such as miscalibration, misreading or overpumping. A 15 percent margin for error above that would constitute a reasonable factor of safety against a damage limit state. Thus, the total load factor recommended is L.F. = 1.25.

On the other side of the inequality is the cracking load from Eq. 3.3 with appropriate modification to account for tendon geometry and supplemental reinforcement. Since Eq. 3.3 was selected as a lower bound prediction, the variance attached to Eq. 3.3 is relatively low, and since quality control is fairly good for prestressed construction, a ϕ-factor of 0.90 is reasonable. Thus

$$P_{nom_{cr}} \geq \frac{(P_{cr})(LF)}{\phi} \geq \frac{(1.25)(0.8f_{pu})(A_s)}{(0.90)} = 1.10f_{pu}A_s \qquad (3.7)$$

3.4.2 Limit State Design for Ultimate. In general considerations of ultimate loading which may come on a structure, there is no practical bound on the upper limit of the load due to misloading. With prestressing forces, the tensile strength of the tendon imposes a practical upper bound. For the ultimate limit state, the nominal maximum stressing load on the structure would be the nominal ultimate capacity of the prestressing tendon ($1.0f_{pu}A_s$). However, this is not the best estimate of the highest load which could come onto the structure. Mill reports and metallurgist recommendations indicate

that the actual steel area for a given tendon could be as much as 2.4 percent above the nominally specified cross-sectional area. Likewise, prestressing steel with a nominally specified ultimate strength of 270 ksi may reach 300 ksi maximum, representing an 11.1 percent rise in strength. Both of these values constitute upper bound limits, ones highly unlikely to occur simultaneously for all tendons in practice. An additional consideration, hard to quantify, is the possibility of a greater number of strands being used than the number specified. This chance seems remote. An appropriate load factor which would account for these effects for ultimate would seem to be about 1.20. This is the value used by CEB-FIP for tendon force. Given the same material and construction quality as before, the capacity reduction factor for ultimate failure should be lower than for cracking, as an explosive anchorage failure may have a disastrous effect on the integrity of the overall structure. For this brittle-type failure, a value of $\phi = 0.75$, similar to that used for spiral columns, is recommended. The design check for ultimate is thus:

$$P_{nom_{ult.}} \geq \frac{1.2 \times f_{pu} A_s}{0.75} = 1.60 f_{pu} A_s \qquad (3.8)$$

3.4.3 Application of Limit State Philosophy. It is anticipated that the application of a reasonable limit state philosophy to post-tensioned anchorage zones will be a controversial subject. A cracking criterion based on a design tendon force of $1.10\ f_{pu} A_{sp}$, as suggested in Sec. 3.4.1, at first glance seems wildly conservative in an industry which takes pride in "load testing" every structure during the post-tensioning process. Yet it is just this "load-testing" that makes the requirement so important. Almost every tendon is loaded to approximately $0.8 f_{pu} A_{sp}$ during jacking. With errors in ram calibration, pressure gauges, and human fallibility, certainly some are loaded beyond that point and probably more than 10 percent beyond. The remaining difference is the "margin of safety" which must not only

account for possible dimensional errors, material understrengths and constructional bloopers like honeycombing, but must provide for the wide variability associated with the imprecision of our knowledge and the general variability of concrete tensile properties.

It is even more important to focus on the ultimate state. The tendon can be called on to develop its full tensile capacity if the structure is overloaded. This tensile capacity is not the guaranteed minimum tensile strength but the actual tensile strength based on actual (not nominal) area and actual tensile properties. The failure of an anchorage may be sudden, explosive, and devastating. A suitable reserve should be provided. The values suggested are actually less than we accept for a ductile beam failure because of the higher confidence in the level of load.

Traditionally in the United States, a consistent design philosophy has not been applied to the anchorage zone. These load levels seem high when compared to what we have used. In the CEB-FIP criteria they have been more realistic. They require a load factor on prestress forces of 1.2 and resistance factors on concrete in the anchorage zone of 1.5. Thus, the comparable ultimate load when adjusted for variations in concrete quality control would be equivalent to $0.8f_{pu}A_{sp} \times 1.2 \times 1.5 \times 1.10 = 1.58\ f_{pu}A_{sp}$ which is very close to the $1.60\ f_{pu}A_{sp}$ recommended. Therefore, the limit states recommended are not revolutionary but represent more of a world norm.

3.5 Design Criteria

The various factors affecting the design of post-tensioned anchorage zones in Refs. 1 and 2 and the preceding chapters are restated in terms of specific design criteria in this section. A complete design may follow one of two routes; to not permit any cracks at all to form at service loads, or, alternatively, to permit the formation of cracks at service load but limit their maximum widths. Both routes must satisfy the serviceability and ultimate limit state requirements of Eqs. 3.7 and 3.8.

3.5.1 Crack Free Design. Although in some instances such as for interior members the formation of anchorage zone cracks at service load levels may be acceptable, for the most part they should not be tolerated for reasons of freeze-thaw durability or corrosion threats and for general aesthetics. There are two means of achieving service load level crack free anchorage zone design:

(1) To proportion the segment to remain uncracked with no dependence on supplementary anchorage zone reinforcement using Eqs. 3.3 and 3.7 while providing sufficient supplementary reinforcement to satisfy the ultimate strength requirement of Eq. 3.8.

(2) If, due to geometric restrictions the section would not remain uncracked at the service level stressing load according to Eq. 3.3, then supplementary reinforcing, either active or passive, should be used to raise the cracking load to a level which satisfies the requirements of Eq. 3.7. The expected increase in cracking load above that given by Eq. 3.3 for a given geometric configuration and reinforcing scheme is given by Eq. 3.4. A final check must be made to satisfy the ultimate strength requirement of Eq. 3.8.

3.5.2 Acceptable Crack Design. If for some reason the requirements of Section 3.5.1 cannot be met, it is possible in some cases to maintain service level crack widths within the general AASHTO-ACI acceptable levels (0.013 in.) through the use of supplementary reinforcement particularly lateral prestressing. Due to scatter in the experimental crack width data the assessment of allowable load increases beyond cracking load is difficult. The following data were obtained from examination of Tables 2.11 and 3.4 in Ref. 2.

	$\bar{X}$	σ	$\bar{X}-\sigma$	$\bar{X}-2\sigma$
Straight tendons with spiral reinforcement	36%	14%	22%	8%
Inclined tendons with spiral reinforcement	51%	26%	25%	0
Inclined tendons with 100 psi lateral post-tensioning	25%	5%	20%	15%

where $\bar{X}$ = the mean percent increase in load above the cracking load before crack widths begin to exceed 0.013 in.

The values for the full-scale inclined tendon specimens were calculated from crack width data measured within a distance of $4a'$ from the loaded face, thus inside the range of influence of the supplemental reinforcement. Crack widths at the point of maximum tendon curvature were generally wider at a given load, but since no supplementary reinforcement was provided at that location the results were not usable. Selection of one standard deviation below the mean values implies that with adequate spirals or lateral post-tensioning, nominal cracking loads approximately 20 percent above the cracking loads calculated from Eq. 3.3 can be tolerated with acceptable crack widths. Specimens with orthogonal supplementary reinforcement exhibited unacceptably wide cracks at first cracking and thus no increase is recommended. The more conservative use of a criterion two standard deviations below the mean would indicate that only lateral post-tensioning would give a useful increase in cracking load (15 percent).

Until more extensive experimental evidence is available concerning crack width control in the anchorage zone, the above recommendations must be considered very tentative and the prudent designer should make every effort to use the more certain "no crack" design procedure of Sec. 3.5.1. Should a large overload occur on a section designed for no cracking, an additional buffer would be available (20 percent) before the section would experience severe cracking distress.

3.5.3 Design of Supplemental Reinforcement. In order to obtain the strength increases indicated in Eqs. 3.4 and 3.5, supplementary anchorage zone reinforcement must meet certain minimum requirements.

3.5.3.1 Spiral Reinforcement. Spiral reinforcement for the anchorage zone should be proportioned to ensure that the spiral confinement is sufficient to confine early cracking. In keeping with the general philosophy of limit state design, a strength reduction factor should be applied to the capacity carried by unconfined concrete. In addition, wherever a spiral is required, an arbitrary minimum diameter of 1/4 in. is suggested so that a sturdy unit which will hold its shape is furnished. Thus,

$$A_{sp} \geq \frac{f_l - \phi(0.85f'_{c_i})}{8.2f_s}(Ds) \geq 0.05s_i \qquad (3.9)$$

or for design,

$$A_{sp} \geq \frac{f_l - 0.6f'_{c_i}}{5\, f_y} Ds \geq 0.05s_i \qquad (3.9a)$$

where A_{sp} = the required cross-sectional area of the rod used to fabricate the spiral

f_l = the post-tension design load divided by the area confined by the spiral

$= 4P/\pi D^2$ (psi)

f'_{c_i} = specified compressive strength of concrete at time of stressing (psi)

D = overall diameter of spiral (in.)

s = pitch of spiral (longitudinal hoop spacing) (in.)

f_s = the allowable stress in the spiral steel = $0.6\, f_y$

f_y = spiral yield strength

ϕ = 0.70 for spiral design

See Fig. 3.3a for details concerning spiral geometry.

For design of a spiral based upon Eq. 3.9a, the following recommendations are made:

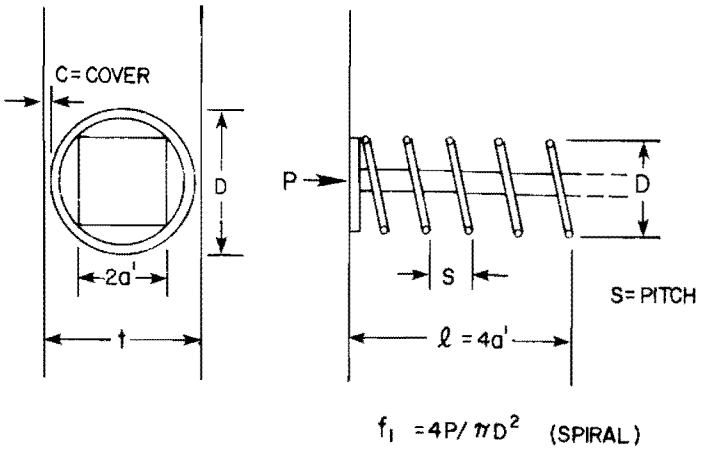

(a) SPIRAL

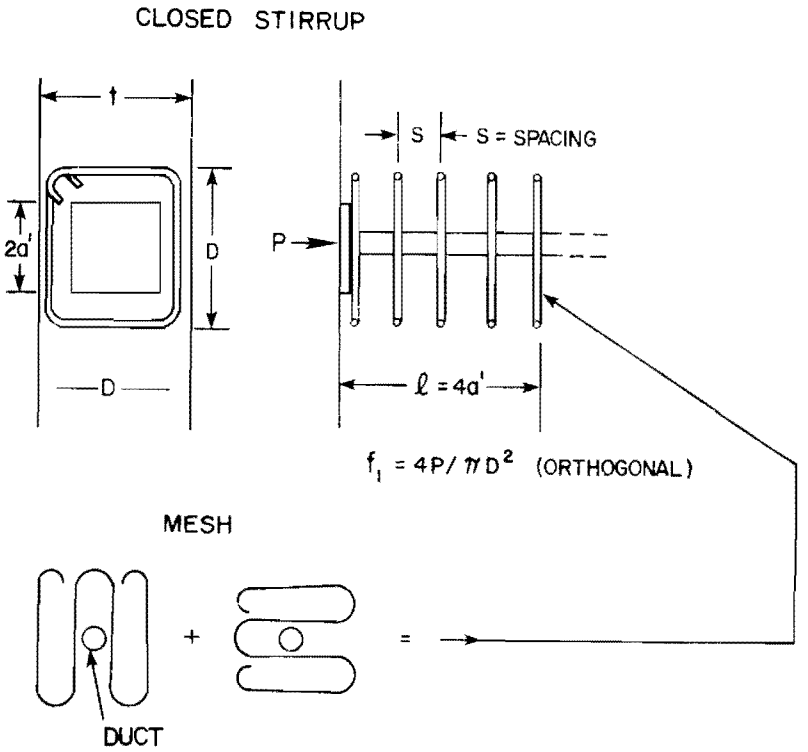

(b) ORTHOGONAL

Fig. 3.3 Passive reinforcement design

(1) The diameter of the completed spiral, D, should be as large as possible within the confines of the web or slab, while still satisfying cover requirements. This recommendation is limited to thin web applications where $0.05 \leq t/2a \leq 0.25$. For tendons located near the side face of thick web sections, the radius of the spiral should be the edge distance less the required cover. For tendons located in the center portions of wider webs, the spiral diameter should be the maximum linear dimension of the anchorage projected bearing surface (or approximately $2a'\sqrt{2}$ for square anchors).

(2) The spiral pitch should be as small as possible, but not less than that required to readily pass the maximum aggregate size used in the concrete mix. The AASHTO Bridge Specifications and ACI Building Code recommend a minimum spiral clear distance pitch of 1 in. or 1-1/3 the maximum aggregate size for column spirals.

(3) The spiral should begin at the anchor bearing plate and the minimum length of the spiral should be $4a'$. Longer spirals affixed to the anchor will not raise the cracking load significantly. The design of spiral reinforcement in regions of tendon curvature to control cracking due to multistrand effects is discussed in Sec. 3.5.3.4.

3.5.3.2 Orthogonal Reinforcement. For passive reinforcement applications where spiral reinforcement cannot be used, an orthogonal grid of closely spaced closed stirrups or a mesh similar to that shown in Fig. 3.3b may be substituted. Since massive amounts of orthogonal reinforcement were shown to have little effect in preventing cracking in the anchorage zone, the required reinforcement can be calculated by using the same procedure and equation presented for spiral reinforcement design in Sec. 3.5.3.1. While this may at first appear unconservative, since it is known that orthogonal reinforcement is substantially inferior to the spiral, the trends presented in Fig. 2.15 clearly show that addition of substantial reinforcement beyond that calculated by Eq. 3.9 is nonproductive.

The only required definition changes from those presented in Sec. 3.5.3.1 are that the spiral diameter, D, becomes the minimum lateral dimension of the orthogonal closed stirrup (see Fig. 3.3b). The desired configurations for confinement are square closed stirrups, or better, a square mesh as shown in Fig. 3.3b. The s term in Eq. 3.9a becomes stirrup spacing, rather than spiral pitch. All other recommendations on placement remain the same as for the spiral.

3.5.3.3 Active Reinforcement. For full utilization of the cracking and ultimate load increases recommended in Eqs. 3.4 and 3.5, active reinforcement in the form of lateral post-tensioning should be designed as follows:

(1) LPT (Lateral Post-Tensioning) tendons should be placed as close as possible to the loaded face and should extend throughout the height of the web.

(2) LPT load levels should be designed to produce a minimum of 100 psi lateral precompression across the web section after losses. Considering the losses to be expected over the short development length, initial stressing should provide between 150 and 200 psi precompression. The lateral precompression stress can be estimated as the total lateral post-tension load divided by a nominal effective area (at) where a is the half height of the web and t is the web thickness (see Figs. 2.18 and 3.6).

(3) LPT tendons should be placed in pairs or as U stirrups with tendons laterally equidistant from the longitudinal tendon duct (see Fig. 2.18) to minimize lateral moments being set up in the web.

(4) LPT tendons should be grouted and should utilize the most positive seating load lock-off mechanism available.

3.5.3.4 Reinforcement for Multistrand Effects. Although no tests were performed in this series to investigate the most effective control measure for multistrand cracking with curved tendons, previous model tests [14] have shown spiral reinforcement to be an

efficient means of control. Until other detailed tests can be performed, the following design method should produce a conservative solution:

(1) Given the internal diameter of the tendon duct and the number of strands to be used, make a scale drawing of the duct with all strands placed as close as possible to the concave side of the duct as would occur when the stressing load is applied. Draw two tangential lines from the center of the duct to the outside of the outermost strands as in Fig. 3.4a. This defines α.

(2) The radial force per unit length, p, as calculated from Eq. 2.7 ($p = P/R$) is assumed to be uniformly applied over the duct bearing arc length between the two lines scribed during step 1. Q is the equivalent uniform pressure along the loaded arc segment, as illustrated in Fig. 3.4b.

(3) The lateral force that would have to be resisted by spiral reinforcing, F, as shown in Fig. 3.4c, can be calculated by a simple equilibrium analysis from $\Sigma F_y = 0$ as:

$$\int_{-\pi/2}^{\alpha-\pi/2} (Qsr\ d\alpha) \cos\alpha - 2F = 0$$

$$Qsr \sin\alpha \Big|_{-\pi/2}^{\alpha-\pi/2} = 2F$$

$$Qsr(1 - \cos\alpha) = 2F$$

$$F = \frac{Qsr(1 - \cos\alpha)}{2} \qquad (3.10)$$

where F = force to be resisted by the spiral (lbs.)

Q = equivalent uniform pressure along the arc segment as calculated in step 2 = $\frac{90P}{R\pi\alpha r}$

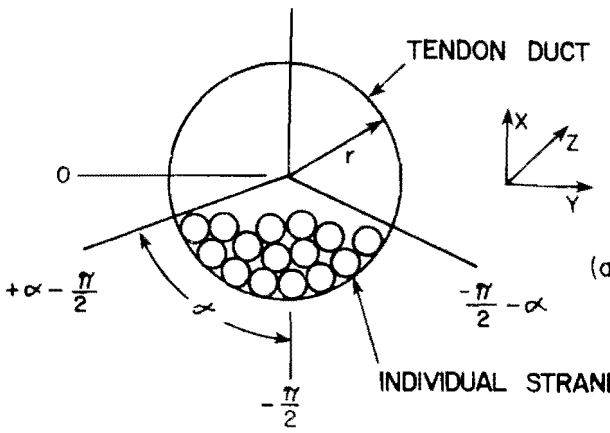

(a) GEOMETRY AT STRESSING LOAD

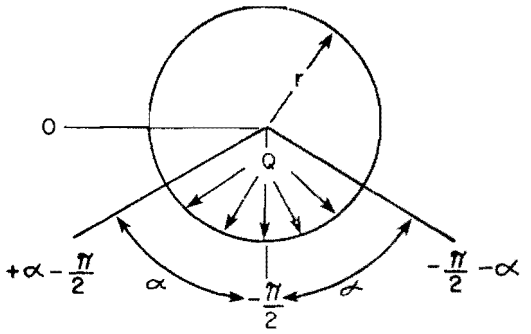

(b) APPROXIMATE LOADING

r = INSIDE RADIUS OF TENDON DUCT

Q = EQUIVALENT PRESSURE

$$Q = \frac{90P}{\alpha \pi r} = \frac{90P}{R \alpha \pi r}$$

$$\text{ARC LENGTH} = 2\alpha \cdot \frac{2\pi r}{360} = \frac{\alpha \pi r}{90} \quad (\alpha \text{ in DEGREES})$$

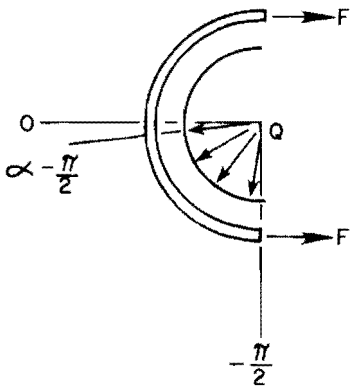

(c) EQUILIBRIUM

$\Sigma F_y = 0$

F = FORCE IN SPIRAL

Fig. 3.4 Spiral confinement for multistrand loading

P = design post-tension load (lbs.)

R = minimum radius of curvature of tendon at critical location (in.)

r = tendon duct radius (in.)

s = pitch of the spiral (in.)

α = 1/2 the loaded arc angle (degree) but not greater than 90°.

If the allowable steel stress in the spiral is given by $f_s = 0.6\, f_y$, then the required rod area to be used in fabricating the spiral would be:

$$A_{sp} = \frac{F}{f_s} = \frac{Qsr(1 - \cos \alpha)}{2f_s} \tag{3.11}$$

Using the expression for Q above

$$A_{sp} = \frac{45Ps(1 - \cos \alpha)}{\pi \alpha R f_s} \geq 0.05 \text{ sq. in.} \tag{3.12}$$

The amount of spiral reinforcement needed to resist the forces set up by the multistrand effect is not excessive. As an example, a 45° inclined, curved tendon with a minimum radius of curvature of 143 in. and duct inside diameter of 2-1/2 in., at a design load of 400 kips, α = 90° (tendon duct 1/2 full), a spiral pitch of 2 in., and an allowable steel stress of $f_s = 0.6f_y = 0.6(60) = 36$ ksi (Grade 60 reinforcement) would require a spiral rod diameter of 3/16 in. In this case the arbitrary minimum size of a 1/4 in. spiral would govern. The spiral hoop diameter, as previously mentioned, should be as large as possible while meeting cover requirements and minimizing placement difficulties.

Spirals to control multistrand effects should be provided throughout any region where significant lateral forces may be set up. This may be conservatively estimated as regions where the nominal shear stress on a horizontal plane through the cover over the tendon would exceed the usual limiting shear diagonal tension stress of $2\sqrt{f'_c}$. This would be where

$$2F_o \geq 2\phi \sqrt{f'_{c_i}}\ (Cs) \tag{3.13}$$

where $2\phi \sqrt{f'_c} = 1.7 \sqrt{f'_{c_i}}$ = nominal shear strength of the concrete (psi)

C = minimum concrete cover on one side of the tendon duct. (in.)

s = spiral pitch (in.)

F_o = lateral force equivalent to that resisted by one leg of a spiral

Combining Eqs. 3.10 and 3.13, the spiral is required throughout those regions where

$$F > F_o \tag{3.14}$$

so

$$Q \geq \frac{2\phi \sqrt{f'_{c_i}}\ C}{r(1 - \cos \alpha)} \tag{3.15}$$

This corresponds to those regions where

$$R \leq \frac{90P(1 - \cos \alpha)}{\pi\alpha C 2\phi \sqrt{f'_{c_i}}} \tag{3.16}$$

This may extend along the tendon for several web thicknesses on either side of the point of minimum radius of curvature (R). Since the designer would use the tendon force P in his calculations, Eq. 3.16 may be written in terms of a side face cracking load, P_o as

$$P_o = \frac{2\phi \sqrt{f'_{c_i}}\ CR\pi\alpha}{90(1 - \cos \alpha)} \tag{3.17}$$

where the minimum value of R should be used and $\phi = 0.85$.

To check the general applicability of these expressions, results of several of the full-scale tests may be examined using $\phi = 1.0$ since all properties are known. For example, specimen FS2B had a 2.5 in. ID duct with a 12 strand 1/2 in. ϕ 270 ksi tendon in a 12 in. wide web. In FS2B the measured P_{cr} was 330 kips, P_{design} was 400 kips, the minimum R was 191 in., α was 67.5°, f'_c was 4627 psi and r = 1.25 in. Thus

$$C = \frac{12 - 2.5}{2} = 4.75 \text{ in.}$$

From Eq. 3.17 with $\phi = 1.0$

$$P_o = \frac{(2.0)\sqrt{4627}(4.75)(191)\pi(67.5)}{90(1 - \cos 67.5)} = 471 \text{ kips}$$

Since $P_{des} = 400$ kips $< P_o$ no side face cracking near the point of minimum radius of curvature would be expected until after anchorage zone cracks had appeared. Similarly, use of Eq. 3.16 would indicate R_o to be 162 in. Since the minimum R was 191 in., $R > R_o$ so no supplementary spiral in the area of maximum curvature is needed. Specimen FS2B did crack in the anchorage zone at 330 kips and did not experience initial side face distress.

For FS4A, first cracking occurred at 400 kips and was definitely due to multistrand effects. A 17 strand 1/2 in. ϕ 270 ksi tendon was used in a 12 in. wide web. The original ductwork was removed to provide extra space so that r = 1.5 in., C = 4.5 in., $\alpha = 90°$ for this case, f'_c was 5200 psi and minimum R = 178 in. Thus from Eq. 3.17 with $\phi = 1.0$

$$P_o = \frac{2\sqrt{5200}(4.5)(178)\pi(90)}{90(1 - \cos 90)} = 363 \text{ kips}$$

Since P_{des} = 567 kips > $P_{o\ initial}$ cracking would be expected to occur in the region of maximum curvature. The 400 kip level at which the cracking occurred is in good agreement with P_o. Equation 3.16 indicates R_o to be 278 in. Since the minimum R was 178 in., a spiral is required in the tendon curvature zone.

In design applications the side face cracking limit state should be checked by using $P_{nom\ cr}$ from Eq. 3.7 for P_o in Eq. 3.17 with ϕ = 1.0 in that expression. In reality such a calculation is only a crude approximation. To achieve ultimate rupture, failure must occur on at least two radial planes connected to the duct (see Fig. 2.8c). This would tend to raise the capacity. Likewise, the use of the value $2\sqrt{f'_c}$ for the limiting shear strength of the concrete in this type application is a very approximate and conservative value. However, the results indicate the use of this model is reasonably consistent with test results. In view of the seriousness of this type failure the provision of spiral reinforcement in areas defined by Eqs. 3.16 and 3.17 is a prudent requirement pending further experimental study.

3.5.4 Anchor Bearing Area. Both the experimental and the analytical results shown in Fig. 2.13 indicated that the cracking load is relatively insensitive to appreciable changes in bearing area and that bearing stress should not be the primary criteria for anchorage zone design. However, it is a useful tool in sizing anchor plates and web thicknesses. In addition, all tests in this investigation were short-term tests and did not reflect possible creep effects at extremely high stressing levels.

Comparison of the results of this study with the various specification trends indicated in Fig. 2.13 show that agreement is much better when an increase in anchorage bearing stress is allowed for increased concrete surrounding the anchor. Thus, AASHTO should consider adoption of an expression similar to ACI and CEB-FIP. As

suggested in Sec. 2.3.3, an effective bearing stress design criterion for post-tensioned anchorages is:

$$f_{b_{all}} = 0.8\, f'_{c_i} \sqrt{A_2/A_1} \leq 1.33\, f'_{c_i} \qquad (3.18)$$

where f_b = permissible concrete bearing stress under the anchor plate of post-tensioning tendons

A_1 = bearing area of anchor plate

A_2 = maximum area of the portion of the anchorage surface that is geometrically similar to, and concentric with, the area of the anchor plate

f'_{c_i} = compressive strength of concrete at time of initial prestress.

3.6 Suggested Code or Specification Requirements

The general design criteria and recommendations contained in Secs. 3.4 and 3.5 are difficult to reduce to simple, concise language suitable for direct inclusion in regulations such as the AASHTO Specifications or the ACI Building Code. The provisions are best expressed as general performance requirements in the Specification or Code but with accompanying commentary indicating possible ways of satisfying the performance requirements.

Section 3.6.1 contains suggested performance requirements and Section 3.6.2 provides more detailed commentary text to assist designers and fabricators in meeting these requirements.

3.6.1 Code Provisions

A.0 Notation

A_{ps} = nominal area of post-tensioning tendon (in.^{2})

f_{pu} = specified tensile strength of prestressing tendons (psi)

A.1 Post-Tensioned Tendon Anchorage Zones

A.1.1 Reinforcement shall be provided where required in tendon anchorage zones to resist bursting, splitting, and spalling forces. Regions of abrupt change in section shall be adequately reinforced.

A.1.2 End blocks shall be provided where required for support bearing or for distribution of concentrated prestressing forces.

A.1.3 Post-tensioning anchorages and supporting concrete shall be designed to resist maximum jacking forces for strength of concrete at time of prestressing.

A.1.4 Post-tensioning anchorage zones shall be designed such that the minimum load producing cracking along the tendon path shall be at least equal to $1.10\ f_{pu}A_{ps}$.

A.1.5 Post-tensioning anchorage zones shall be designed such that their minimum strength shall be at least equal to $1.60\ f_{pu}A_{ps}$.

A.1.6 Supplementary anchorage zone reinforcement required for control of cracking or development of minimum strength may consist of passive reinforcement such as spirals or orthogonal closed hoops or mats. Active reinforcement such as lateral post-tensioning may be used.

A.1.7 Supplementary reinforcement such as spirals shall be provided to resist web face rupture in regions of high tendon curvature when multiple strand tendons are used.

A.1.8 Unless structural adequacy is demonstrated by comprehensive tests or a more comprehensive analysis, anchorage bearing stress at $1.1\ f_{pu}A_{ps}$ shall not exceed

$$f_b = 0.8f'_{c_i}\sqrt{A_2/A_1} \leq 1.33f'_{c_i}$$

where f_b = maximum concrete bearing stress under the anchor plate of post-tensioning tendons

A_1 = bearing area of anchor plate

A_2 = maximum area of the portion of the anchorage surface that is geometrically similar to, and concentric with, the area of the anchor plate.

f'_{c_i} = compressive strength of concrete at time of initial prestress.

3.6.2 Commentary

C.A.1 The general problems of anchorage of post-tensioned tendons are significantly different from the development of pretensioned reinforcement. Items concerning pretensioned element anchorage zones such as now included in AASHTO Sec. 1.6.15 should be put in a separate section.

C.A.1.1 This general performance statement alerts the user to the fact that the actual stresses around post-tensioning anchorages may differ substantially from those obtained by means of usual engineering theory of strength of materials. Consideration must be given to all factors affecting bursting, splitting, and spalling stresses. A refined strength analysis should be used whenever possible considering both the cracking and ultimate limit states.

C.A.1.2 Where convenient, widening of the anchorage region to distribute the high localized forces is an effective way of reducing bursting and spalling stresses and raising the cracking and ultimate capacities. The effect of increased width is indicated in Eq. A in Sec. A.1.4.

C.A.1.3 In application of all anchorage zone design the level of prestress applied and the concrete strength at time of application must be considered. This is particularly important with stage prestressing.

C.A.1.4 It is highly desirable that the anchorage zone remain uncracked at service levels to protect this vital area from corrosive and freeze-thaw deterioration. This can be ensured by proportioning the anchorage zone so that the cracking load is greater than any anticipated stressing load. In this proportioning the anchor zone can be designed to remain crack free without supplementary anchorage zone reinforcement by use of Eqs. A through D. The zone can be designed to remain surface crack free through provision of supplementary reinforcement which will raise the level of the cracking loads as indicated by Eqs. E through G. The service load level specified $1.10\ f_{pu} A_{ps}$ contains allowances for jacking errors, material tolerances, and a margin of variability.

C.A.1.4.1 Cracking Loads. The cracking load for thin web post-tensioned sections without supplementary anchorage zone reinforcement can be determined for certain conditions as:

$$P_{cr} = t\left[\frac{f_{sp}}{24}(38a - 120) - \frac{t}{81}[2\theta - 252(e/a)f_{sp}] - \frac{103}{9}(e/a) - 7 + 39a' + \frac{f_{sp}}{5}[166 - 975(a'/t)^2] - 9.1\right] \quad (A)$$

where P_{cr} = cracking load in kips

e = tendon eccentricity (in.)

$2a$ = section height (in.)

$2a'$ = width of anchor plate (assumed square, in.)

t = section thickness (in.)

θ = tendon inclination at loaded face (degrees)

f_{sp} = split cylinder tensile strength (ksi) may be estimated as $6.5\sqrt{f'_c}$ psi)

All variables are illustrated in Fig. A.1 (Fig. 3.1 in text, not repeated). Limitations on the use of Eq. A assume

a. e, θ are both positive as defined in Fig. A.1
b. $0.05 \leq t/2a \leq 0.25$
c. anchors are assumed square, plate type
d. single tendon anchored in the web.

The equation can be easily extended to other practical applications as shown in Fig. A.2 (Fig. 3.2 in text, not repeated).

For sections which do not meet the above criteria cracking loads can be obtained using three-dimensional finite element analysis techniques, or by comprehensive physical tests.

The cracking load can be calculated from a three-dimensional finite element computer analysis which has been calibrated to extensive physical tests. One such calibration indicates:

1. The maximum spalling strain (transverse tensile strain parallel to the loaded face) at the anchor plate edge must be calculated. For most cases this will require a detailed mesh refinement in the vicinity of the anchor plate edge following a preliminary analysis with a coarse grid. This is particularly necessary for inclined tendon blockouts with square corners. Anchorage zone reinforcement need not be modeled for this analysis.

2. The peak spalling strain corresponding to a load of 1 kip should be computed. The approximate cracking load (for a section without supplementary reinforcement) can be calculated as follows:

$$P_{cr} = \frac{\epsilon_{cr}}{\epsilon_{1\ kip(FEM)}} \qquad (B)$$

where P_{cr} = cracking load (kips)

ϵ_{cr} = threshold cracking strain ($\mu\epsilon$)

$\epsilon_{1\ kip(FEM)}$ = peak spalling strain at plate edge from program with unit post-tension load of 1 kip.

Calibration studies indicate that appropriate values of ϵ_{cr} are 172 $\mu\epsilon$ for plate anchors with straight tendons and 1092 $\mu\epsilon$ for plate anchors with inclined tendons in which a right angle blockout is used.

For other than plate bearing-type anchorages, the cracking loads obtained from Eqs. A and B should be modified as follows:

Conical Anchor $P_{cr} = 0.61\ P_{cr}$ (plate) (C)

Bell Anchor $P_{cr} = 1.08\ P_{cr}$ (plate) (D)

These coefficients apply only when the anchorages present approximately the same projected bearing area.

In any physical tests to determine cracking loads, the conditions to be expected during construction of the actual structure must be replicated as precisely as possible. These include the effects of tendon eccentricity, inclination, curvature and multiple strands, as well as anchor size, section width and height, and supplementary reinforcement.

C.A.1.4.2 Effect or Reinforcement on Cracking --Cracking loads as calculated from Eqs. A through D represent the minimum value to be expected for a section with no supplementary reinforcing in the anchorage zone. The addition of supplementary reinforcing will raise both the cracking and ultimate load. For sections provided with spiral, orthogonal, or active reinforcement designed in accordance with A.1.4.6, the cracking load can be determined as

Spiral Reinforcement: $P'_{cr} = (2.03 - 0.032\theta)P_{cr}$ (E)

Orthogonal Reinforcement: $P'_{cr} = (1.61 - 0.019\theta)P_{cr}$ (F)

Active Reinforcement: $P'_{cr} = (2.37 - 0.0372\theta)P_{cr}$ (G)

where P'_{cr} = cracking load for the reinforced section (kips)

θ = angle of tendon inclination (degrees)

P_{cr} = cracking load for the unreinforced section as calculated above (kips)

C.A.1.5 The proper development of the post-tensioning force in unbonded tendons and prior to completion of grouting in bonded tendons is completely dependent on proper anchorage of the tendons. The anchorage capacity must be greater than any anticipated tendon load with a reasonable factor of safety. The capacity specified 1.60 $f_{pu}A_{ps}$ contains allowance for tendon tolerances, actual strength range rather than guaranteed minimum strength, and a margin of safety against the explosive type failure which would occur if an anchorage zone failed.

The ultimate load for sections without supplementary anchorage zone reinforcement is conservatively assumed to be equal to the cracking load. With the addition of reinforcement designed according to A.1.6 the ultimate load will be:

No Supplementary Reinforcement: $P_{ult} = P_{cr}$ (H)

Spiral Reinforeement: $P_{ult} = (3.18 - 0.053\theta)P_{cr}$ (I)

Orthogonal Reinforcement: $P_{ult} = (1.71 - 0.017\theta)P_{cr}$ (J)

Active Reinforcement: $P_{ult} = (3.89 - 0.0640\theta)$ (K)

where P_{ult} = ultimate load for the reinforced section (kips)

θ = angle of tendon inclination (degrees)

P_{cr} = cracking load for the unreinforced section as calculated above.

C.A.1.6 In order to obtain the strength increase indicated in Eqs. E through K, supplementary anchorage zone reinforcement must meet the following minimum requirements.

C.A.1.6.1 Spiral Reinforcement--Spiral confinement must be adequate to resist cracking and fully develop the anchorage. To

ensure a sturdy unit the minimum spiral wire diameter is 1/4 in. Minimum spiral area is

$$A_{sp} \geq \frac{f_l - 0.6f'_{c_i}}{5f_y} Ds \geq 0.05 \text{ si}$$

where A_{sp} = spiral wire cross-sectional area, $in.^2$

f_l = post-tension load divided by the area confined by the spiral = $4P_u/\pi D^2$, psi

f'_{c_i} = specified concrete compressive strength at time of stressing, psi

D = overall diameter of spiral, in.

s = pitch of spiral, in.

f_y = spiral yield strength.

In thin webs, the spiral diameter, D, should be as large as possible while still satisfying cover requirements. In general, the spiral diameter should be the maximum linear dimension of the anchor projected bearing surface (the diagonal for square anchor plates). Spiral pitch should be as small as possible but must allow for concrete placement. The spiral should begin at the anchor plate and have a minimum length of twice the anchor plate depth or width, whichever is larger.

C.A.1.6.2 Orthogonal Reinforcement--While spiral reinforcement is usually superior to orthogonal reinforcement, in some applications an orthogonal grid of closely spaced closed stirrups or a mesh of orthogonal bars may be used. The minimum area of bars in such closed stirrups or meshes should be calculated using the expression given in A.1.6.1 with the minimum lateral dimension of the orthogonal closed stirrup or mesh substituted for D and the stirrup spacing substituted for s.

C.A.1.6.3 Active Reinforcement--Lateral post-tensioning (LPT) is highly effective as active reinforcement. Such reinforcement should be designed on the following basis:

1. LPT tendons should be placed as close as possible to the loaded face and should extend throughout the height of the web.
2. LPT tendons should produce a minimum lateral precompression in the anchor zone of 100 psi after losses. Initial stressing should provide 150 to 200 psi. The nominal effective area for stress calculation should be taken as the web thickness times a length equal to half the section height.

3. LPT tendons should be placed in pairs equidistant from the tendon centerline to minimize lateral moments in the web.

4. LPT tendons should be grouted and should utilize the most positive seating load lock-off mechanism available.

C.A.1.7 Reinforcement for Multistrand Effects--For post-tensioning applications with significant tendon curvatures and with multiple strand tendons, a side face failure mechanism may govern the failure of the section. Any time a loaded tendon follows a curved path, normal and friction forces are set up along the length of the duct. In regions of small radius of curvature lateral forces due to the flattening out of the multi-strand tendon under stressing loads can cause tendon path cracking at loads below those which would initiate cracking in the anchorage zone proper. Such cracking will be likely if

$$P_{des} \geq P_o = \frac{2\phi \sqrt{f'_{c_i}}\, CR\pi\alpha}{90(1 - \cos \alpha)}$$

or

$$R_{min} \leq R_o = \frac{90P(1 - \cos \alpha)}{\pi\alpha C 2\phi \sqrt{f'_{c_i}}}$$

where P_{des} = P = the minimum cracking design load ($1.10 f_{pu} A_{ps}$)

P_o = side face cracking load

ϕ = strength reduction factor for shear = 0.85

f'_{c_i} = compressive strength of concrete at time of stressing, psi

C = minimum concrete cover on one side of duct

R = minimum radius of curvature of tendon, in.

α = 1/2 the duct loaded arc angle, degrees (but not more than 90°)

If $P_{des} \geq P_o$ or $R_{min} \leq R_o$ then supplementary reinforcement will be required in the region where $R \leq R_o$. Since the region of minimum radius of curvature is typically some distance removed from the anchorage zone (and the benefit of the supplemental reinforcement there) additional reinforcement must be provided. This can be accomplished most efficiently through the use of spiral reinforcement designed as follows:

1. The radius of curvature along the tendon profile is calculated as:

$$R = \frac{\left[1 + (dx/dz)^2\right]^{3/2}}{\left|d^2x/dz^2\right|}$$

where x is the dependent vertical variable and
z is the longitudinal variable.

Most tendon profiles can be defined by the equation

$$x = Az^3 + Bz^2 + Cz + D$$

The minimum radius of curvature R can thus be calculated.

2. Given the internal diameter of the tendon duct and the number of strands used, make a scale drawing of the duct with all strands placed as close as possible to the concave side of the duct as would occur when the stressing load is applied. Draw two tangential lines from the center of the duct, to the outside of the outermost strand, as in Fig. A.3 (Fig. 3.4 in text, not repeated). This defines α. The area of spiral required is then

$$A_{sp} = \frac{45Ps(1 - \cos \alpha)}{\pi \alpha R 0.6 f_y} \geq 0.05 \text{ sq. in.}$$

General spiral proportioning should follow the requirements in Sec. A.1.6.1. The spiral should extend throughout those regions where $R \leq R_o$ but at least 2t (where t = web thickness) to either side of the point of minimum radius of curvature. Such spiral reinforcement designed for multistrand cracking need not be placed in areas where equivalent or stronger primary anchorage zone reinforcement has already been supplied.

C.A.1.8 Bearing Stress--In many cases the adequacy of anchorage assemblies will have been demonstrated by comprehensive tests or analyses. However, in other cases it is desirable to have a relatively simple method to proportion the size of bearing plates. Comprehensive tests and analyses show the tendon anchorage cracking load is relatively insensitive to bearing area and bearing stress. However, the confinement provided by concrete surrounding the bearing plate does increase the cracking load somewhat. The value of allowable bearing stress given in

Sec. A.1.8 reflects recent test experience and tends to be a conservative bearing stress for use in sizing bearing plates. The expression given represents a slight liberalization over ACI 318-77 values and a substantial liberalization over current AASHTO values for anchors which do not extend fully across the web.

3.7 Illustrations of Design Procedure

3.7.1 Example 1. Assume a preliminary design for a post-tensioned, segmental precast box girder bridge has developed a tendon profile and cross section as shown in Fig. 3.5. The maximum temporary prestress in each web section is 495 kips (tendon has fifteen 1/2 in. diameter 270 ksi strands), and a plate bearing-type anchor 13.25 in.^{2} will be used to anchor the tendon. The compressive strength of the concrete will be 5000 psi within tolerance levels to be expected at the precast yard. Given the above data:

(a) Will the anchor plate satisfy the bearing stress requirements of A.1.8?

(b) Will the section satisfy Sec. A.1.4 and A.1.5 with no supplementary reinforcement?

(c) If the answer to (a) is no

(1) Design a reinforcing scheme that will satisfy all requirements of Secs. A.1.4 and A.1.5.

(2) Redesign the section for no cracking with no supplemental reinforcement. Then supply a suitable passive reinforcing scheme to meet ultimate strength requirements.

(d) Since the tendon is curved, check to see if the section satisfies A.1.7 (multi-strand effects). Reinforce as needed.

Solution

Available information:

$t = 14$ in. $\quad 2a' = 13.25$ in. $\quad A_1 = (13.25)^2 = 176$

$2a = 120$ in. $\quad \theta = 25$ degrees $\quad A_2 = (14)^2 = 196$

$e = 12$ in. $\quad f_{sp} = 6.5\sqrt{f'_c} = 6.5\sqrt{5000}$

$= 460$ psi $= 0.46$ ksi

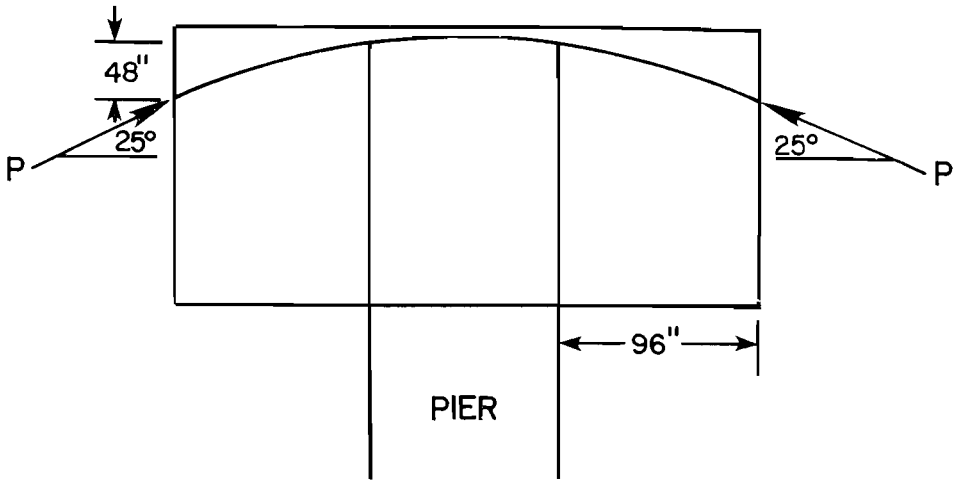

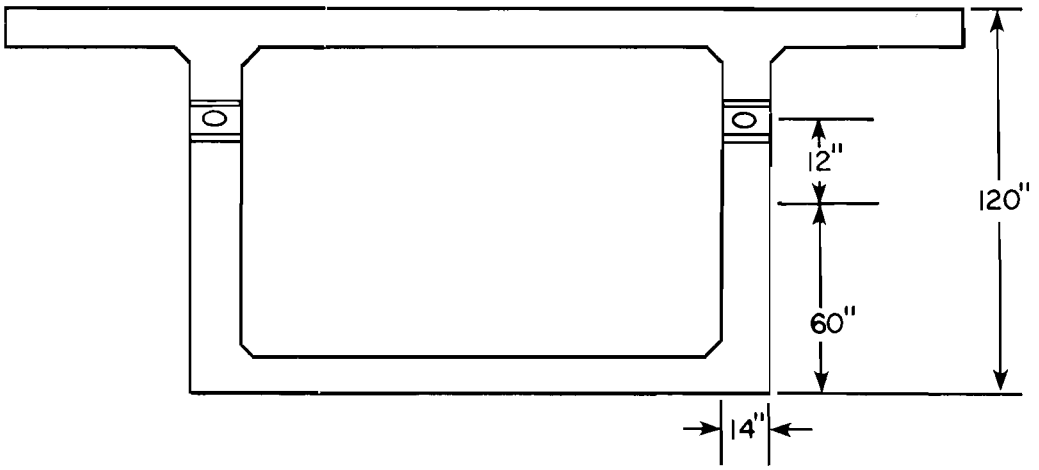

Fig. 3.5 Example 1 cross section and tendon profile

$$P_{nom} = 0.8 f_{pu} A_{ps}$$

$$= 495 \text{ kips}$$

$$1.10\, f_{pu} A_{sp} = 680 \text{ kips}$$

$$1.60\, f_{pu} A_{sp} = 990 \text{ kips}$$

a) Check Sec. A.1.8 Bearing Stress

$$f_b = \frac{1.1 f_{pu} A_{sp}}{A_1} \leq 0.8 f'_{c_i} \sqrt{A_2/A_1} < 1.33 f'_{c_i}$$

$$f_b = \frac{680000}{176} = 3864 \text{ psi} \leq (0.8)(5000)\sqrt{\frac{196}{176}} < 4221 \leq 6620$$

$\therefore$ bearing stress OK

b) Check Sec. A.1 4 Service Level Cracking

$$P = 1.10 f_{pu} A_{sp} = 680 \text{ kips}$$

From Eq. A:

$$P_{cr} = 14\left[\frac{0.46}{24}[38(60) - 120] - \frac{14}{81}[2(25) - 252(12/60)(0.46)]\right.$$

$$\left. - \frac{103}{9}(12/60) - .7\right] + 39\frac{(13.25)}{2} + \frac{0.46}{5}\left[166 - 975\left(\frac{13.25}{2(14)}\right)^2\right] - 9.1$$

$$= 630 \text{ kips}$$

$\therefore$ $P = 680$ kips $> P_{cr} = 630$ kips

Therefore, the section does not meet the cracking strength requirement of Sec. A.1 4.

If spiral reinforcement is provided the new cracking load from Eq. E would be

$$P'_{cr} = (2.03 - 0.032\theta)P_{cr} = [2.03 - 0.032(25)](630)$$

$$= 775 \text{ kips}$$

This is greater than the 680 kips required by Sec. A.1.4, and thus the section will not crack. This spiral reinforcement can be designed as shown later. Alternatively, from Eq. G active reinforcement in the form of lateral post-tensioning will also provide the necessary increase in cracking load:

$$P'_{cr} = (2.37 - 0.0372\theta)P_{cr} = [2.37 - 0.0372(25)]630$$

$$= 907 \text{ kips}$$

which is considerably higher than the required 680 kips. A.1.4 OK if either a spiral or active reinforcement is provided.

c) Check Sec. A.1.5 Minimum Strength

$$P_u = 1.60 f_{pu} A_{ps} = 990 \text{ kips}$$

To meet service load cracking requirements either spiral reinforcement or active reinforcement is required in the section. Therefore the minimum strength check should be made for these cases.

With spiral reinforcement, from Eq. I

$$P_{ult} = (3.18 - 0.053\theta)P_{cr}$$

$$= [3.18 - (0.053)(25)](630) = 1169 \text{ kips}$$

$$P_u = 990 \text{ kips} \leq 1169 \text{ kips} \qquad \text{OK}$$

with active reinforcement, from Eq. K

$$P_{ult} = (3.89 - 0.064\theta)P_{cr}$$

$$= [3.89 - (0.064)(25)](630)$$

$$= 1443 \text{ kips} \qquad \text{OK}$$

Either type of reinforcement must be provided to allow the section to meet A.1.5.

d) Proportion active reinforcement to meet A.1.6.3

The recommended minimum initial lateral precompression of 150-200 psi across the web can be achieved by:

$$0.200 \text{ ksi} = \frac{0.8 f_{pu} A_{ps}}{ta} = \frac{0.8(270)A_{ps}}{(16)(60)}$$

$$A_{ps} = 0.888 \text{ sq. in.}$$

The required area A_{ps} (LPT) can be provided by three sets of 1/2 in. 270 ksi U stirrups with grouted tendons placed so that the resultant load will act as close as possible to the primary load face as shown in Fig. 3.6.

e) Proportion spiral reinforcement to meet A.1.6.1

From Commentary A.1.6.1

$$A_s \geq \frac{(f_l - 0.6f'_{c_i})}{5f_y} (Ds) = \text{cross-sectional area of bar} \geq 0.05 \text{ sq. in. used to fabricate the spiral}$$

where $f_l = 4P_u/\pi D^2 = (4)(990)/\pi(13)^2 = 7460$ psi

$f'_c = 5000$ psi

$D = 9$ in.

$s = 1\text{-}1/2$ in. pitch

$$A_s = \frac{7460 - 0.6(5000)}{(5)(60000)} (9)(1.5) = 0.20 \text{ in.}^2$$

$$d_{bar} = \sqrt{\frac{4(0.20)}{\pi}} = 0.50 \text{ in.}$$

Use 1/2 in. ϕ 60 ksi smooth rod spiral 9 in. overall diameter, at 1-1/2 in. pitch. The length of the spiral should be $4a' = 27$ in.; details as shown in Fig. 3.7.

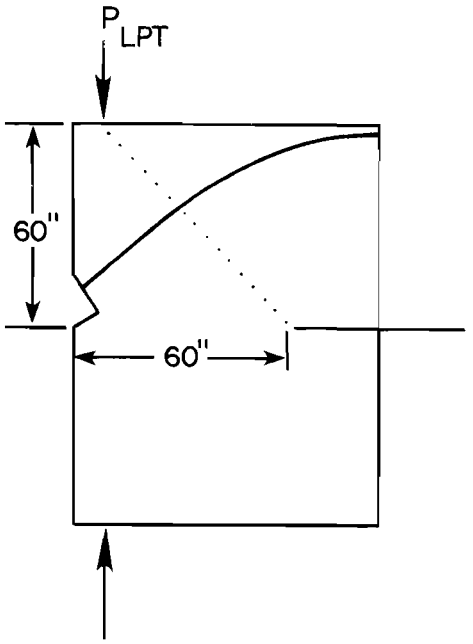

$$\sigma_{\text{Initial LPT}} \cong \frac{P_{LPT}}{\frac{(2a)t}{2}} = 200 \text{ psi.}$$

$$P_{LPT} = .8\,P_{ULT} = 200\text{psi}\,(60)(15)$$

$$P_{ULT} = 240 \text{ kips}$$

USE (3) - 1/2" 270 ksi U GROUTED STIRRUPS

Fig. 3.6 Lateral post-tensioning details

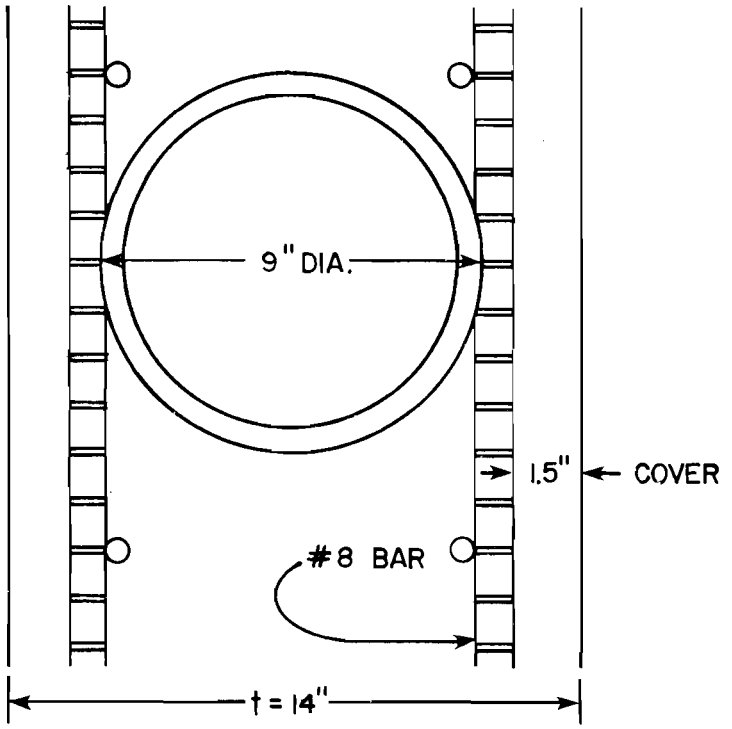

Fig. 3.7 Sizing spiral diameter

f) Check Sec. A.1.7 multistrand effects

The tendon profile shown in Fig. 3.8 can be described by the following equation:

$$x = x_2 - A(z_2 - z)^3 - B(z_2 - z)^2$$

where the boundary conditions are assumed to be:

at x_1 $\theta = 0.436$ radians (25°)

$x = x_1 = 72$ in.

$z = z_1 = 0$ in.

at x_2 $\theta = 0.0$ radians

$x = s_2 = 114$ in.

$z = z_2 = 96$ in.

based upon these assumptions

$$A = \frac{-2(x_2 - x_1)}{(z_2 - z_1)^3} + \frac{\theta}{(x_2 - z_1)^2}$$

$$B = \frac{3(s_2 - x_1)}{(z_2 - z_1)^2} - \frac{\theta}{(z_2 - z_1)}$$

for this problem

$$A = -4.75\ (10)^{-5}$$

$$B = 9.13\ (10)^{-3}$$

substituting these values into the tendon profile equation and differentiating yields

$$x' = -1.425(10)^{-4}(96 - z)^2 + 1.826(10)^{-3}(96 - z)$$

$$x'' = 2.85(10)^{-4}(96 - z) - 1.826(10)^{-3}$$

The radius of curvature is given by

$$R = \frac{\left[1 + [-1.425(10)^{-4}(96 - z)^2 + 1.826(10)^{-3}(96 - z)]^2\right]^{1.5}}{\left|2.85(10)^{-4}(96 - z)^2 - 1.826(10)^{-3}\right|}$$

These values are tabulated in Fig. 3.8. A survey of these values shows that the minimum radius of curvature is 81.9 in. at which point Q is calculated to be 2045 psi for a tendon duct with a diameter of 2.75 in. (the recommended flexible duct for a 15 strand commercial anchor). This minimum value of R can be checked against the expression for R_o in Sec. C.A.1.7

$$R_o = \frac{90P(1 - \cos \alpha)}{\pi\alpha C 2\phi \sqrt{f'_{c_i}}}$$

For 15 strands the duct will be half full so $\alpha = 90°$. $C = 1/2(14 - 2.75) = 5.625$ in. Thus

$$R_o = \frac{(90)(680000)(1 - \cos 90)}{\pi(90)(5.625)(1.7)\sqrt{5000}} = 320 \text{ in.}$$

Thus the spiral to resist multistrand effects is required wherever the curvature radius is less than 320 in. From Fig. 3.8 it can be seen that a confining spiral for approximately 78 in. in horizontal projection extending from the anchor over 80 percent of the curved zone is required.

The spiral area is given by

$$A_{sp} = \frac{45Ps(1 - \cos \alpha)}{\pi\alpha R 0.6 f_y} \geq 0.05 \text{ si}$$

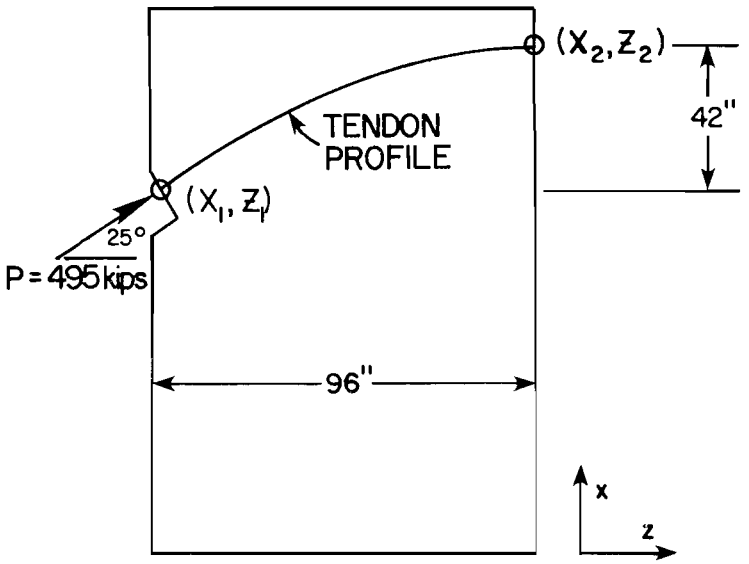

z(inches)	R(inches)	(lb/inch) p = P/R	(psi) Q = p/20r
0	136.1	5319	1231
10	106.8	6779	1568
20	89.7	8071	1867
30	82.3	8497	1965
35	81.9	8840	2045
40	83.7	8649	2001
50	94.98	7621	1763
60	121.	5983	1384
70	179.7	4022	930
80	366.	1978	457
90	547	1323	306

Fig. 3.8 Data for design of spiral reinforcement to resist multistrand cracking

$$A_{sp} = \frac{(45)(680000)(1\text{-}1/2)(1 - \cos 90)}{\pi(90)(82)(0.6)(60000)} = 0.054 \text{ sq. in.}$$

Thus a 1/4 in. diameter spiral rod with a pitch of 1-1/2 in. and an overall diameter of 9 in. should be used.

3.7.2 Example 2. Determine the web thickness required for the box girder in Example 1 if no supplementary reinforcement is to be provided in the anchorage zone at cracking load levels. Determine if supplementary anchorage zone reinforcement is required at ultimate strength levels.

In Example 1 the design cracking load to meet A.1.4 was 680 kips. The original box girder with 14 in. webs had P_{cr} = 630 kips from Eq. A. Thus the cracking load has to be raised (680/630 = 1.08) about 8 percent to satisfy this requirement with no supplementary reinforcement. Of the three major geometric variables (inclination, eccentricity, and cover) the most practical and most effective change in the cracking load can be achieved through modification of web thickness. Since the ultimate capacity of a section with no supplementary reinforcement as indicated by Eq. H is the same as the cracking load, it is obvious that a section designed to just satisfy the cracking load requirement (680 kips) will not meet the ultimate requirements (990 kips) without additional confining reinforcement. Assume that in this case the required increase (990/630 = 1.57) of 57 percent is considered excessive to handle by web thickening. The designer decides to increase the web width to control cracking without relying on confinement, but to provide confinement for ultimate.

On this basis, an approximate web width is selected for trial as 110 percent t = (1.10)(14) = 15.4 in. Thus t = 16 in. is selected as a practical dimension checking Eq. A for:

$t = 16$ in. $\qquad 2a' = 13.25$

$2a = 120$ in. $\qquad \theta = 25°$

$e = 12$ in. $\qquad f_{sp} = 0.46$ ksi

$P_{nom} = 495$ kips $\qquad A_1 = 176$ sq. in.

$1.10 f_{pu} A_{sp} = 680$ kips $\qquad A_2 = 256$ sq. in.

$1.60 f_{pu} A_{sp} = 990$ kips

$$P_{cr} = 16\left[\frac{0.46}{24}((38)(60) - 120) - \frac{16}{81}\left[(2)(25) - (252)\frac{(12)}{(60)}(0.46)\right]\right.$$

$$\left. - \frac{103}{9}\frac{(12)}{(60)} - 7\right] + (39)\frac{(13.25)}{2} + \frac{.46}{5}\left[166 - 975\left(\frac{13.25}{(2)(16)}\right)^2\right]$$

$$- 9.1 = 669 \text{ kips}$$

This is still less than the 680 kips required although it is close. The next practical increase would use a web width t of 18 in. Rechecking Eq. A for t = 18 in. yields $P_{cr} = 712$ kips which satisfies the requirement $P_{cr} = 712 \text{ kips} \geq 1.10 f_{pu} A_{sp} = 680$ kips.

However, with no supplementary reinforcement the section does not satisfy the ultimate load requirement of $1.60\ f_{pu} A_{sp}$. Further widening of the webs to meet this requirement would probably result in webs over 2 ft. wide so it is necessary to include confining reinforcement for satisfying the ultimate conditions. This indicates that most sections will require such confinement so that it might as well be considered for crack control. Using Eq. I for spiral reinforcement

$$P_{ult} = (3.18 - 0.053\theta)P_{cr}$$

$$= (3.18 - (0.053)(25)(712) = 1321 \text{ kips}$$

This more than satisfies the requirement

$$P_{ult} = 1321 \text{ kips} \geq 1.60\ f_{pu} A_{sp} = 990 \text{ kips}$$

For a web width of 18 in., a maximum spiral diameter D of 13 in. can be used. Rechecking the spiral equation

$$A_s \geq \frac{(f_l - 0.6f'_{c_i})}{5f_y} Ds$$

$$A_s \geq \frac{(7460 - 0.6(5000))}{(5)(60000)}(13)(1.5) = 0.29 \text{ sq. in.} > 0.05$$

Thus a 5/8 in. ϕ rod at a pitch of 1-1/2 in. would be required. The larger diameter of 13 in. results in a slightly heavier spiral than in Example 1. Bearing stress would be no problem for this wider web.

Side face multistrand effect confining reinforcement should be rechecked because of the greater side face cover thickness.

Checking R_o for the new cover C = 1/2(18 - 2.75) = 7.625

$$R_o = \frac{(90)(680000)(1 - \cos 90)}{\pi(90)(7.625)(1.7)\sqrt{5000}} = 236 \text{ in.}$$

Since the minimum R is 82 in., a confining spiral is still required. The expression for spiral area is not affected by the cover so a 1/4 in. diameter spiral rod with a pitch of 1-1/2 in. and an overall diameter of 9 in. should be used along the tendon path for approximately 75 in. in the horizontal direction.

3.7.3 Example 3. Suppose that the cracking load is desired for a section identical to that of prototype specimen FS2B (t = 12 in., 2a = 82 in., 2a′ = 10.5 in., f'_c = 5000 psi, e = 0, θ = 30°) with the exception that the angle of inclination θ is to be 45° rather than 30°. Since no experimental data were obtained beyond a 30° inclination, an approximate solution is to be determined using a three-dimensional finite element analysis. In this case the program PUZGAP 3D was used. The mesh used is shown in Figs. 3.9 through 3.13. The rezoned portion of the mesh (indicated by the

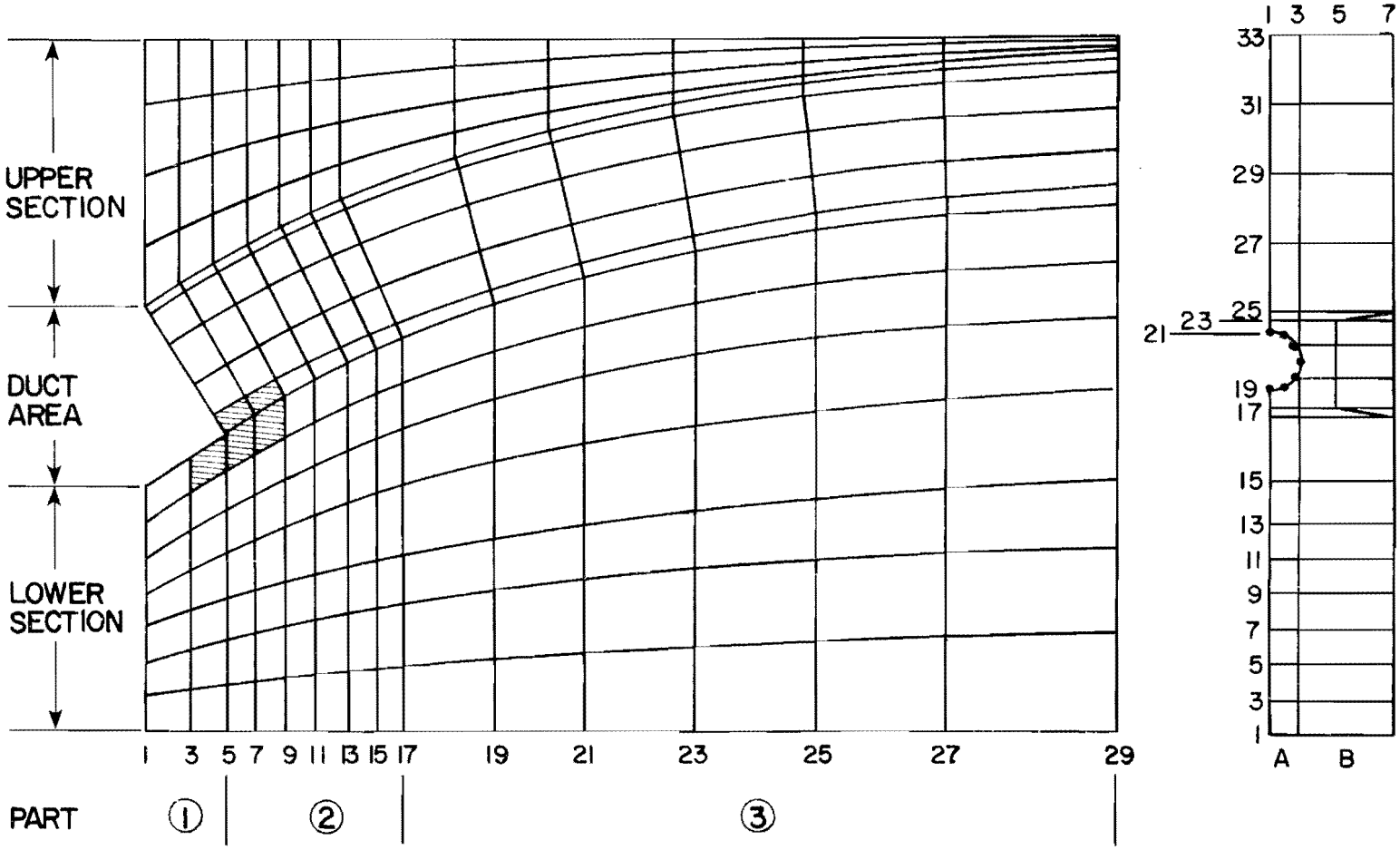

Fig. 3.9 Overall mesh pattern--inclined tendon prototype specimen

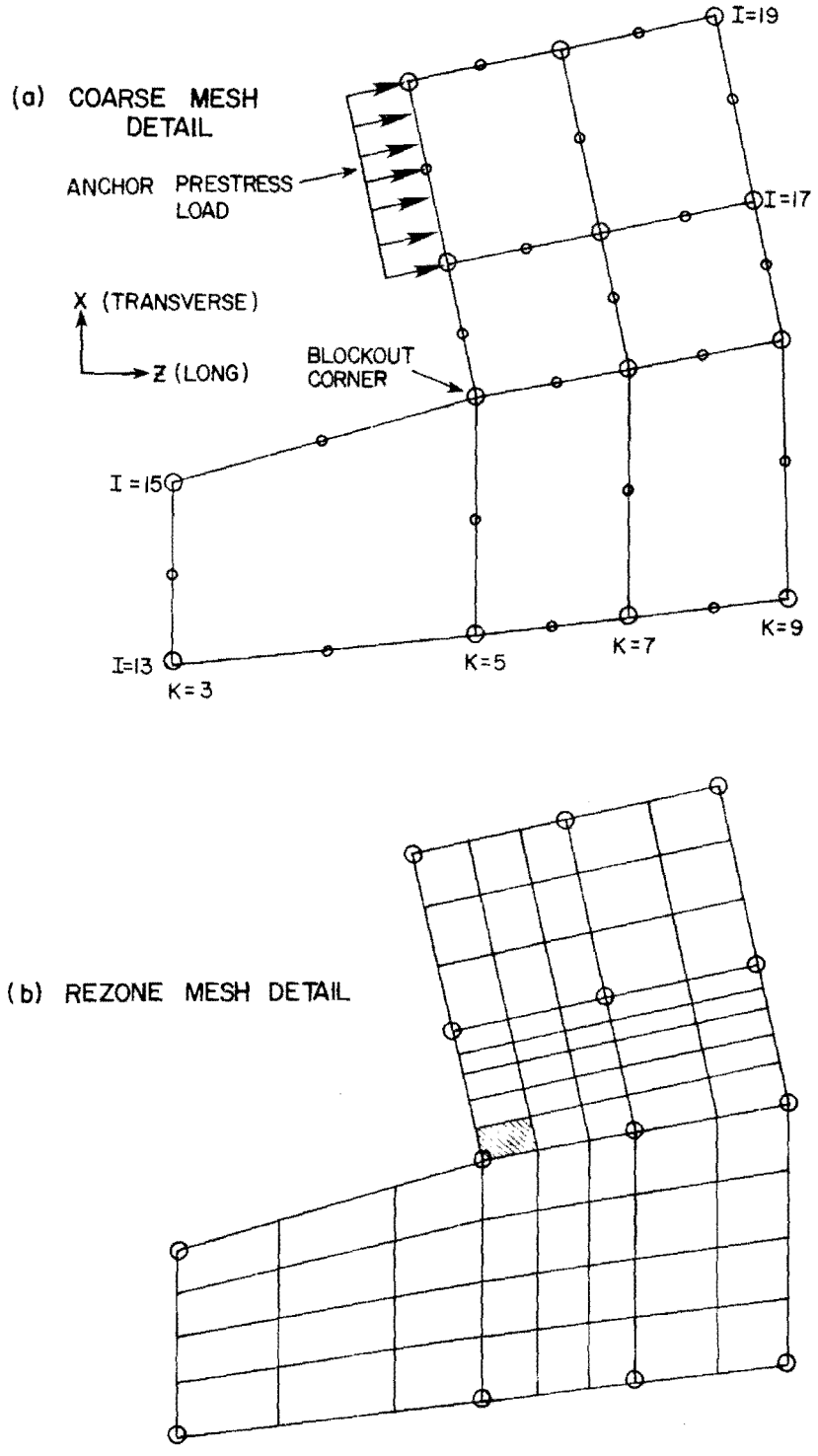

Fig. 3.10 Rezone mesh detail

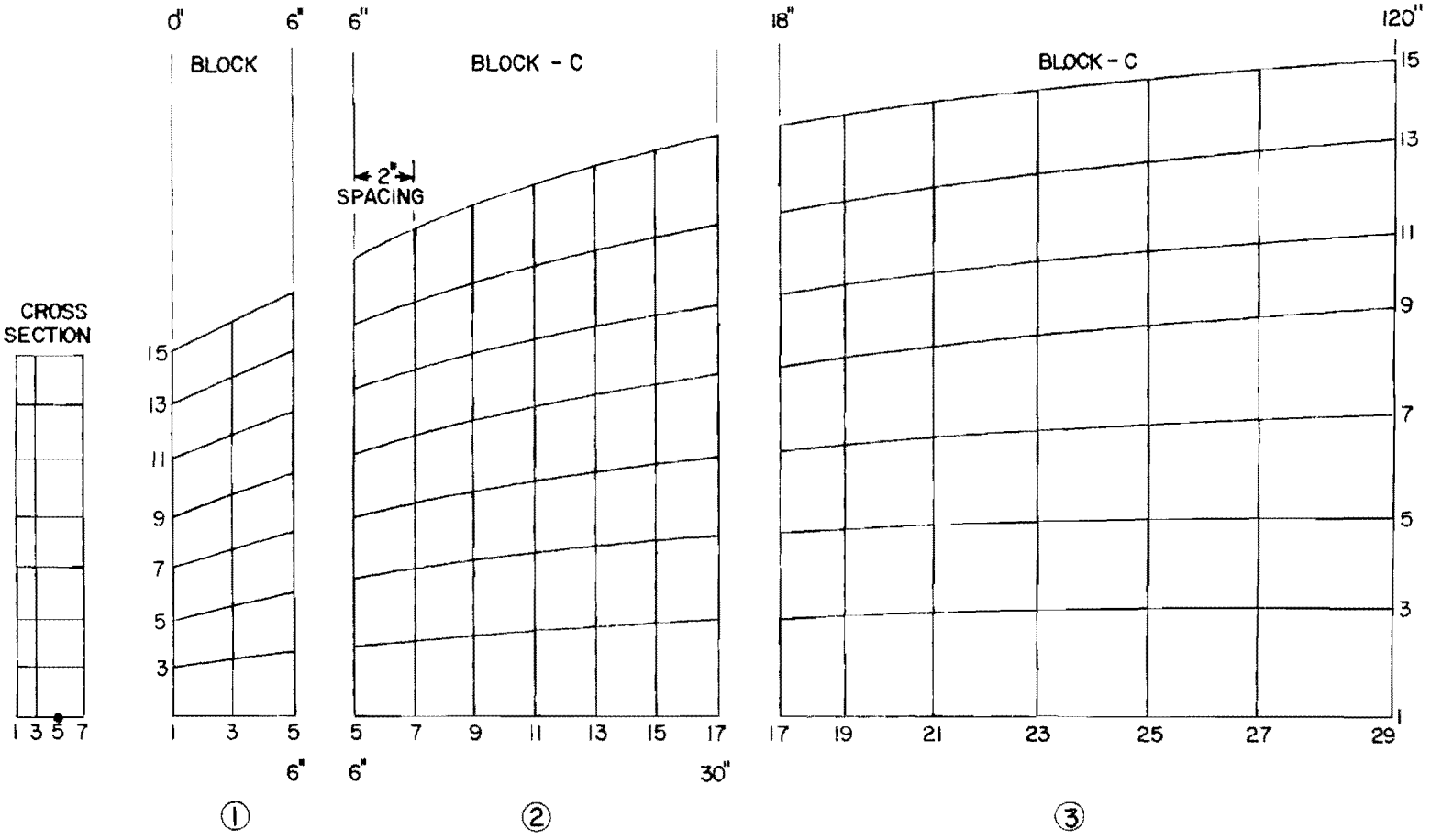

Fig. 3.11 Bottom mesh detail

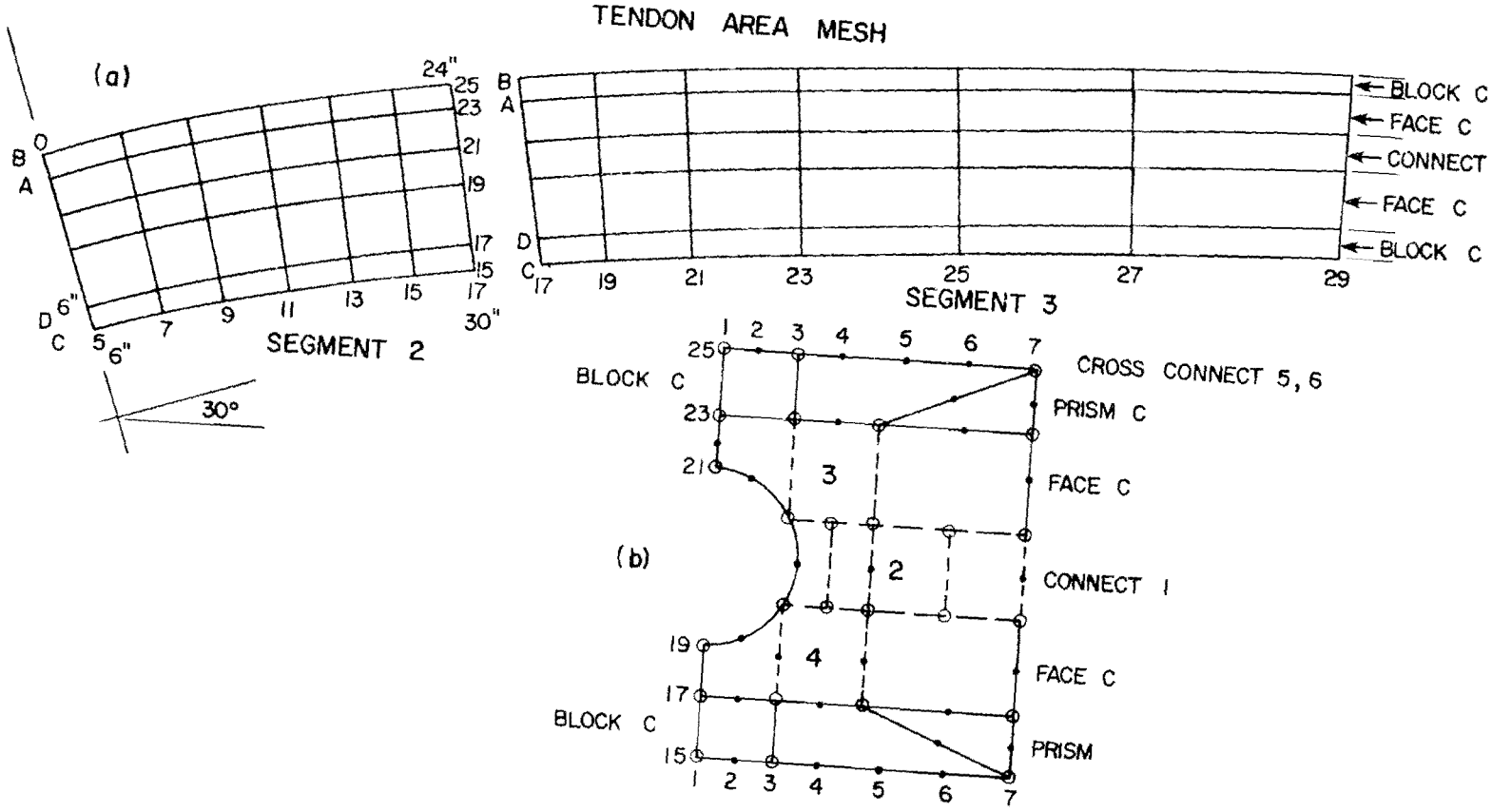

Fig. 3.12 Duct mesh detail

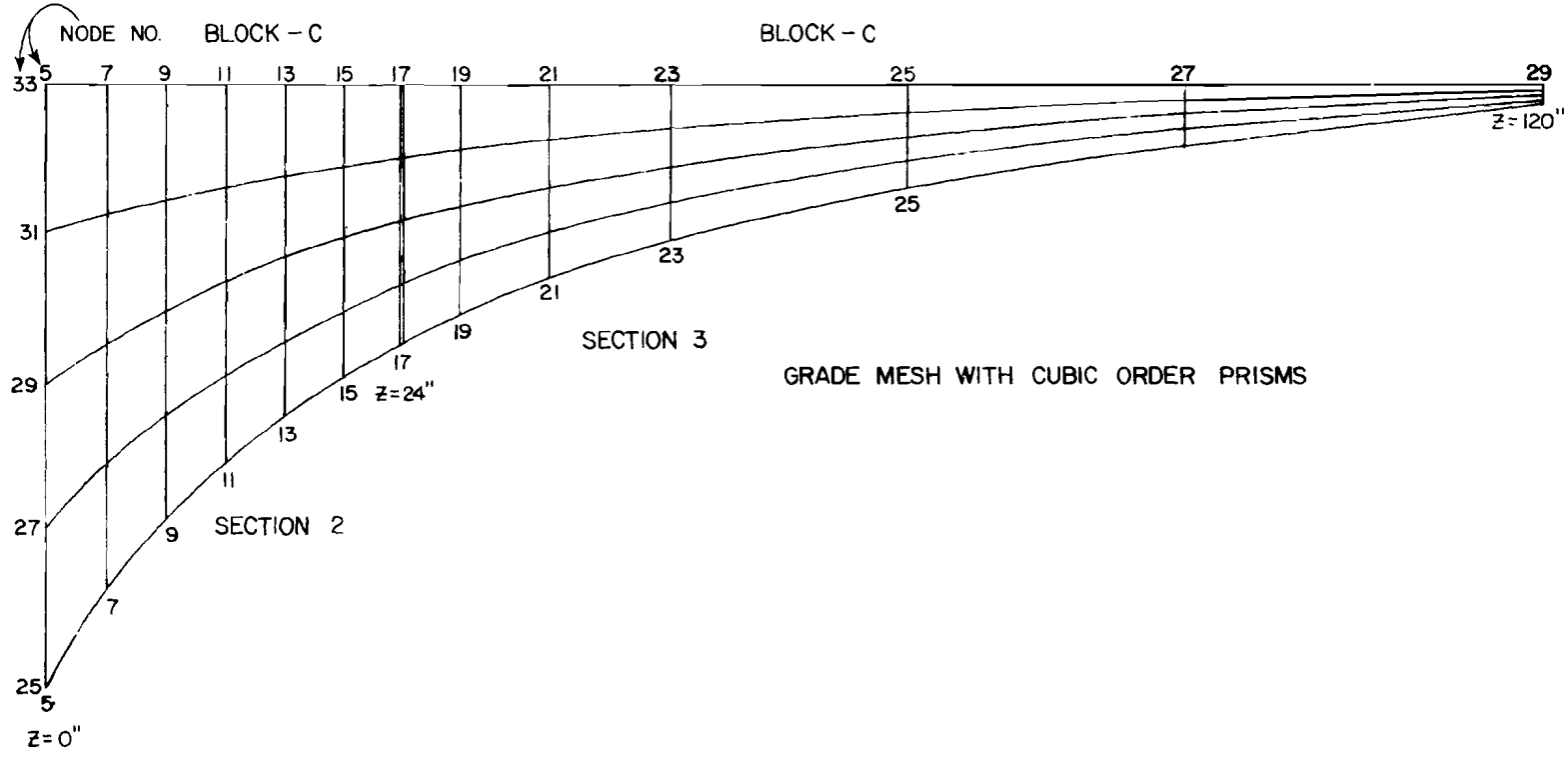

Fig. 3.13 Top mesh detail

shaded area in Fig. 3.9) is detailed in Fig. 3.10. The peak spalling strain calculated was on the shaded element shown in Fig. 3.10b. At a load of 200 kips this value was 1010 microstrain. The unit load value is then 1010/200 = 5.05 microstrain, and the cracking load, as determined from the inclined tendon threshold strain, is: $P_{cr}(45°)$ = 1092/5.05 = 216 kips. For f'_c = 5000 psi the value of f_{sp} is approximately $6.5\sqrt{f'_c}$ = 0.459 ksi. Thus the value of P_{cr}/f_{sp} for $\theta = 45°$ in Fig. 2.12 was calculated as 216/0.459 = 470 (full-scale) or 29.4 (model-scale). ($P_{cr}/2$at f_{sp} = 0.487.) This illustrates the level of detail required in an analysis to extrapolate to other cases.

3.8 Summary

This chapter dealt with the development of a limit state design procedure for proportioning supplemental anchorage zone reinforcement. Two methods were presented. The first is used to design the section to remain uncracked at the maximum temporary post-tensioning load. The second is used to allow cracking at the maximum load, but maintain crack widths within acceptable limits. The former procedure is recommended for conservative design.

The concept of limit state design of the post-tensioned anchorage is discussed and factors of safety are developed with respect to cracking and ultimate load.

A generalized equation based upon regression analysis of experimental data was presented for calculating the expected cracking load for an unreinforced section. The major variables include the tensile splitting strength of concrete, the section width and height, the anchor width, and tendon eccentricity and inclination. The cracking and ultimate load can be increased through the addition of supplemental anchorage zone reinforcement and appropriate factors are presented for calculating the increases to be expected for a given reinforcing scheme. The recommendations are presented in typical Specification or Code and Commentary format. Example problems are solved to illustrate the design procedure.

CHAPTER 4

CONCLUSIONS AND RECOMMENDATIONS

4.1 General

At the inception of this study in 1975 the common American practice for post-tensioned anchorage zone reinforcement design was for the structural designer to specify tendon force and location and to allow the contractor to choose a post-tension system. Both then usually relied on the hardware supplier to furnish detailed advice on the use of the system. Often the suppliers' knowledge was based on limited tests, on practical experience (generally with enlarged cast-in-place end blocks), and on the published work of such investigators as Guyon or Zielinski and Rowe who relied on the classical bursting stress approach to design of supplementary anchorage zone reinforcement.

Although these designs usually worked well for straight tendon applications with little eccentricity, they were insufficient to control anchorage zone cracking in some thin member applications such as in precast segmental box girder bridge web sections. In these applications, the tendons were often not only eccentric, but also highly inclined in order to pick up a portion of the dead load shear. Because of the highly proprietary nature of the industry those companies which did have experience with such problems were often reticent to publish this knowledge in the public literature. American specifications such as AASHTO and the ACI Building Code were framed in very limited terms of allowable bearing stresses, and did not reflect the effects of section aspect ratio, of tendon eccentricity, curvature, and inclination, nor of the effect of supplementary reinforcement.

This investigation provides a starting point for the practicing engineer to address many common thin web post-tensioning applications as well as a separate check method to evaluate the recommendations of the hardware supplier.

The results of this study reflect a composite formed from three sources. These include physical tests of approximately forty quarter-scale microconcrete models, physical tests of nine full-scale prototype concrete specimens designed to replicate post-tensioning conditions found in thin web sections and results of an extensive series of three-dimensional linear elastic finite element computer analyses.

The model test results were found to match the prototype behavior when scaled properly through the use of the geometric scale factor and the measured split cylinder tensile strength of the concrete. A linear regression analysis of the experimental data yielded an empirical equation for the load causing formation of the tendon path crack in sections without supplementary anchorage zone reinforcement. This type of crack has previously been referred to as the "bursting" crack in the literature. These values could then be modified by appropriate factors to yield results where reinforcement was present. The effect of variable trends indicated was also observed in the computer analysis results. The empirical equation for cracking load has the following limitations:

(1) For inclined tendons, the eccentricity e and inclination θ must always be assumed positive.

(2) Thin web sections are assumed. $0.05 \leq \frac{\text{web thickness}}{\text{section depth}} \leq 0.25$.

(3) Multiple tendons anchored in the same web section are not expressly covered.

(4) The anchorage is assumed to be square. Rectangular plates with the long dimension oriented parallel to the web face can also be used. Equivalent areas of circular plates may be used.

For those applications which fall outside these limits, such as multiple tendons, solutions can be obtained from comprehensive three-dimensional finite element analysis programs such as the program PUZGAP using calibration techniques described in Secs. 2.2.6 and 3.6.2.

An extensive strain analysis was performed using both physical strain gage data and the results of the analytical program. Good correlation was found between the predicted and measured strains. The end result of this study was a theory which explains tendon path crack initiation based upon attainment of specified peak spalling strains at the edge of the anchorage. Two threshold spalling strains were presented, one for straight tendon applications and one for inclined tendons where right angle block-outs are used to achieve tendon inclination. The theory agreed well with experimental data over a wide range of variables, and thus was used to extrapolate cracking loads beyond the range of physical test data by use of the 3D FEM analysis.

Various reinforcing schemes (both active and passive) were investigated and a general reinforcement design procedure was developed. Experimental data from the prototype tests revealed an interesting additional failure mechanism due to "multistrand" effects. Sections with significant tendon curvature and with multiple strands in the same duct generated large lateral splitting forces at the point of minimum radius of curvature due to the flattening out of these multiple strands within the confines of the duct. A method of designing reinforcement to resist this effect was presented.

4.2 Major Conclusions

The results of this study indicate a radical departure from previous methods of analyzing the anchorage zone cracking problem which were basically limited to concentric, straight tendon anchors.

For the general range of variables investigated, the major conclusions are:

(1) Design of anchorage zone reinforcement using bursting stress criteria is erroneous when the tendon is inclined or eccentric.

(2) Bearing stresses as high as $2.5f'_c$ were routinely achieved before ultimate failure. Specifications limiting allowable bearing stresses to less than f'_c are overly conservative and inappropriate for controlling the complex anchorage phenomena.

(3) While anchorage zone design based upon the ACI Building Code Commentary formula using the square root of relative bearing areas will be conservative under certain circumstances, it cannot be relied upon to be conservative when the tendon is highly eccentric or inclined, or when very thin web sections are used.

(4) A new failure theory which recognizes the complex role of the end face spalling stress in the vicinity of the anchor as the trigger mechanism for an anchorage zone shear failure was confirmed experimentally. Application of this failure theory and experimentally determined spalling strain limits resulted in a general solution to the problem using a three-dimensional finite element analysis. This analysis predicts cracking loads which were confirmed experimentally over a wide range of variables.

(5) The load required to cause formation of the tendon path crack increases with increasing web width. Increasing the angle of inclination, or the eccentricity of the tendon decreases the cracking load. The cracking load for plate-type bearing anchors with no supplementary anchorage zone reinforcement can be calculated as:

$$P_{cr_{plate}} = t\left[\frac{f_{sp}}{24}(38a - 120) - \frac{t}{81}[2\theta - 252(e/a)f_{sp}] - \frac{103}{9}(e/a) - 7\right]$$

$$+ 39a' + \frac{f_{sp}}{5}[166 - 975(a'/t)^2] - 9.1$$

where P_{cr} = cracking load in kips for section without supplementary anchorage reinforcement

e = eccentricity of tendon (in.) (always positive)

$2a$ = section height (in.)

$2a'$ = width and depth of bearing plate (assumed square) (in.)

t = section thickness (in.)

θ = tendon inclination at loaded face (degrees)(always positive)

f_{sp} = split cylinder tensile strength (ksi) = approx. $6.5\sqrt{f'_c}$ (psi) for normal readymix concrete.

(6) Tendon path cracks can occur at points well removed from the anchorage zone in sections where the tendon profile has significant curvature and multiple strand tendons are used. This is due to the tendency for the bundle to flatten out within the confines of the duct, thus creating lateral forces sufficiently high to cause not only cracking but side face rupture as well.

(7) The failure mechanism for plate type anchors is:

(a) The large friction forces developed beneath the anchor plate locally constrain the lateral expansion of the concrete due to Poisson's ratio effect.

(b) A complex, triaxial compressive stress state is set up which permits development of extremely high direct bearing stresses (up to $3f'_c$) beneath the plate.

(c) The confining lateral forces at the edge of the plate are reduced by the presence of the spalling tensile stresses.

(d) At some load level which depends on section and tendon geometry, the confining stress is sufficiently reduced that a shear failure occurs along the plate of approximately 45°, and thus the shear crack propagates to form a 45° pyramidal "cone" beneath the anchor.

(e) Simultaneous with the formation of the cone, a tendon path crack propagates from the tip of the cone. The cone is then forced into the anchorage zone setting up large lateral forces which eventually produce a set of "upper and lower" diagonal cracks which typically form at the corners of the anchor and propagate away from the tendon path at angles of approximately 45°.

(f) Increases in load above that required for formation of the diagonal cracks lead to ultimate explosive failure of the side faces, bounded by the upper and lower diagonal cracks.

(8) Anchor geometry can affect the cracking load. Tests using plate-, bell- and cone-type anchors indicate the following factors should be applied to calculated cracking loads for plate anchors:

	P_{cr}
Plate	1.00 P_{cr} plate
Bell	1.08 P_{cr} plate
Cone	0.61 P_{cr} plate

These values are for sections without supplementary anchorage zone reinforcement. Ultimate loads for unreinforced plate- and cone-type anchors occurred at loads only nominally above the cracking load. Unreinforced bell anchors exhibited ultimate failure at loads approximately 25 percent above those which cause cracking.

Tests of spirally reinforced plate and cone anchorages indicated nearly identical factors were still applicable. No tests were done on spirally reinforced bell anchors. Since the bell action somewhat simulates the spiral action, it was felt further confinement was redundant.

4.3 Reinforcement Conclusions

(1) When using passive reinforcement, spirals exhibit much better performance than standard orthogonal reinforcement both for increasing cracking and ultimate loads, and for controlling crack widths. Spiral reinforcement has the effect of changing the cracking pattern from a single tendon path crack to a series of parallel cracks which exhibit a reduction in the average crack width. The spiral advantage

is greater for thinner web sections, making it the preferred choice of passive reinforcement. Design equations for the spirals are presented which are similar to those used for design of spiral column reinforcement.

(2) The ultimate load for anchorages with spiral reinforcement is as much as 45-60 percent higher than that for anchorages with orthogonal reinforcement (bar grid) with ten times the reinforcement ratio of the spiral.

(3) For a given volumetric percentage of spiral reinforcement, the spirals fabricated from smaller wires performed better than spirals fabricated from larger wires. This indicates that spirals should use close pitch.

(4) Within the range investigated long spirals (2t to 2.5t in length affixed to the anchor) performed no better than short spirals (t in length).

(5) With inclined, curved, multiple strand tendons careful attention must be paid to the possibility of cracking along the tendon path at the point of maximum curvature. In most practical applications that point would be well removed from the anchorage zone, and from the influence of any short spiral reinforcement in the anchorage zone. Continuing anchorage zone reinforcement into the zone of maximum curvature is logical in some cases. However, calculations indicate that the reinforcement required to resist multi-strand effects is usually much smaller than that required in the anchorage zone. A secondary calculation method is presented in Sec. 3.5.3.4 to design the additional reinforcement required for curved tendon applications.

(6) Active reinforcement (lateral post-tensioning) is the most efficient means of controlling anchorage zone cracking. A relatively small precompression of 100 psi across the anchorage zone of a section with an inclined, curved, multiple strand tendon raised

the cracking load 33 percent above that for an unreinforced section. The optimum location for the lateral prestress is as close to the loaded face as is feasible.

4.4 Similitude Conclusions

(1) The tensile strength of the microconcrete used for constructing the models was found to be substantially higher than that for the corresponding prototype concrete.

(2) Cracking and ultimate loads must be normalized with respect to the indirect tensile strength (f_{sp}) when using model results for prediction of cracking in corresponding prototype structures.

(3) When adjusted for geometric scale factor and split tensile strength, excellent reliability (+/- 10%) can be expected for model tests using straight tendons, including the effects of cover, eccentricity, and bearing area.

(4) Specimens with inclined tendons can also be accurately modeled; however, careful attention must be made to detailing the model tendon, when sharply curved multiple strand prototype sections are to be modeled. Due to the importance of multistrand effects in full-scale structures the model tendon should be a precise scaled-down version of the prototype tendon and duct system.

(5) Crack patterns observed in prototype specimens can be accurately reproduced in the models. However, crack widths in the models (after adjustment by the scale factor) were on the average 40 percent smaller than those observed in the full-scale specimens.

(6) As with the full-scale tests, the formation of upper and lower diagonal cracks around the anchor act as a visual indicator of the proximity of ultimate failure. For unreinforced plate anchors a cone of crushed concrete was observed beneath the anchor at failure.

4.5 Analytical Study Conclusions

(1) Static, linear elastic, three-dimensional finite element analyses can be used to predict the state of stress of the anchorage zone with reasonable accuracy up to the cracking load.

(2) Calibration studies show that for straight tendons, a peak spalling tensile strain of 172 $\mu\epsilon$ near the edge of the anchorage as calculated by the program corresponded to initiation of tendon path cracking in test specimens without supplementary reinforcement. The corresponding strain for inclined tendons in which a right angle blockout is modeled is 1150$\mu\epsilon$, due to the high stress concentration induced by the presence of the idealized corner.

4.6 Recommendations for Further Research

The limitations imposed on the empirical cracking equation indicate most directly the areas where further research would be useful. Specifically these would include:

(1) A small series of microconcrete models to investigate the effect of inclined tendons which have "negative" eccentricities (e.g., below the section centroid) or "negative" inclinations.

(2) Extension of the 3D FEM analytical study to investigate the effect of multiple tendons anchored in the same web section. Experimental test results from Cooper [3] and Kashima [14] are presently available for checking the analytical model predictions.

(3) A small series of microconcrete models, backed by analytical predictions to investigate the effect of rectangular-shaped anchors and their orientation with respect to the end face geometry.

(4) A similar series to investigate the effect of lateral eccentricity of the anchor, a subject of some importance when several anchors are placed across a wider web section.

(5) A series of full-scale tests to investigate the most efficient reinforcement design for resisting multistrand effects.

B I B L I O G R A P H Y

1. Stone, W. C., and Breen, J. E., "Analysis of Post-Tensioned Girder Anchorage Zones," Research Report 208-1, Center for Transportation Research, The University of Texas at Austin, August 1980.

2. Stone, W. C., Paes-Filho, W., and Breen, J E., "Behavior of Post-Tensioned Girder Anchorage Zones," Research Report 208-2, Center for Transportation Research, The University of Texas at Austin, August 1980.

3. Breen, J. E., Cooper, R. L., and Gallaway, T M., "Minimizing Construction Problems in Segmentally Precast Box Girder Bridges," Research Report No. 121-6F, Center for Highway Research, The University of Texas at Austin, August 1975.

4. Dilger, W. H., and Ghali, A., "Remedial Measures for Cracked Webs of Prestressed Concrete Bridges," Journal of the Prestressed Concrete Institute, Vol. 19, No. 4, July-August 1974.

5. American Association of State Highway and Transportation Officials, Standard Specifications for Highway Bridges, 12th Edition, 1977.

6. American Concrete Institute, Building Code Requirements for Reinforced Concrete and Commentary (ACI 318-77), Detroit, Michigan, 1977.

7. Guyon, Y., The Limit State Design of Prestressed Concrete, Vol. II: The Design of the Member, Translated by F. H. Turner, John Wiley & Sons, New York, 1974.

8. Rhodes, B., and Turner, F. H., "Design of End Blocks for Post-Tensioned Cables," Concrete, December 1967.

9. Comité Euro-International Du Béton (CEB) and the Féderation Internationale de La Précontrainte (FIP), Model Code for Concrete Structures, English Translation, 1978.

10. Rüsch, H., Grasser, E. and Rao, P. S., "Fundamentals of Design for Uniaxial Stress-conditions in Concrete Members," Munich, August 1961 (Translation from German, Oct. 1963, by J. V. McMahon and J. E. Breen, University of Texas at Austin).

11. Peterson, R. E., Stress Concentration Design Factors, New York, Wiley, 1953.

12. Berezovytch, W. N., "A Study of the Behavior of a Single Strand Post-Tensioning Anchor in Concrete Slabs," unpublished Master's thesis, The University of Texas at Austin, May 1970.

13. MacGregor, J. G., "Safety and Limit States Design of Reinforced Concrete," Canadian Journal of Civil Engineering, Vol. 3, No. 4, 1976.

14. Kashima, S., and Breen, J. E., "Construction and Load Tests of a Segmental Precast Box Girder Bridge Model," Research Report 121-5, Center for Highway Research, The University of Texas at Austin, February 1975.